Mitigation Effects on Urban Flood by Installing an Underground Storage Box

KO Dongwoo

2015

Mitigation Effects on Urban Flood by Installing an Underground Storage Box

A dissertation submitted in partial fulfillment for the requirement

Doctoral Degree in Civil and Earth Resources Engineering

by

KO Dongwoo

Supervised by Prof. NAKAGAWA Hajime

Laboratory of Hydro-science and Hydraulic Engineering

Department of Civil and Earth Resources Engineering

Graduate School of Engineering

Kyoto University

Japan

2015

Abstract

Recently, urban inundation disasters resulting from torrential rain have led to serious problems in many countries all over the world, especially in Asian countries. In recent years, numerous cities have been inundated by storm water, which is the major cause of urban flooding. The frequency and intensity of natural disasters are increasing because of interactions between natural and artificial factors. Protecting people and critical network infrastructure, and taking effective countermeasures are of the highest importance during flooding and natural disasters. Although the chance is slim, we should always be prepared for natural disasters.

To mitigate the damage of urban inundation, various structural strategies have been carried out, one of which is creating underground storage boxes attached to sewerage systems. In the strategy, part of the storm water within a sewer pipe is diverted over the side weir into the storage box. The function of this storage box is to manage storm water runoff on a developed site to prevent flooding, and it works as an essential part to provide a temporary storage area for excess storm water. In this way, the underground storage boxes are assumed to drain the surcharged water in the urban area efficiently and keep the urban area from inundation.

However, there are no criteria on the degree of mitigation effect that can be expected from such underground storage systems. In order to evaluate the mitigation effect of this facility, there must be appropriate diversion of overflow discharge from a sewerage system over the side weir. Therefore, it is essential to study the overflow discharge over the side weir related to underground storage systems.

Side weirs are hydraulic structures that are usually used as flow dividers in urban drainage systems, irrigation channels and flood protection works (Granata et al, 2013). The main contributor to the understanding of the hydraulic behavior of side weirs is De Marchi (1934). He presented a theory based on the assumption of a constant energy head along the side weir and the overflow discharge being calculated by the classical weir formula, which overlooks the effect of lateral outflow direction, local velocity and the type of flow (pressurized or non-pressurized) in the system. In this regard, De Marchi's approach seems appropriate for the open-channel flow condition. However, no study has verified the suitability of De Marchi's equation to the pressurized flow condition. Considering overflow from the sewerage system during urban flooding, pressurized flow conditions are often.

The present study was undertaken to determine the appropriate equation to estimate the diversion discharge to a storage box. The experiment was to obtain the overtopping discharge

under different conditions, like upstream discharge and weir condition, and to determine the discharge coefficient. Also, the numerical model was used to validate the experimental results using the discharge coefficient obtained by experiment. Therefore, the applicability of De Marchi's equation must also be verified in my experimental cases, and the correlation equation of discharge coefficient in the changing hydraulic structure conditions, like side weir length and height, was suggested under pressurized flow conditions.

Finally, actual field application studies on the effects of underground storage box were carried out using a numerical model, adopting the suggested correlation equation of the discharge coefficient. An integrated model consisting of a two-dimensional ground surface model was developed, and a one-dimensional sewer model was used.

The current study was applied to the Nakahama area in Osaka, where 90% of the city area is prone to flooding by heavy rain and storm water has to be drained by pumps. In addition, most storm water cannot infiltrate into the ground due to the city's high pavement ratio. Therefore, flood control is one of the most important roles of the sewerage system.

The main objective of the study was to maximize flood mitigation by installing the underground storage box. Firstly, the differences in the storage box's effects were verified due to rainfall type and weir shape changes. Secondly, the lowland, middle, and upstream portions of the Nakahama area were investigated to verify the storage box's effect along locations that have different area features. Thirdly, the differences in the storage box's effect were verified by the changes in storage capacity volume. Lastly, a suitable installation site was verified though assessments of inundation damage costs.

Keywords*: underground storage box, De Marchi's equation, side weir, discharge coefficient, integrated urban inundation model*

Acknowledgements

The completion of this thesis was made by the contributions, knowledge, kindness, and support of many individuals. First of all, I would like to express my sincere gratitude to my supervisor, Professor Dr. Hajime Nakagawa, Disaster Prevention Research Institute to (DPRI), Kyoto University, for his patient guidance, support, encouragement, and excellent advice throughout my study period.

I am deeply grateful to Professor Dr. Kenji Kawaike, Disaster Prevention Research Institute to (DPRI), Kyoto University, for his academic guidance, keen insight, invaluable comments and suggestions to refine the thesis.

I wish to express my sincere gratitude to Professor Dr. Hao Zhang, Kochi Unversity, for his guidance, suggestions, comments and friendly help in all aspects of my study.

I am deeply grateful to my thesis reviewer, Professor Dr. Masaharu Fujita, Disaster Prevention Research Institute to (DPRI), Kyoto University, for his valuable comments and suggestions to refine the thesis.

I am deeply thankful to Professor Dr. Jongsung Yoon, Inje University, Dr. Sunbong Woo, Dr. Dongkeun, Dr. Myoungkyu, Dr. Yeonjoong Kim for their guidance, and for leading me to interested topic and coming to Japan.

I would like to thank Mr. Ueda who can make an experimental model for his kindness, consideration, experimental invaluable comments.

I would like to warmly thank Ms. Natsuyo Iguchi and Ms. Tomoko Himuro for their support in routine administrative. Had it not for their help, I could have experienced the difficulties in Japanese life.

I am indebted to my all colleagues of Reseach Center for Fluvial and Costal Disaster, DPRI, Kyoto University for their kind cooperation and unforgettable friendship. I am especially grateful to Dr. Seungsoo Lee, Dr. Masakazu Hashimoto, Dr. Namgyun Kim, Mr. Bhattarai

Pawan, Mr. Rocky Talchabhadel, Mr. Taku Oomoto, Mr. Nanahiro Tanaka, Mr. Shunsuke Hiratsuka, Mr. Osamu Kitaguchi, Mr. Kei Nishio, Mr. Shogo Harigae, Mr. Synnichi Sugihara, Ms. Wang Yu, Ms. Shoko Fujita, Ms. Miki Yamazaki and all the staffs in Ujigawa Open Laboratory, Disaster Prevention Research Institute of Kyoto University for their kind cooperation, support in routine administrative process and experiments.

I gratefully acknowledge the financial support of the Monbukagakusho (Ministry of Education, Culture, Sports, Science and Technology, Japan)

I take this opportunity to express my profound gratitude to my grandmother Boksoon Kim, beloved parents, Moonyong Ko, Okyeol Jeong, my sister and brother, and close relatives for their encouragement, loving support, and praying for me throughout the course of this study. All the time they gave me the feeling of doing something special.

Last but not least, I am sincerely gratitude to my girlfriend, Hyunju Hong, for her persistent love, continuous support, and enormous patience.

Table of contents

Chapter 1

Introduction

1.1 General

With the increase of urbanization, original surface and climate conditions have been changed by human activities. Excessive rain, a ruptured dam or levee, and rapid ice melting in the mountains can overwhelm a river and send water spreading over the adjacent land, called a floodplain. Most floods take hours or even days to develop, giving residents plenty of time to prepare or evacuate. Other floods generate quickly and with little warning. These flash floods can be extremely dangerous, instantly turning a babbling brook into a thundering wall of water and sweeping away everything in its path downstream.

Disaster experts classify floods by their possibility of occurring in a given time period. A hundred-year flood, for example, is an extremely large, devastating event that would theoretically be expected to happen only once every century, but this is a theoretical number. In reality, this classification means there is a one-percent chance that such a flood could happen in any given year. Over recent decades, maybe due to global climate change, hundred-year floods have been occurring worldwide with frightening regularity.

Recent years have seen major flooding, which involves inland flooding caused by a lack of drainage capacity and drainage pump systems, as well as insufficient water retention due to increasing runoff flow by urbanization in towns. Drainage systems are relatively well established, but urban inundation sill occurs. This means that the flow in sewers is much greater during a heavy storm and can reach maximum capacity. Impervious areas have increased rapidly over the past several years, and most drainage systems are insufficient to control normal storms. Due to this, urbanization has increased peak flows and surface runoff volume over pre-urban levels, as shown in Figure 1.1. This is a typical hydrograph of an urban stream during heavy rain.

It illustrates that the peak flows of urbanized streams respond more quickly and are much higher than they were during the pre-development situation. This increase in discharge also causes erosion of the stream banks due to higher flow velocities.

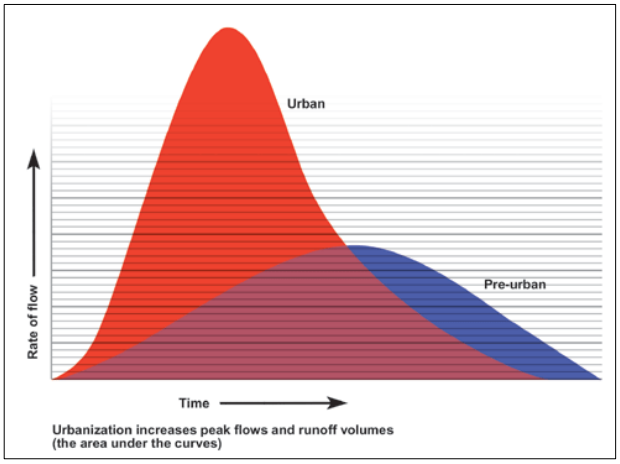

Figure 1.1 Effects of urbanization on volume and rates of surface water runoff
(Source: Adapted from Drainage Manual, Roads and Transportation Association of Canada)

Impervious surfaces include roads, parking lots, rooftops, sidewalks, and driveways. Such constructed surfaces prevent rainfall from penetrating the soil. Since a large portion of the rainfall in urban areas no longer infiltrates the ground, it is intentionally routed to storm drains and directly enters into urban streams as runoff, as shown in Figure 1.2. In many cases the need for development of additional storm water infrastructure depend on changes in land use within or upstream of a community. In general, increases in the extent of impervious surfaces are associated with higher rates of flooding. Although these effects may not lead to serious flooding in the short term, over time even minor rain events will begin to culminate in larger quantities of water flowing into storm water systems at faster rates. Flood control structures can mitigate the deleterious side effects of urbanization by creating or enhancing areas within the developed landscape that provide opportunities for increased infiltration, evaporation, transpiration.

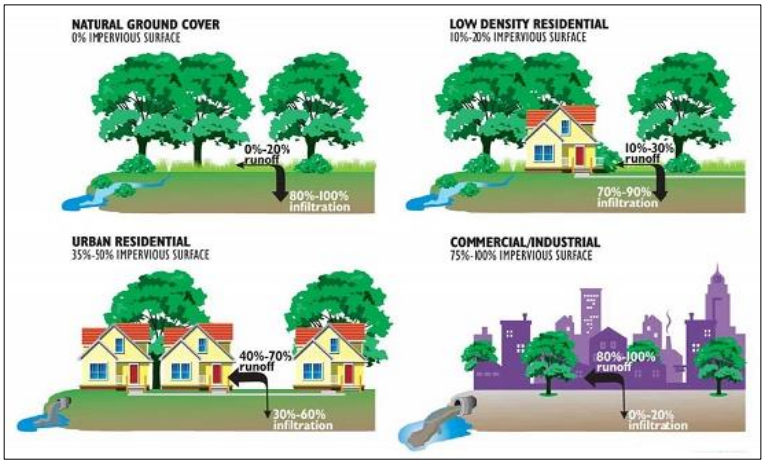

Figure 1.2 Effects of urbanization on volume and rate of surface water runoff
(Source: http://www.lincoln.ne.gov/city/pworks/watrshed/educate/runoff/)

1.2 Recent inundation damage

1.2.1 South Korea

On July 25, 2011, over 495 mm of rain poured down during two days of heavy rain and thunderstorms in Seoul, South Korea, the heaviest such event in July since 1907. A total of 587 mm of rain was recorded in the area after three days. These events caused a series of flash floods and landslides that killed at least 49 people and left more than 77 dead or missing. Flood waters inundated main roads, residential areas, and basement facilities in and around Seoul, cutting the power supply to 14,000 homes and leaving thousands of vehicles submerged on flooded roads, as shown in Figures 1.3 ~ 1.4. The damage in Seoul was greater than in other areas of Korea due to its urbanized areas.

On August 25, 2014, a maximum of 130mm/hour of rain poured down in Gumjung-gu, South Korea (near Busan University). A total of 242mm/day of rain poured down, which was a 200 year frequency rainfall, as shown in Figures 1.5 ~ 1.6. Five people were killed, and five others were missing after the heavy rains pummeled the area. The storm water of this area gathered together in a short time, including flowing rainfall from a mountain, resulting in serious flash-flooding damage. The problem was that the heavy rainfall had inundated the area, yet the flood control structures were insufficient.

Figure 1.3 Vehicles submerged in floodwater (Source: Daily Mail Reporter)

Figure 1.4 Cars trapped on a flooded road (Source: Daily Mail Reporter)

Figure 1.5 Flooded areas near Busan Subway Station

Figure 1.6 Flooded Dongnae Subway Station

1.2.2 Japan

On September 13, 2013, a typhoon made over 400mm of rain pour down onto Kyoto, Japan, for three days. In addition, 93 houses flooded in Arashiyama District, 289 houses became flooded in Rokujizo, near Ogurisu, and about 270 cars were submerged. Figure 1.7 shows water erupting through a manhole near Rokujijo Station.

Figure 1.7 Water erupting through a manhole (Source: Kawaike K.)

1.3 Countermeasures for urban inundation.

Since the severe storm surge disaster caused by Isewan Typhoon in 1959, Japan, various laws related to flood disasters have been established and revised, and flood control structures have been constructed. These have been based on the concept that storm water should be collected into river channels as soon as possible. In fact, they have significantly reduced casualties due to flood disasters.

However, flood disasters still remain a serious problem. Therefore, storage facilities have been created within urban areas. Moreover, both non-structural and structural countermeasures have been adopted, such as the arrangement of evacuation systems and publication of areas with flood hazards. As an effective way to promote those countermeasures, local governments are strongly recommended to publish “flood hazard maps” (Kawaike and Nakagawa, 2006). Figure 1.8 is an example of a flood hazard map published by Neyagawa City, Osaka Prefecture.

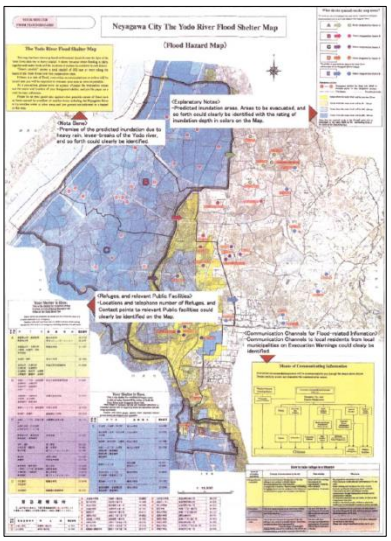

Figure 1.8 Flood hazard map for Neyagawa City
(Source: http://www.adrc.asia/publications/TDRM2003June/28P201.pdf)

In Osaka, the Neyagawa basin cannot naturally drain into rivers because the population and assets have been rapidly concentrated through urbanization. 90% of the city's area is prone to flooding, and storm water has to be drained by pumps. The flood control and other comprehensive measures are not only important to repair the river but also to promote the development of storage facilities.

Two underground tunnels are planned to be constructed: Neyagawa North Tunnel and Neyagawa South Tunnel. The completed parts of these tunnels have been utilized as storm water storage facilities. Neyagawa North Tunnel is 14.3km long (3.7km completed), has a 5.4 ~ 11.5m diameter, a maximum storage capacity if 680,000m^3 (130,000m^3 completed), and 250m^3/s maximum flow discharge. The Neyagawa South Tunnel is 13.4km long (11.2km completed), has a 6.9 ~ 9.8m diameter, a 790,000m^3 maximum storage capacity (630,000m^3 completed), and 180m^3/s maximum flow discharge. Since the installation of this tunnel as a large storage tank, the inundation damage to the surrounding area has decreased greatly, especially under precipitation of less than 40mm/hour. However, building these kinds of tunnels is time-consuming and expensive. Accordingly, the construction of underground storage boxes is a cost-effective solution. Storm water storage boxes can be adapted to the sewer system relatively easily, and storage boxes are an essential part of drainage systems that provide a temporary storage space for excessive storm water. Figure 1.9 provides an example of underground storage facility from Kadoma, Mitsujima, in Osaka Prefecture, with a storage capacity of approximately 24,300m^3. The ground zone of this storage system is used as tennis courts.

Figure 1.9 Mitsujima storage facility
(Source: Neyagawa Water System Renovation Engineering Camp)

1.4 Objectives of the study

The main objective of this study is to propose effective countermeasures to urban inundation. As a method of protection, underground storage box can be considered under experimental and numerical models. Such storage boxes are attached to sewerage systems, and some portion of the storm water within a sewerage pipe is diverted over the side weir into the storage box. Therefore, an evaluation of the mitigation effects of storage box requires an appropriate estimation of overflow discharge from a sewerage system over the side weir.

Experiment

- To determine the overtopping discharge regarding the side weir's condition to calculate the discharge coefficient made by the downscaling of a prototype.

Simulation

- To validate the experimental results using the discharge coefficient obtained by the experiment.
- The constant coefficient value is easy to handle when estimating the actual overflow discharge from the weir. Therefore, the applicability of the constant value derived from these experiments will be investigated.

Simulation (application in the actual field, Nakahama, Osaka)

- To verify the differences in the storage box's effects due to rainfall type and weir shape changes.

- To verify the storage box's effect at locations with different area features, like the lowland, middle, and upstream portion of the Nakahama area.
- To verify the differences in the storage box's effects due to the storage box's capacity changes.
- To verify the differences in the storage box's effects due to the storage box's capacity changes.
- To verify a suitable installation site though assessments of inundation damage costs.

1.5 Literature review

1.5.1 Side weirs

Side weirs are hydraulic structures that are usually used as flow dividers in urban drainage systems, irrigation channels, and flood protection works (Granata et al., 2013). De Marchi (1934) is the main contributor to the understanding of side weirs' hydraulic behavior. He presented a theory based on the assumption of a constant energy head along the side weir and the overflow discharge being calculated by the classical weir formula, which overlooks the effect of lateral outflow direction, local velocity, and the type of flow (pressurized or non-pressurized) in the system.

Many studies have suggested the discharge coefficients regarding the side weir with subcritical flow and supercritical flow in several channel conditions. Subramanya et al. (1972), Yu-tech (1972), Hager (1987), Cheong (1991), and Borghei et al. (1999) obtained equations for the discharge coefficients of rectangular, sharp-crested side weirs based on experimental results. Ghodsian (2003) studied the behavior in rectangular side weirs with supercritical flow. Khorchani et al. (2004) studied overtopping discharge through weirs with a full-scale experiment using digital cameras. Muslu (2002) and Yüksel (2004) used numerical evaluations to analyze the flow over rectangular side weirs.

Some previous theoretical analyses and experimental studies have reported on flow over rectangular side weirs in circular open channels. Generally, the method assumes one-dimensional flow conditions, thus neglecting the variations of overflow direction and the velocity distribution (Allen, 1957; Uyumaz and Muslu, 1985; Hager 1987; Vatankhah, 2012; Granata, 2013).

1.5.2 Effect of underground storage facilities

Research on the effects of underground storage facilities has been actively pursued in South Korea. Song et al. (2007) studied the runoff reducing effects of infiltration storage systems in an experimental hydraulic study. The infiltration characteristics of runoff reduction facilities were verified under varying rainfall conditions and infiltration layer materials, which were used to consider the influences of urban development.

Kim et al. (2010) analyzed the effects underground installations on flood damage mitigation through an actual field application. The SWMM model was used for a runoff and pipe network analysis on Typhoon Maemi, in 2003. A 2-D inundation analysis model based on diffusion waves was employed for inundation analysis and to verify the computed inundation areas with an observed inundation trace map.

Choi et al. (2012) verified existing drainage capacities during flash floods and analyzed the mitigation effect of inundation damage with underground storage facilities installed. The rainfall runoff analysis was carried out on the probable rainfalls at 10, 20, 50, and 100 year frequencies.

Ryu et al. (2012) developed an optimal model to decide adequate capacities and locations according to the numbers of facilities. A genetic algorithm was utilized for this optimal technique and SWMM 5.0 DLL was constructed accordingly for better hydraulic and hydrological interpretation. Furthermore, a method of reducing inundation while installing underground storage facilities was analyzed by adapting various excess rainfall conditions.

Song et al. (2013) focused on storage amounts based on the storage tank, reductions in the outflow and peak water surface elevation, changes in the phase lag time, and the design of new boxes at the inlet and outlet of the storage tank. They concluded that combined management of a previous storage facility and a new underground storage tank would control excessive rainfall runoff efficiently.

1.5.3 Urban inundation modeling

An integrated numerical model is developed in the study to simulate runoff processes in urban areas. A 1-D model is used to calculate the rainfall runoff hydrographs and the flow conditions in drainage networks. A 2-D model is employed for routing flow on overland surfaces. Both models are solved by different numerical schemes and using different time steps, with the flow through manholes adopted as the model's connections. The effluents and influents via manholes are determined by the weir or orifice equations. Timing synchronization between both models is taken into account to guarantee suitable model linkages (Chen et al., 2007).

Iwasa and Inoue (1982) and Inoue et al. (1994) developed numerical solutions for 2-D overland flood flows using the finite difference scheme based on Cartesian meshes, while Kawaike et al. (2000) applied the finite volume method, based on unstructured meshes and the

finite difference. The method based on unstructured meshes has advantages in describing complicated areas more exactly.

Chen et al. (2005) showed that incorporating the linear ratio of building areas to the total area of interest may be considered to reflect complex flow phenomena in simulating dynamic flow interactions regarding the urban inundation model. An accurate method for modeling urban flooding may be obtained by covering buildings with a flexible grid system to capture the wall effect on the flow.

Tayefi et al. (2007) developed a coupled 1D-2D treatment that is likely to provide the best modeling approach with currently available technology for complex floodplain configurations. It should be noted, however, that floods in urban areas have different characteristics from floods in rural areas.

One of the challenges in modeling urban flooding is the effects of buildings. Chen et al. (2008) concluded that buildings in a densely developed urban area have a crucial influence on flood propagation progress. The presence of buildings, particularly in high-density urban areas, changes flow paths and patterns due to blockage, which leads to an effect on flood inundation. This phenomenon needs to be accounted for in an urban flood model to accommodate physical processes under real conditions.

Schubert et al. (2008) simulated urban flooding using unstructured mesh generation with resistance values estimated from satellite images. Nevertheless, the computation time may increase significantly when the unstructured mesh is applied to a large or dense area. Moreover, a pixel-based estimation of resistance depends heavily on the satellite image's resolution.

Farid et al. (2012) developed a flood inundation model that considered the building's effects in a high density urban area. A 2D overland flow model was coupled with a 1D channel model to simulate flood inundation, with the exchange of flows between the river and surface floodplains. A momentum equation in the overland flow model was modified in order to consider the urban flooding characteristics. The sharing rate, defined as the occupancy area of buildings in each grid of a model domain, was applied to accommodate the effects of buildings. Drag force occurring due to the reaction of force acting on buildings was also included. The tank model, which is widely used to model the hydrology process in a basin or sub-basins, was combined into the model.

Lee et al. (2015) developed a new urban inundation model that can reflect real field situations. They carried out two kinds of simulations with homogeneous and non-homogeneous meshes using manholes and storm drains as discharge exchange spots, respectively. These results were compared to estimate the effects of road networks and building groups according to different discharge exchange spots. A 2-D runoff flow model and a 1-D slot-model were used to simulate ground surface runoff flow and sewer pipe flow. To connect both models, they used a newly

suggested bi-directional model and its coefficients.

1.6 Outlines of the dissertation

This research concerns effective countermeasures to reduce urban flooding in metropolitan areas. Therefore, a process to verify the effects of underground storage box is described.

Chapter 1 presents the background of the work, the study's objectives, and a brief review of previous literature.

Chapter 2 presents experimental laboratory studies and also describes the experimental objectives, method, and major measurement apparatus, as well as the experimental results.

Chapter 3 presents a one-dimensional model to validate the experimental results. The applicability of the constant values derived from these experiments is verified.

Chapter 4 presents a 1D-2D integrated inundation model to verify a storage box's effects along locations and along changes in its capacity and side weir condition when applied to an actual field in Osaka.

Chapter 5 summarizes the conclusions based on the present study and recommendations for future research.

Chapter 2

Experimental studies for estimating inflow discharge to an underground storage box

2.1 Introduction

Even though numerous studies have been conducted on reducing urban inundation damage, such damage remains a serious problem every year. Urban inundation has caused immense property damage and many personal injuries due to short-term, local heavy rainfall and extreme climate conditions worldwide. Although wide, permeable areas such as farming land and forest may exist before urbanization, permeable areas decrease after urbanization as a result of increased road areas, building construction, etc. Due to this, most storm water does not infiltrate into the ground and the total amount of storm water runoff increases, which can lead to urban inundation.

To mitigate this problem, underground storage boxes have been implemented as an effective countermeasure, especially in highly urbanized areas. However, there are no criteria on the degree of mitigation that can be expected from installing such underground storage boxes. In many cases, these storage boxes are attached to sewerage systems, and some portion of the storm water within a sewerage pipe is diverted over the side weir into the storage box. Therefore, an evaluation of storage boxes' mitigation effects requires an appropriate estimation of overflow discharge from a sewerage system over the side weir. In this regard, it is essential to study the overflow discharge over the side weir related to underground storage systems. Figure 2.1 briefly shows the structure of an underground storage system.

The present study was undertaken to determine the appropriate equation to estimate the diversion discharge to a storage box. Moreover, as seen in Table 2.1, several studies have obtained discharge coefficient equations for rectangular side weirs based on experimental results, where F is the Froude number at the upstream end of the side weir and h is the flow

depth at the side weir. De Marchi(1934) is the main contributor to the understanding of hydraulic behavior at side weirs. He presented a theory based on the assumption of a constant energy head along the side weir and the overflow discharge being calculated by the classical weir formula, which overlooks the effect of lateral outflow direction, local velocity, and type of flow (pressurized or non-pressurized) in the system.

De Marchi's equation is usually employed in cases of open channel flow, and many researchers have suggested its discharge coefficient. However, no study has verified the suitability of De Marchi's equation in the pressurized flow condition. When considering overflow from a sewerage system during urban flooding, the pressurized flow condition would occur often and the applicability of De Marchi's equation must also be verified in that condition. Hence, in this study, an experimental set-up is proposed, in order to determine the discharge coefficient for pressurized flow in a circular channel with different side weir lengths. Such experimental data is then expected to be used to validate numerical models for estimating the effects of underground storage box.

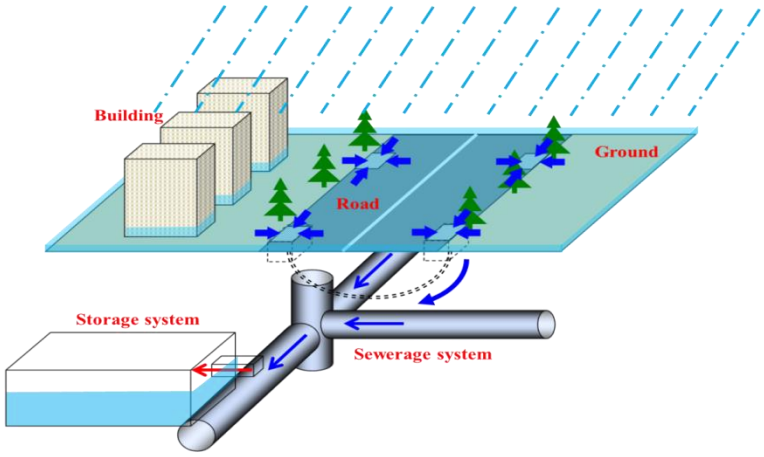

Figure 2.1 Underground storage system

Table 2.1 Discharge coefficient of side weir

Researcher	Equation
Subramanya et al. (1972)	$C_d = 0.611\sqrt{1-(\frac{3F^2}{F^2+2})} = 0.864(\frac{1-F^2}{2+F^2})^{0.5}$
Yu-Tech (1972)	$C_d = 0.623 - 0.222F$
Hager (1987)	$C_d = 0.485(\frac{2+F^2}{2+3F^2})^2$
Cheong (1991)	$C_d = 0.45 - 0.221F^2$
Borghei et al. (1999)	$C_d = 0.7 - 0.48F - 0.3\left(\frac{p}{h}\right) + 0.06\frac{L}{D}$

2.2 Experimental set-up

2.2.1 Description of hydraulic model

The experiments were conducted at the Ujigawa Open Laboratory of the Disaster Prevention Research Institute (DPRI), Kyoto University, as shown in Figure 2.2.

Figure 2.2 Experimental setup

A rectangular side weir in a circular pipe is shown in Figure 2.3, where D is the diameter of the main pipe, p is the height of the side weir, and L is the length of the side weir. The experimental setup consists of a side weir with two circular acrylic pipes that are 4m in length and 0.05m in internal diameter. An upstream supply tank with a recirculation pump system is present, as is a downstream collecting tank with a movable gate to adjust the downstream water level. The recirculation system can be controlled by an RPM controller, which controls motor speed to supply constant inflow discharge to the upstream tank. A flowmeter was used to measure the upstream input discharge. All of the experiments were conducted using a horizontal pipe. The experiments were conducted with three different side weir lengths, 10cm, 15cm, and 20cm, and three different side weir heights, 3cm, 3.5cm, and 4cm in all cases. The standard weir elevation is the dashed line on the bottom of the pipe in Figures 2.3 and 2.4. Figure 2.5 shows a design drawing for combining the pipe and weir processes; this side weir height can be adjusted up and down easily by controlling the bolt. The fundamental length and height of the side weir model were determined according to the actual size of the pipe diameter and the side weir in Moriguchi City, which can be regarded as a typical overflow system of side weirs. Table 2.2 shows the ratios between the proto-type and the physical model's scale based on the similarity law.

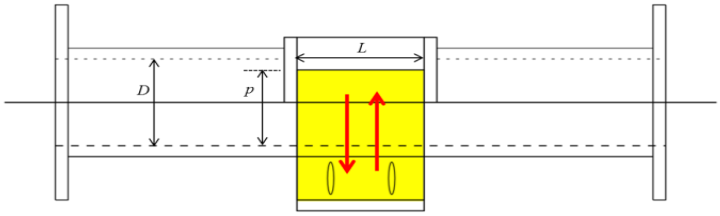

Figure 2.3 Definition sketch of rectangular side weir

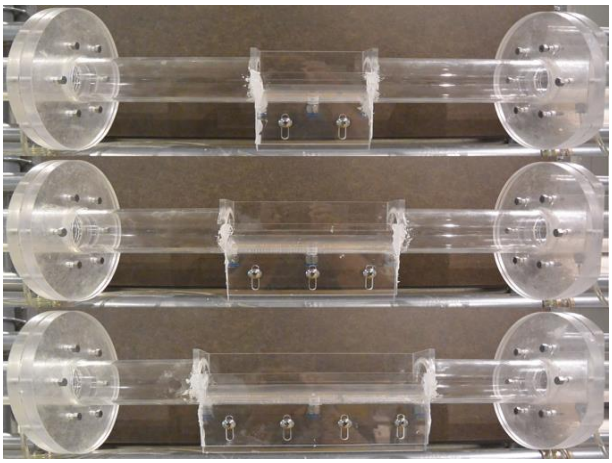

Figure 2.4 Side weirs

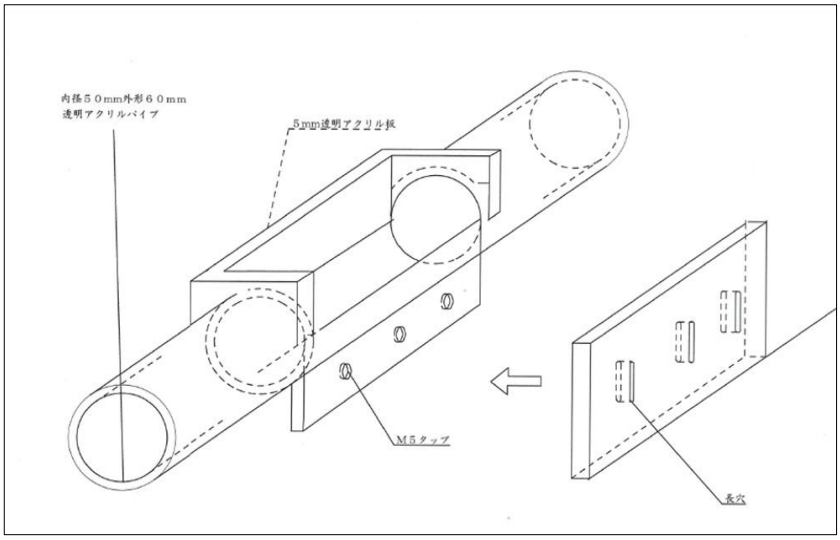

Figure 2.5 Design drawing for combining of pipe and weir processes

Table 2.2 Ratios between the proto-type and physical model's scale

Index	Ratio
Diameter	1/22
Weir length	1/23 ~ 1/45
Weir height	1/24 ~ 1/32

2.2.2 Experimental conditions

63 experimental cases in total were conducted to determine the overflow discharge coefficient, with steady conditions but different side weir lengths and heights. The water heads were measured by a total of 17 piezometer tubes placed at the lowest bottom of the pipe. In particular, there are 3 measuring points along the bottom of the side weir section, as shown in Figure 2.6. Seven experiments were carried out for each different side weir condition, and the discharge supplied to the upstream tank differed from 0.5 ℓ/s to 1.1 ℓ/s. The downstream movable gate level was set to the bottom of the main pipe. The detailed hydraulic conditions are summarized in Tables 2.3, 2.4, and 2.5, which contain the observed water head at the downstream end of the pipe. Each experiment under the same conditions was repeated three times to consider the consistency of the overflow discharge rate.

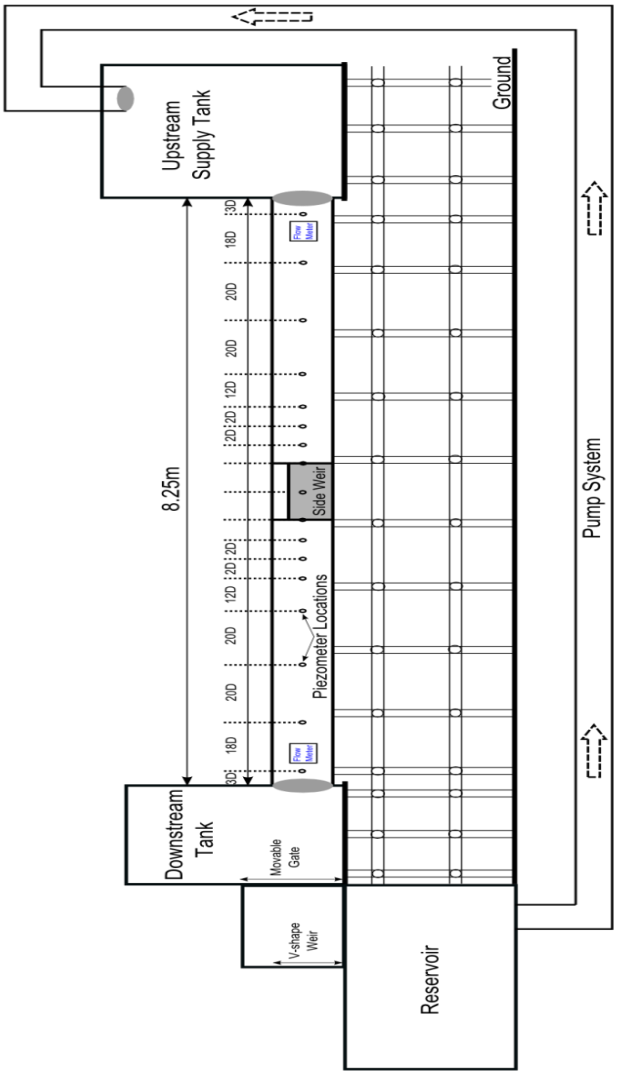

Figure 2.6 Side view of experimental arrangement

Table 2.3 Experimental conditions (Weir length = 10m)

Weir length(cm)	Weir height(cm)	Case 1	Case 2	Case 3	Case 4	Case 5	Case 6	Case 7
Upstream discharge(ℓ/s)								
10	3, 3.5, 4	0.5	0.6	0.7	0.8	0.9	1.0	1.1
Water depth at the downstream end of the pipe(cm)								
10	3	2.8	2.9	3.0	3.2	3.3	3.4	3.5
	3.5	2.9	3.0	3.0	3.2	3.3	3.4	3.5
	4	3.1	3.2	3.3	3.3	3.4	3.5	3.6

Table 2.4 Experimental conditions (Weir length = 15m)

Weir length(cm)	Weir height(cm)	Case 1	Case 2	Case 3	Case 4	Case 5	Case 6	Case 7
Upstream discharge(ℓ/s)								
15	3, 3.5, 4	0.5	0.6	0.7	0.8	0.9	1.0	1.1
Water depth at the downstream end of the pipe(cm)								
15	3	2.6	2.7	2.8	3.0	3.2	3.3	3.4
	3.5	2.9	3.0	3.0	3.2	3.2	3.3	3.4
	4	3.1	3.2	3.3	3.3	3.4	3.5	3.6

Table 2.5 Experimental conditions (Weir length = 20m)

Weir length(cm)	Weir height(cm)	Case 1	Case 2	Case 3	Case 4	Case 5	Case 6	Case 7
Upstream discharge(ℓ/s)								
20	3, 3.5, 4	0.5	0.6	0.7	0.8	0.9	1.0	1.1
Water depth at the downstream end of the pipe(cm)								
20	3	2.6	2.7	2.8	3.0	3.2	3.2	3.3
	3.5	2.8	2.9	3.0	3.1	3.2	3.3	3.4
	4	3.1	3.2	3.3	3.3	3.4	3.4	3.5

2.3 Measurement apparatus

2.3.1 Magnetic flowmeter

The ADMAG AXF magnetic flowmeter, which adopts the dual frequency excitation method to ensure quicker response and stability in high-concentration slurries, was used to measure the inflow discharge from the upstream tank and the outlet discharge to the downstream tank, as shown in Figure 2.7. The standard accuracy is 0.35% of the reading.

Figure 2.7 Magnetic flowmeter

2.3.2 RPM controller

To supply the inflow discharge to the upstream tank, an RPM controller was used to control the motor speed of the recirculation pumping system, as shown in Figure 2.8. It can be easily operated while adjusting the frequency and can create constant discharge conditions. The frequency accuracy is within 0.5% with the analog setting.

Figure 2.8 Controller

2.3.3 HD video camera (HDR-CX630)

As mentioned above, there were 17 measurement points along the bottom of the pipe. The video cameras were located in front of the side weir to observe the surface flow pattern from the upstream to downstream section on the side weir and panel of the piezometric tubes in order to measure the changes by piezometric heads in the pipe along the different upstream discharge rates. Figure 2.9 shows a panel of the piezometric tubes.

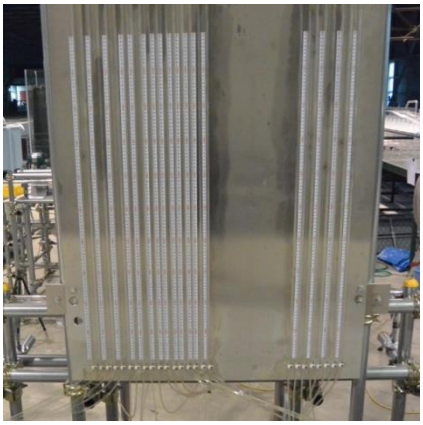

Figure 2.9 Piezometric tubes

2.4 Experimental procedure

Upstream inflow discharge was supplied along each case. All of the experimental conditions here were considered steady. Although the phenomenon is actually unsteady, the steady-state condition was selected to simplify the problem; the unsteady-state will also be analyzed as an advancement of the research. Then, the water heads of the upstream and downstream tanks were read with the naked eye; also, the water heads regarding each measurement point placed at the bottom of pipe were recorded. The overtopping water over the side weir was captured for 5 seconds by a sampler box directly, which was weighted, and the discharge was calculated by considering the time of sampling, as shown in Figures 2.10 and 2.11. This situation was repeated three times to estimate the amount of overtopping water accurately and to reduce the inevitable error. Afterwards, the overtopping water along the different upstream inflow discharges was determined by averaging the values. Figure 2.12 shows a drain system to a reservoir using another pump to protect the temporary water scarcity in the reservoir, because if the stored water in a reservoir decreases, then the power supplied through the circulation pumping system will also decrease. Therefore, it is difficult to maintain the steady-state condition.

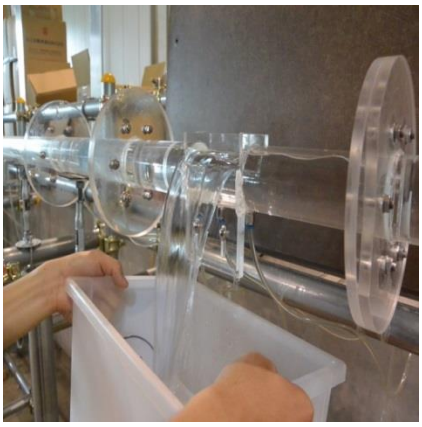

Figure 2.10 Sampling the overtopping water

Figure 2.11 Measuring the captured water

Figure 2.12 Drain system to the reservoir

2.5 Experimental results

2.5.1 Water head profile

The water surface profiles around the side weir for all of the cases are described in Figures 2.13 ~ 2.21. As can be seen in all of the figures, the water head at the upstream end of the side weir was lower than that at the downstream end of the side weir. This phenomenon was due to the water spurting quickly from the upstream to downstream portion, so that it takes the pressure at the downstream portion. The same results have been observed in all previous experimental studies. As the upstream discharge increased, the hydraulic gradient became steeper, compared with the results of the smaller discharge cases. However, the variation of the water heads at the upstream end of the side weir was small, compared with the water head at the downstream end of the side weir for all of the cases. Due to this, if the water head at the

upstream end of the side weir was used to calculate the discharge coefficient, the values increased in the greater discharge cases, with unstable values. When the height of the side weir became lower or the length became longer, the water head values on the side weir decreased.

As mentioned above, generally, the surface profiles on the side weirs shown by previous studies also rose toward the downstream end of the side weir. However, the rate of the rise in pressurized flow conditions was larger than that in the open channel condition, and a high water head at the downstream end of the side weir has an effect on the water heads of the downstream pipe. The reason for this may be the strength of the lateral flow under pressurized flow conditions. This result shows the difference between open channel flow and pressurized flow conditions.

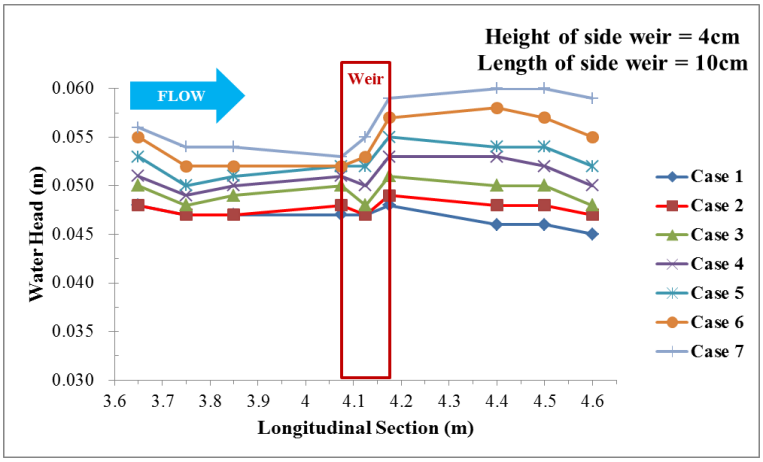

Figure 2.13 Surface profiles around the side weir (p = 4cm, L = 10cm)

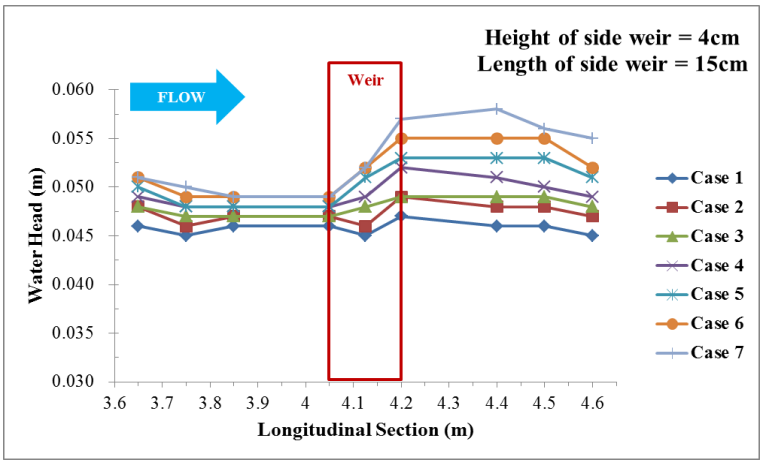

Figure 2.14 Surface profiles around the side weir (p = 4cm, L = 15cm)

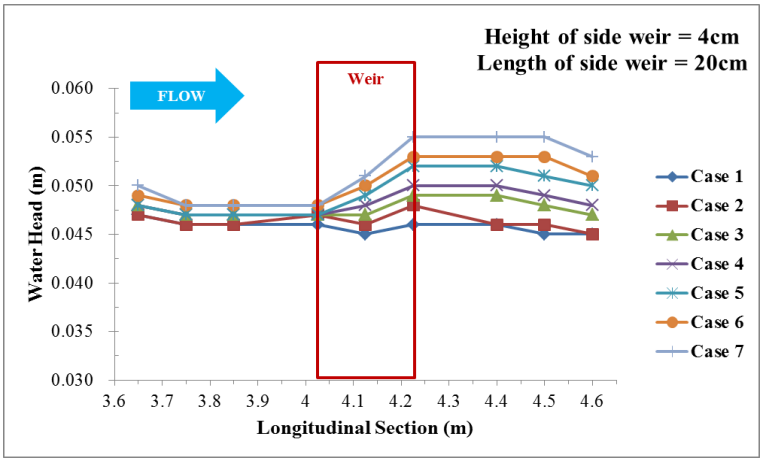

Figure 2.15 Surface profiles around the side weir (p = 4cm, L = 20cm)

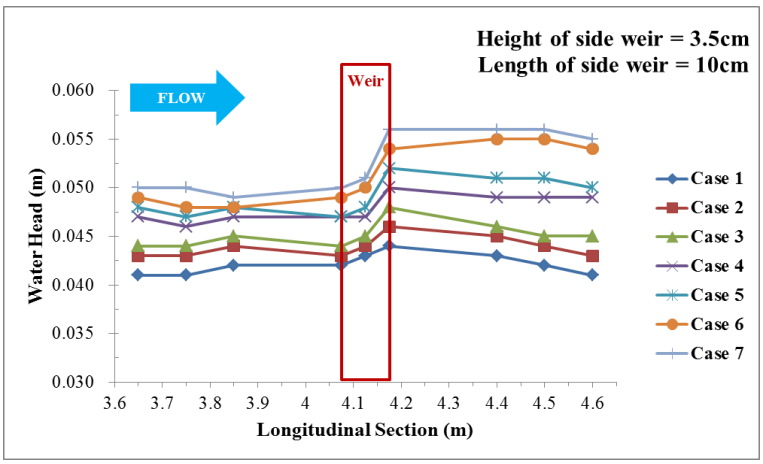

Figure 2.16 Surface profiles around the side weir (p = 3.5cm, L = 10cm)

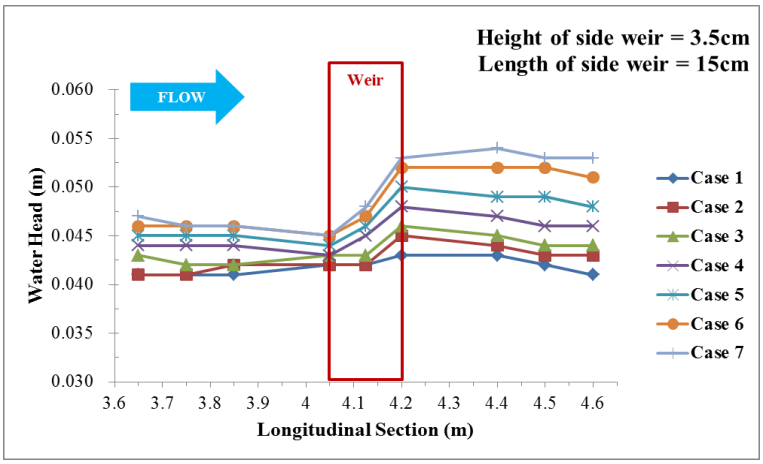

Figure 2.17 Surface profiles around the side weir (p = 3.5cm, L = 15cm)

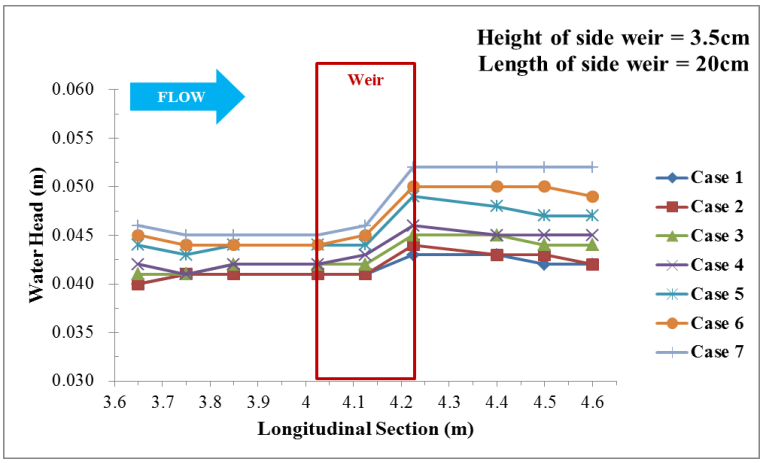

Figure 2.18 Surface profiles around the side weir (p = 3.5cm, L = 20cm)

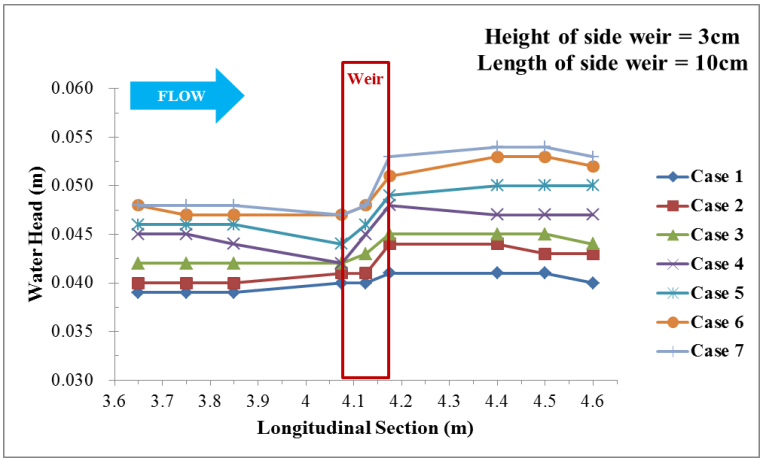

Figure 2.19 Surface profiles around the side weir (p = 3cm, L = 10cm)

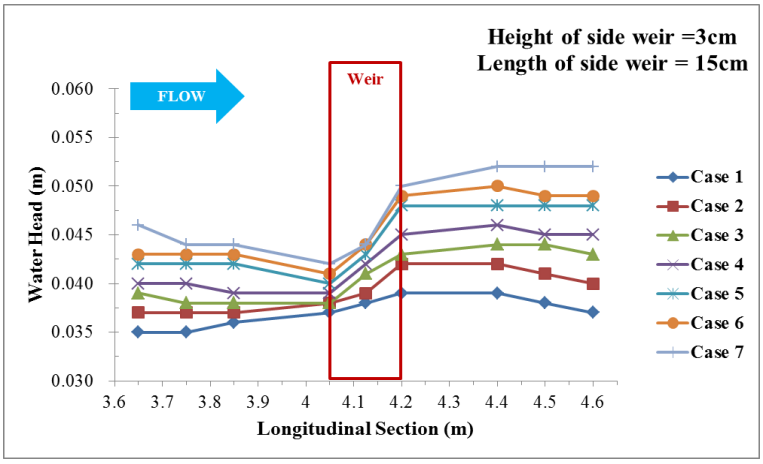

Figure 2.20 Surface profiles around the side weir (p = 3cm, L = 15cm)

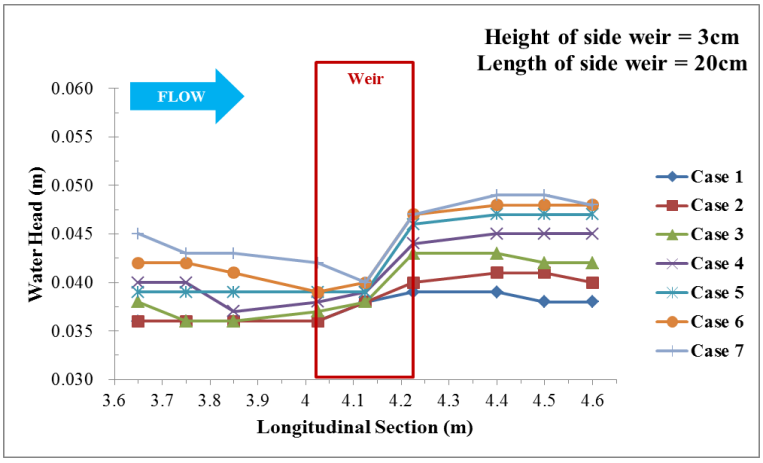

Figure 2.21 Surface profiles around the side weir (p = 3cm, L = 20cm)

2.5.2 Mean integral water head

In Figure 2.22, (a), (b), and (c) indicate the measuring points placed at the bottom of the pipe in the side weir section. The red dotted line represents the top position of the side weir. The blue portion was drawn to show the area where different water heads were observed by the piezometer tubes. The water head was obtained using the painted surface area divided by the weir's length. The black dotted line represents the mean of the water heads calculated by this method.

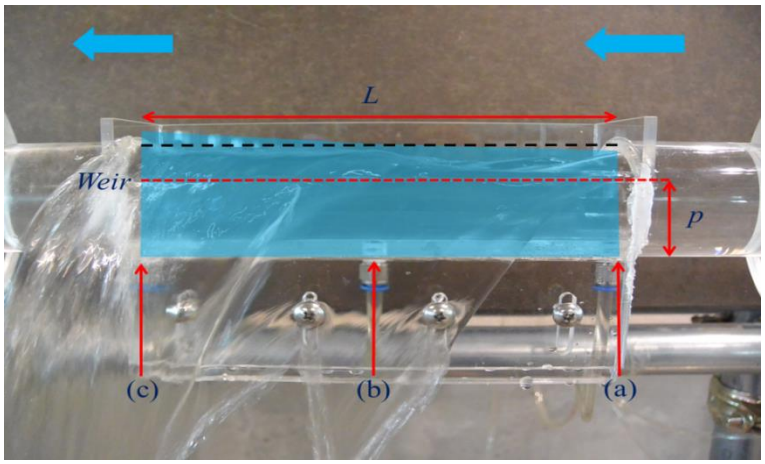

Figure 2.22 Photo of mean of water heads

2.5.3 Discharge coefficient

The discharge coefficient can be derived from De Marchi's equation, as shown in Equation (2.1):

$$C_d = \frac{\frac{3}{2} Q_{out}}{\sqrt{2g} L (h-p)^{1.5}} \quad (2.1)$$

This discharge coefficient depends on the hydraulic conditions including the weir length, weir height, and water head on the side weir and the overflow discharge. As the upstream discharge increases, the overflow rate also increases, in comparison with the results under the low-discharge conditions. The Table 2.6 shows the overflow discharge along each weir condition, which increases in accordance with the lower height and longer length of the side weir.

Table 2.6 Experimental results (overflow discharge)

Weir length(cm)	Weir height(cm)	Case 1	Case 2	Case 3	Case 4	Case 5	Case 6	Case 7
Experiment-Overflow discharge(ℓ/s)								
10	3	0.132	0.194	0.238	0.304	0.344	0.418	0.456
	3.5	0.094	0.154	0.204	0.268	0.320	0.380	0.424
	4	0.063	0.113	0.168	0.233	0.279	0.324	0.366
15	3	0.136	0.224	0.264	0.320	0.384	0.426	0.504
	3.5	0.112	0.168	0.236	0.290	0.350	0.404	0.466
	4	0.065	0.122	0.179	0.246	0.304	0.377	0.430
20	3	0.164	0.224	0.284	0.324	0.394	0.448	0.514
	3.5	0.118	0.174	0.240	0.300	0.360	0.414	0.480
	4	0.069	0.130	0.199	0.253	0.330	0.407	0.468

The seven discharge coefficients were derived using the above hydraulic conditions for each different weir condition. The water head was the most important parameter from which to derive the discharge coefficient in this study. Some previous studies used the water head at the upstream end of the side weir to calculate the discharge coefficient.

However, as I have already mentioned above, there is excessively larger variation in the water heads on the side weir, compared with those of previous studies on the characteristics of pressurized flow. From this perspective, the mean of the integral water heads along the entire side weir length was adopted, which was derived from the side weir's length and the water head integrated along the side weir.

Uyumaz et al. (1985) also reported that the water head is not constant on a side weir. The mean of the upstream and downstream water heads on the side weir did not produce satisfactory

solutions. Calculating the average of several intermediate heads provided more satisfactory results.

In this study, the coefficient value increased gradually when the water head at the upstream end of the side weir was used. In contrast, the discharge coefficient remained almost constant when the mean of the integral water heads was adopted, instead of the water head at the upstream end of the side weir. In particular, these coefficient values became close to the constant value, even though the upstream discharge increased, implying the applicability of a constant coefficient value. Figures 2.23 ~ 2.31 show the discharge coefficient distribution along the different water head on the side weir.

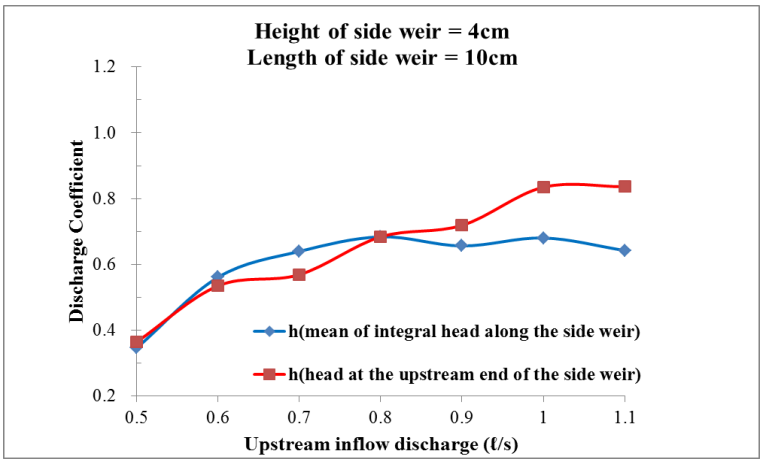

Figure 2.23 Discharge coefficient distribution (p = 4cm, L = 10cm)

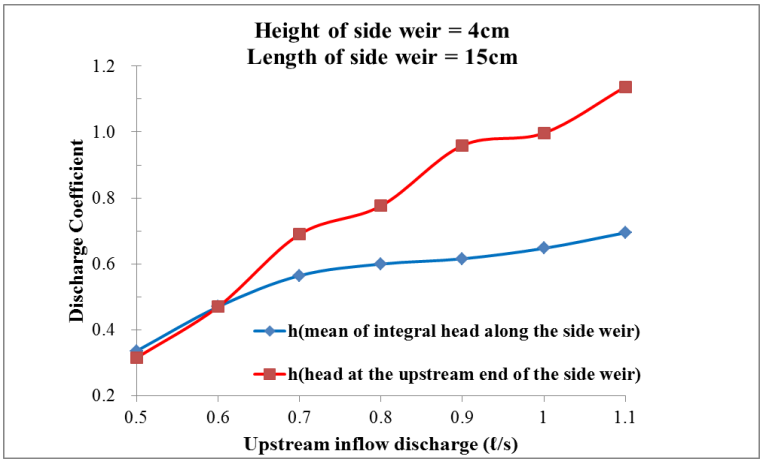

Figure 2.24 Discharge coefficient distribution (p = 4cm, L = 15cm)

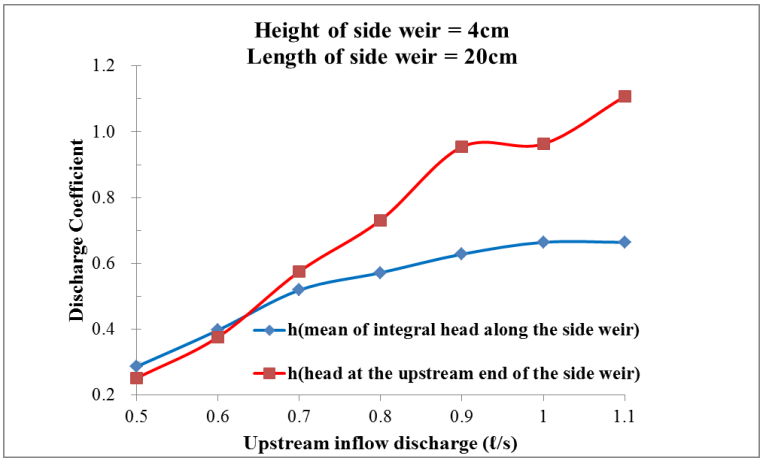

Figure 2.25 Discharge coefficient distribution (p = 4cm, L = 20cm)

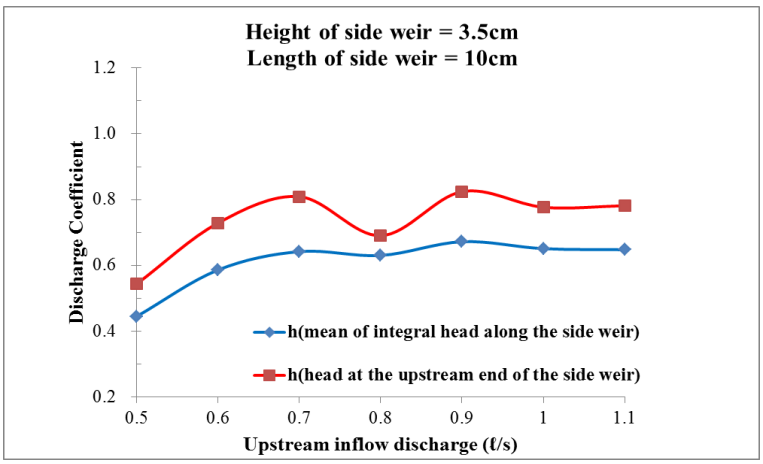

Figure 2.26 Discharge coefficient distribution (p = 3.5cm, L = 10cm)

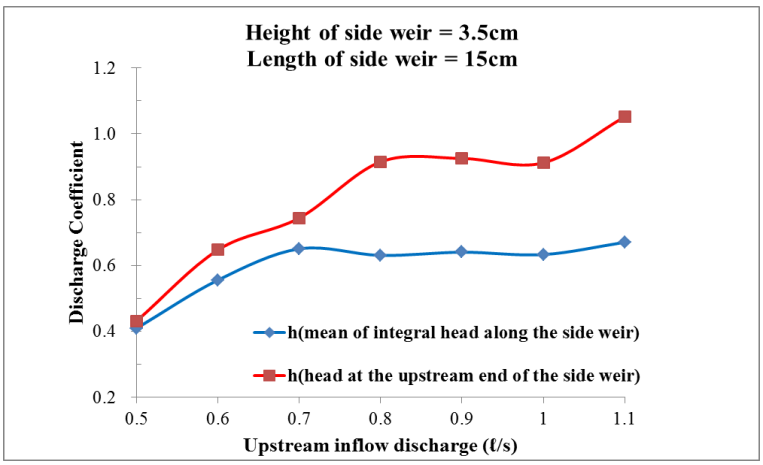

Figure 2.27 Discharge coefficient distribution (p = 3.5cm, L = 15cm)

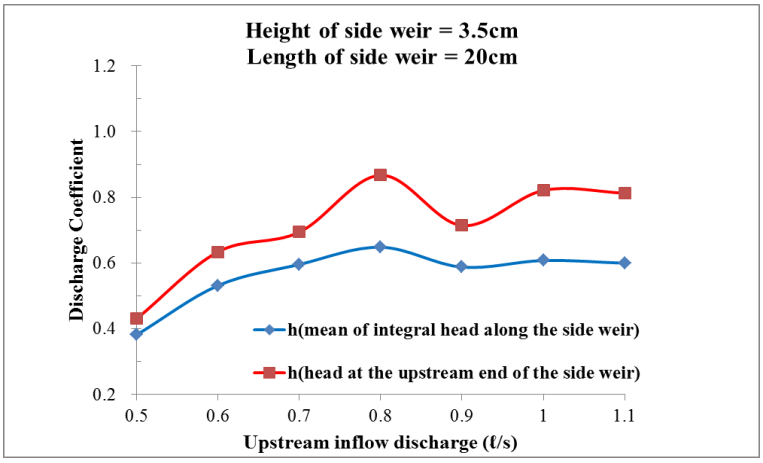

Figure 2.28 Discharge coefficient distribution (p = 3.5cm, L = 20cm)

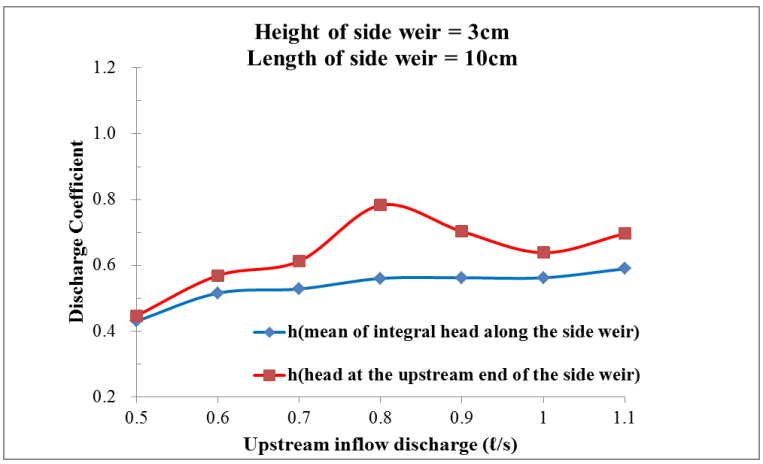

Figure 2.29 Discharge coefficient distribution (p = 3cm, L = 10cm)

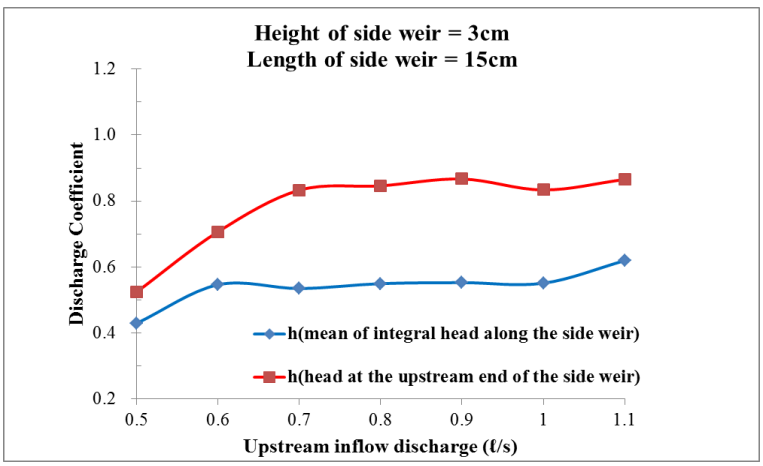

Figure 2.30 Discharge coefficient distribution (p = 3cm, L = 15cm)

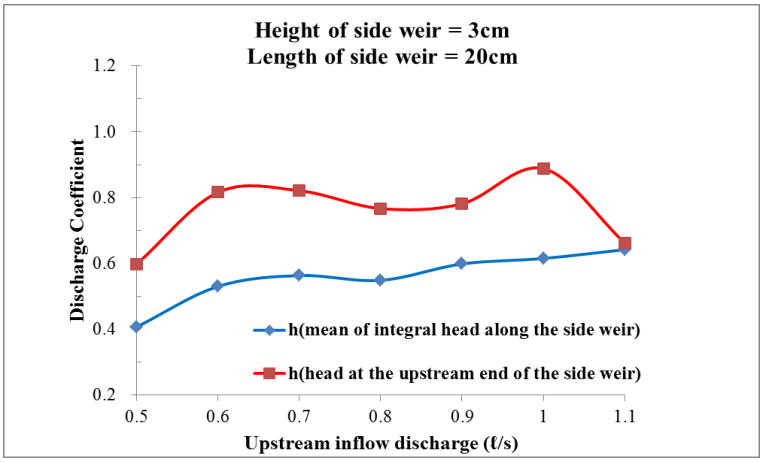

Figure 2.31 Discharge coefficient distribution (p = 3cm, L = 20cm)

2.6 Summary

The present study was investigated to determine the discharge coefficient for pressurized flow in a circular channel with different side weir condition. Several studies have obtained discharge coefficient equations for rectangular side weirs based on experimental results. De Marchi's equation is usually employed in cases of open channel flow, and many researchers have suggested its discharge coefficient. However, no study has verified the suitability of De Marchi's equation in the pressurized flow condition.

The surface profiles on the side weirs shown by previous studies also rose toward the downstream end of the side weir. As the upstream discharge increased, the hydraulic gradient became steeper, compared with the results of the smaller discharge cases. The variation of the water heads at the upstream end of the side weir was small, compared with the water head at the downstream end of the side weir for all of the cases. Due to this, if the water head at the upstream end of the side weir was used to calculate the discharge coefficient, the values increased in the greater discharge cases, with unstable values. The reason for these phenomena may be the strength of the lateral flow under pressurized flow conditions. This result shows the difference between open channel flow and pressurized flow conditions.

This discharge coefficient depends on the hydraulic conditions including the weir length, weir height, and water head on the side weir and the overflow discharge. As the upstream discharge increases, the overflow rate also increases, in comparison with the results under the low-discharge conditions. The seven discharge coefficients were derived for each different weir

condition. The water head was the most important parameter from which to derive the discharge coefficient in this study. Some previous studies used the water head at the upstream end of the side weir to calculate the discharge coefficient. However, there is excessively larger variation in the water heads on the side weir, compared with those of previous studies on the characteristics of pressurized flow. From this perspective, the mean of the integral water heads along the entire side weir length was adopted, which was derived from the side weir's length and the water head integrated along the side weir.

In fact, in application to actual estimation of overflow discharge, the constant coefficient value is easy to handle. Therefore, the applicability of the constant value derived from these experiments will be investigated by using a numerical model.

Chapter 3

Numerical modeling to reproduce the experimental results

3.1 Introduction

The experimental results, including the discharge coefficient calculated by mean of the water heads in pressurized flow conditions, were discussed in the previous chapter. A model is developed here based on the results of the experiments. In this chapter, under the assumption that De Marchi's equation is applicable to the pressurized flow conditions, a numerical model is used to validate the experimental results, like the discharge coefficients obtained by the experiment, so that effective conclusions can be drawn regarding the suitability of De Marchi's equation for these cases.

Even though two flow patterns in sewer pipes may occur in the actual field, like open channel and a fully surcharged flow condition, it is difficult to treat both hydraulic conditions using the previous governing equations, as follows (3.1 ~ 3.4):

Open flow

$$\frac{\partial h}{\partial t} + v\frac{\partial h}{\partial x} + \frac{A}{B}\frac{\partial v}{\partial t} = 0 \tag{3.1}$$

$$g\frac{\partial h}{\partial x} + \frac{\partial v}{\partial t} + v\frac{\partial v}{\partial tx} = g\left(S_0 - S_f\right) \tag{3.2}$$

Fully surcharged flow

$$\frac{\partial H}{\partial t} + v\frac{\partial H}{\partial x} + \frac{a^2}{g}\frac{\partial v}{\partial t} = 0 \tag{3.3}$$

$$\mathrm{g}\frac{\partial h}{\partial x} + \frac{\partial v}{\partial t} + v\frac{\partial v}{\partial tx} = g\left(S_0 - S_f\right) \tag{3.4}$$

where v is the velocity in x direction, h is the water depth, S_o is the slope of the pipe, S_f is the friction slope of the pipe, A is the cross-section area, B is the water surface width, a is the pressure propagation velocity, and H is the piezometric head.

The fundamental problem was that no equations have yet been developed that adequately represent the transition from free surface flow to pressurized flow, which exists in pipes that are completely full. It is accepted practice to circumvent this by applying the so-called Preissmann slot, as shown in Figure 3.1. The idea of this piezometric slot originated from Preissmann (1961) and was further developed by Cunge and Wagner (1964) for practical application. Chaudhry (1979) developed a hypothetical slot model, which considers a sewer pipe with a narrow slot on its ceiling. The pipes that are usually free surfaces and only rarely surcharged are modelled using the Preissmann slot approximation. In fact, the cross-sectional geometry of a circular pipe was slightly changed in order to avoid the occurrence of a transition between free surface flow and pressurized flow by adding a slot with a small width on the top of the pipe. In this manner, the water level directly flows from the mass-balance equation. The width of the slot is so narrow that its volume is negligible. Consequently, the open channel flow dynamic equation can be applied to the slot-modified surcharge flow. However, many pipes are surcharged at any given time, the solution becomes very expensive because the flow equations for all of the surcharged pipes (often for non-surcharged pipes as well) must be solved simultaneously (Yen, 1980).

The width of the slot is defined theoretically by setting the celerity of a disturbance at the free surface in the slot equal to the celerity of a disturbance in the full-pressurized case. The celerity of a surface wave is defined as follows (3.5):

$$c = u \pm \sqrt{gH_h} \tag{3.5}$$

where H_h is the hydraulic depth.

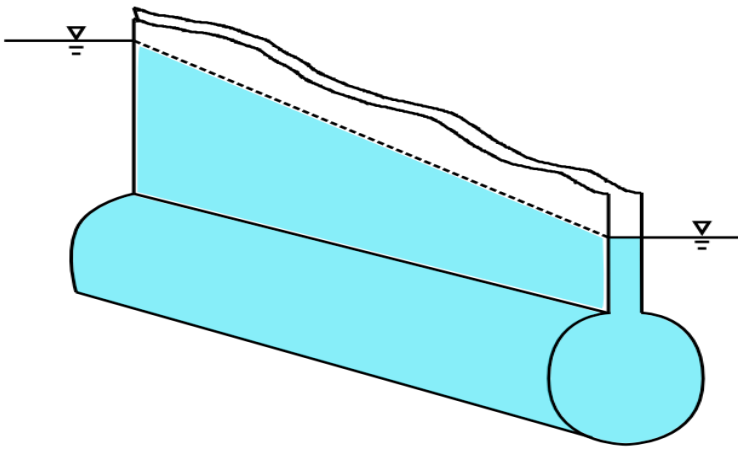

Figure 3.1 Concept of a slot model

3.2 One-dimensional sewer model

3.2.1 Governing equation

The storm water in the sewer pipe is dynamically calculated based on the following 1D continuity (3.6) and momentum (3.7) equations:

$$\frac{\partial A}{\partial t} + \frac{\partial Q}{\partial x} = q_{out} \tag{3.6}$$

$$\frac{\partial Q}{\partial t} + \frac{\partial (uQ)}{\partial x} = -gA\frac{\partial H}{\partial x} - \frac{gn^2|Q|Q}{R^{\frac{4}{3}}A} \tag{3.7}$$

where A is the cross-sectional area of flow, Q is the discharge, q_{out} is the overflow discharge per unit length over the side weir, u is the flow velocity, n is the Manning's roughness coefficient, R is the hydraulic radius, H is the piezometric head ($H = z + h$), z is the bottom elevation of the pipe, and h is the water depth in the pipe measured from the bottom, which is calculated as follows (3.8):

$$h = \begin{cases} f(A) & : (A \le A_p) \\ B` + \frac{A - A_p}{B_s} & : (A > A_p) \end{cases} \tag{3.8}$$

where f is a function that expresses a relationship between the flow cross-section area and water depth in a circular pipe, the case of $A \le A_p$ is the open-channel flow condition and $A > A_p$ is the pressurized flow condition, $B`$ is the height of the pipe ceiling, A_p is the cross-sectional area of the pipe, and B_s is the slot width, which is calculated as follows (3.9):

$$B_s = \frac{gA}{a^2} \tag{3.9}$$

where a is the pressure propagation velocity for the pipe and 5 m/s was used. Figure 3.2 shows the expressions for the area, top width, depth, and θ of a circular channel, which were obtained as follows (3.10), (3.11), (3.12), (3.13):

$$A_p = \frac{D^2}{8}(\theta - sin\,\theta) \tag{3.10}$$

$$W = D\ sin\frac{\theta}{2} \tag{3.11}$$

$$h = \frac{D}{2}\left(1 - \cos\frac{\theta}{2}\right) \tag{3.12}$$

$$\text{and } \theta\ = 2\ cos^{-1}(1 - \frac{2h}{D}) \tag{3.13}$$

where *D* is the pipe diameter and θ is the central angle of the wetted radius.

The types of flow conditions found in conventional circular pipes and pipe-arch culverts are illustrated in (a). The velocity and discharge obtained commonly respond to any of the depths using hydraulic characteristic curves. The maximum rate of discharge in such section occurs at slightly less than full depth. The maximum discharge will pass through such a section when the flow depth becomes 0.95D, and the maximum velocity was found to occur at 0.8D. Solid lines 1 and 2 of (b) in Figure 3.2 indicate the top width position in the partially full pipe flow condition.

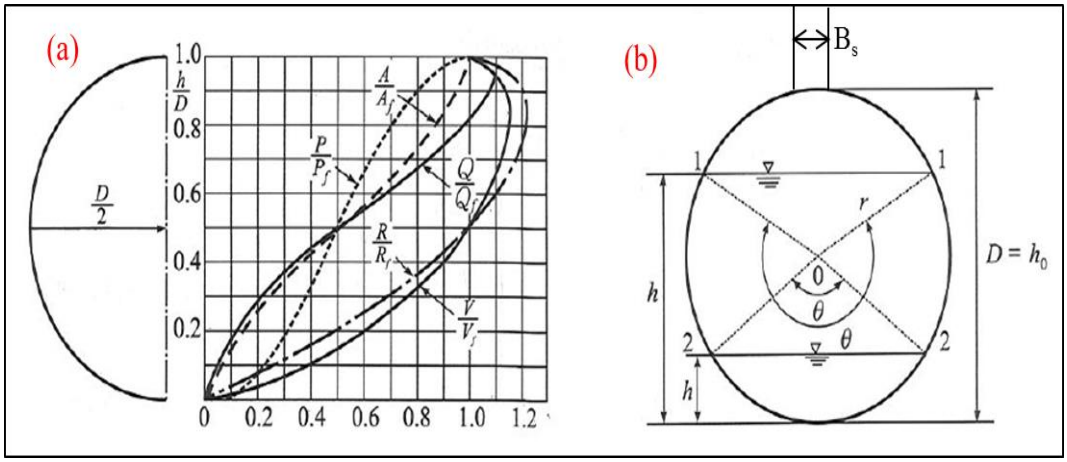

Figure 3.2 Hydraulic characteristic curves

3.2.2 Overflow equation

De Marchi's equation was adopted to calculate the overflow discharge in this model, which is as follows (3.14):

$$q_{out} = \frac{dQ_{out}}{dL} = \frac{2}{3}C_d\sqrt{2g}(h - p)^{1.5} \tag{3.14}$$

where q_{out} is the discharge per unit length of the side weir, Q_{out} is the overflow discharge, L is the distance along the side weir measured from the upstream end of the side weir, g is the acceleration of gravity, p is the height of the side weir, h is the flow depth at the section L, and C_d is the discharge coefficient of the side weir.

The discharge coefficient is influenced by the following parameters (3.15):

$$C_d = f(v, D, g, h, p, L, S \cdots) \tag{3.15}$$

where S is the slope of the main channel.

A rectangular mesh was used, and the mesh generated depends upon the length of the side weir used in the model. That is to say, the weir length was reflected by the grid size, and a finite different method was adopted.

3.2.3 Discretization methods

Equations (3.16) and (3.17) show the discretization of the one-dimensional continuity equation and the momentum equation for a sewer pipe. Figure 3.3 shows the arrangements of each parameter, and Figure 3.4 shows the calculation process using the leap-frog method.

Continuity equation

$$\frac{A_j^{n+3} - A_j^{n+1}}{2\Delta t} + \frac{Q_{j+1/2}^{n+2} - Q_{j-1/2}^{n+2}}{\Delta x_j} = {q_{out}}_j^{n+2} \tag{3.16}$$

Momentum equation

$$\frac{Q_{j-1/2}^{n+2} - Q_{j-1/2}^{n}}{2} + \frac{\left(u_j^* \frac{Q_{j-1/2}^* + Q_{j+1/2}^*}{2} + \left|u_j^*\right| \frac{Q_{j-1/2}^* + Q_{j+1/2}^*}{2}\right)}{\Delta x_{j-1/2}} + \frac{\left(u_{j-1}^* \frac{Q_{j-3/2}^* + Q_{j-1/2}^*}{2} + \left|u_{j-1}^*\right| \frac{Q_{j-3/2}^* + Q_{j-1/2}^*}{2}\right)}{\Delta x_{j-1/2}}$$

$$= -g \frac{A_j^{n+1} - A_{j-1}^{n+1}}{2} \cdot \frac{H_j - H_{j-1}}{\Delta x_{j-1/2}} - gn^2 \frac{\frac{Q_{j-1/2}^{n+2} + Q_{j-1/2}^{n}}{2} \left|Q_{j-1/2}^{n}\right|}{\left(\frac{R_j^{n+1} + R_{j-1}^{n+1}}{2}\right) \frac{A_j^{n+1} + A_{j-1}^{n+1}}{2}} \tag{3.17}$$

Treatment of convection term

To stabilize the calculation here, non-liner convection terms were calculated using the average values of $t = (n-2)\Delta t$ and $t = n\Delta t$, as suggested by Inoue (1986).

$$Q^*_{j-1/2} = \frac{Q^{n-2}_{j-1/2} + Q^n_{j-1/2}}{2} \tag{3.18}$$

$$u^*_j = \frac{u^*_{j+1/2} + u^*_{j-1/2}}{2} \tag{3.19}$$

$$u^*_{j-1} = \frac{u^*_{j-1/2} + u^*_{j-3/2}}{2} \tag{3.20}$$

$$u^*_{j-1/2} = \frac{Q^*_{j-1/2}}{\frac{A_j + A_{j-1}}{2}} \tag{3.21}$$

$$u^*_{j+1/2} = \frac{Q^*_{j+1/2}}{\frac{A_j + A_{j+1}}{2}} \tag{3.22}$$

$$u^*_{j-3/2} = \frac{Q^*_{j-3/2}}{\frac{A_{j-1} + A_{j-2}}{2}} \tag{3.23}$$

where, u^*_j and u^*_{j-1} are calculated by equations (3.18), (3.21), (3.22), (3.23) as follows (3.24), (3.25):

$$u^*_j = \frac{Q^*_{j+1/2}}{A_{j-1} + A_j} + \frac{Q^*_{j-1/2}}{A_j + A_{j+1}} \tag{3.24}$$

$$u^*_{j-1} = \frac{Q^*_{j-3/2}}{A_{j-2} + A_{j-1}} + \frac{Q^*_{j-1/2}}{A_{j-1} + A_j} \tag{3.25}$$

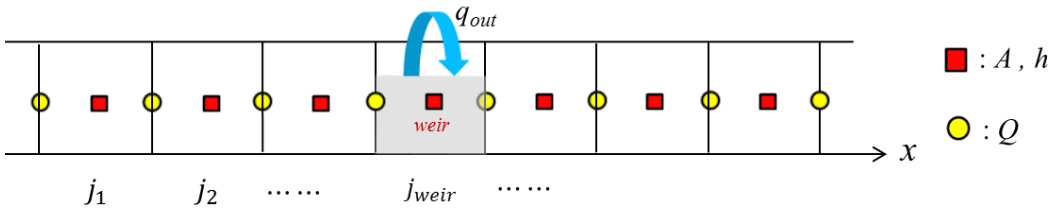

Figure 3.3 Arrangements of each parameter

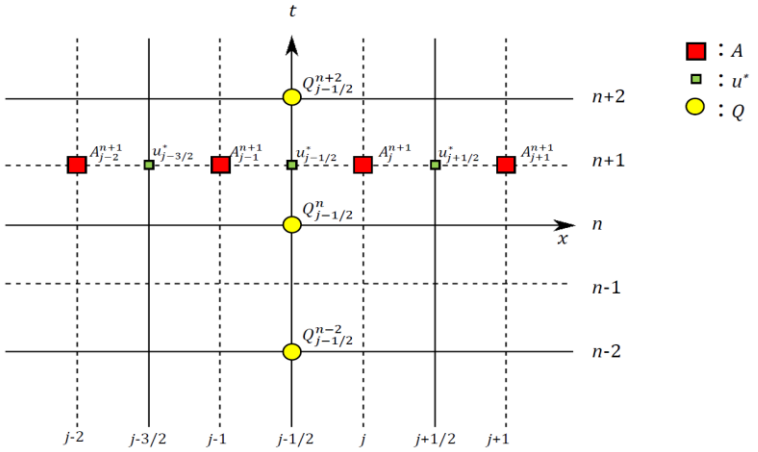

Figure 3.4 Calculation process by leap-frog method

3.2.4 Treatment of cut-edge section in pipe

When performing a flow analysis at a discontinuous section with an adjacent grid, the complete overflow (3.26) and waterfall equations (3.27) are used to calculate the discharge, instead of the governing equation. Figure 3.5 shows a treatment of a cut-edge section in pipe.

Complete overflow case

If the water elevation in the grid at the lower-bottom elevation is higher than the other bottom elevation of the adjacent gird, discharge (Q) is calculated using the difference in water elevation (H_{ls}) and the other bottom elevation (Z_{ls}), as follows (3.26):

$$Q = \mu_1 D h_{ls} \sqrt{2 g h_{ls}} \tag{3.26}$$

where Q is the discharge, D is the pipe diameter, H_{ls} is the water elevation on the pipe grid, Z_{ls} is the bottom elevation of the adjacent grid, h_{ls} is the water depth (H_{ls} – Z_{ls}), and μ_1 is the discharge coefficient (0.35 was used).

Waterfall case

If the water level in the grid at the lower-bottom elevation is lower than the other bottom elevation of the adjacent gird, discharge (Q) is calculated using the water depth (h_{hs}) in the grid of the high-bottom elevation, as follows (3.27):

$$Q = \mu_2 D h_{hs} \sqrt{2 g h_{hs}} \tag{3.27}$$

where Q is the discharge, h_{hs} is the water depth in the grid at high-bottom elevation, and μ_2 is the discharge coefficient (0.544 was used).

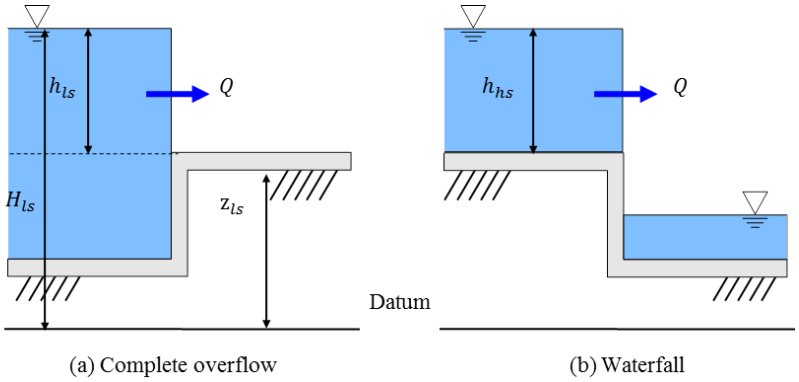

Figure 3.5 Treatment of cut edge section

3.2.5 Calibration of the roughness coefficient

To determine a suitable roughness coefficient, a simple calibration was carried out using the same experimental flume. The upstream supply discharge used to form the pressurized flow condition was 0.3 ~ 0.6 liters. Then, the water heads along the entire pipe were compared using experimental and simulated results. As a result, 0.013 was found to be a suitable roughness coefficient for this experimental flume, which this value was used in this study.

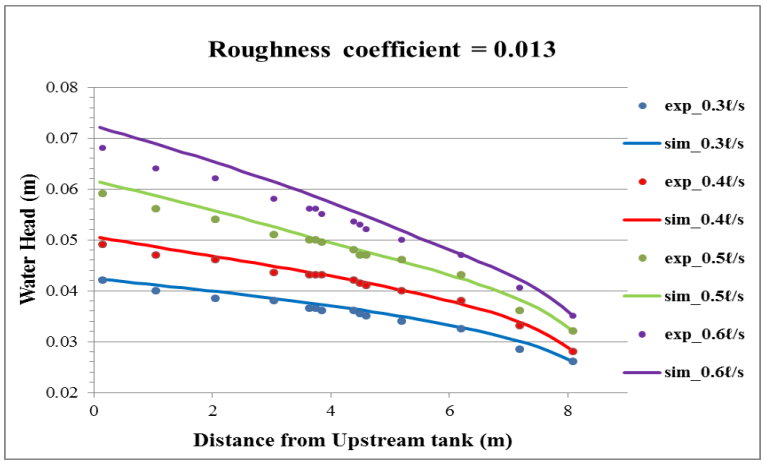

Figure 3.6 Suitable roughness coefficient

3.3 Model verification

Under the assumption that De Marchi's equation is applicable to the pressurized flow condition, the numerical simulation was carried out to verify the suitability of the discharge

coefficient obtained from the experiment. First, the discharge coefficients for each different weir condition were applied to numerical simulation. Secondly, each overflow discharge simulated was compared with the overflow discharge data obtained from the experiment, as shown in Figures 3.7 ~ 3.15. Consequently, the overflow discharge simulated could reproduce the experimental results, although there are still small differences as a whole, as shown in Figure 3.16. Even if all of the data became close to around line, small differences would occur under the lower side weir's height, caused by inevitable measuring errors in the sampling method, due to significant overtopping discharge compared with other cases. Judging the applicability of De Marchi's equation to pressurized flow, this reproduction implies the suitability of De Marchi's equation within my experimental conditions based on upstream discharge, Froude number, side weir length, and height.

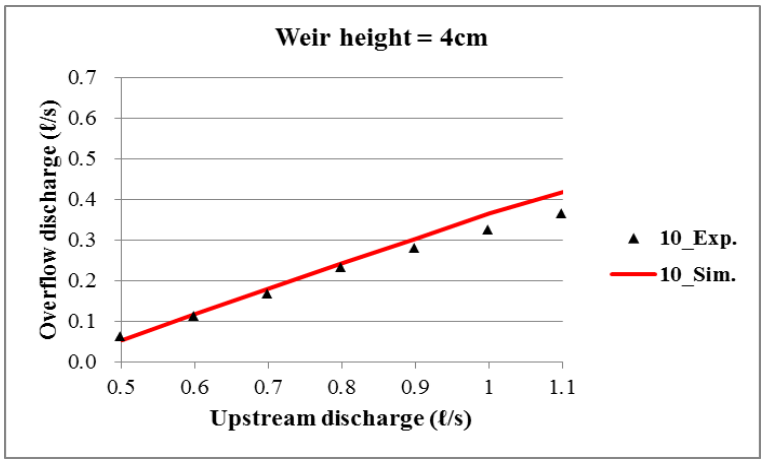

Figure 3.7 Comparisons between the experimental and simulated results (p = 4cm, L = 10cm)

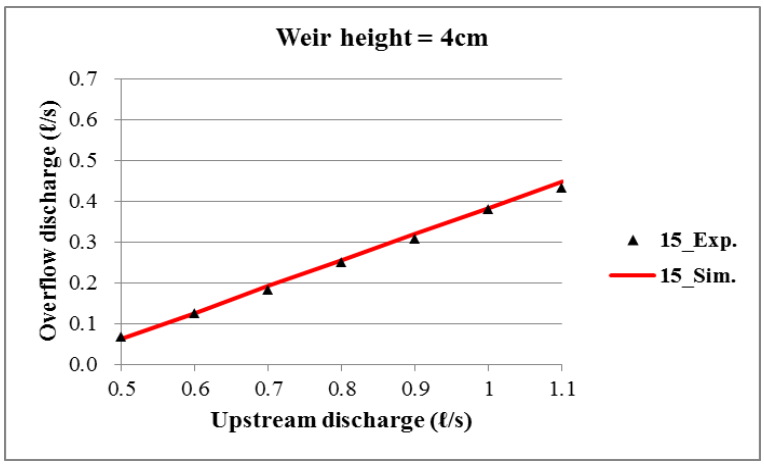

Figure 3.8 Comparisons between the experimental and simulated results (p = 4cm, L = 15cm)

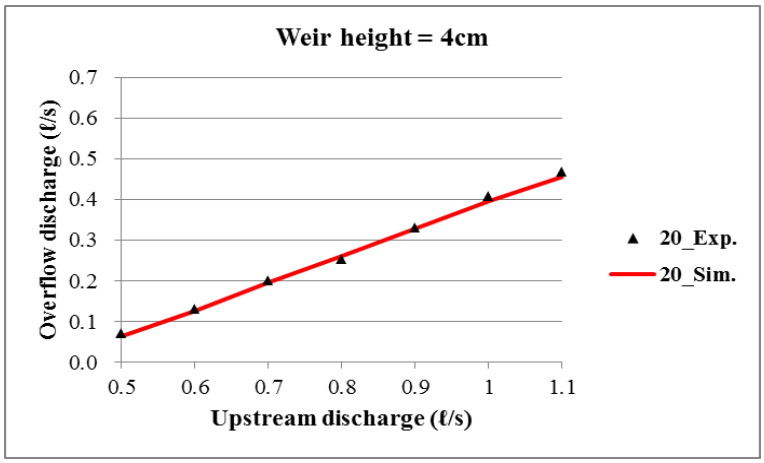

Figure 3.9 Comparisons between the experimental and simulated results (p = 4cm, L = 20cm)

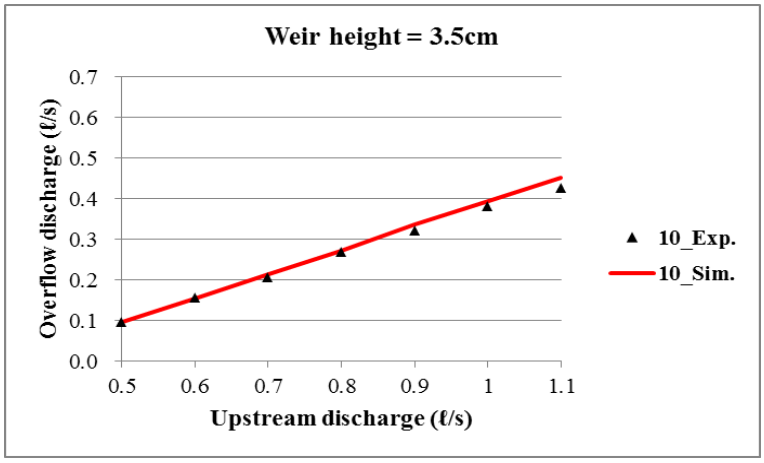

Figure 3.10 Comparisons between the experimental and simulated results (p = 3.5cm, L = 10cm)

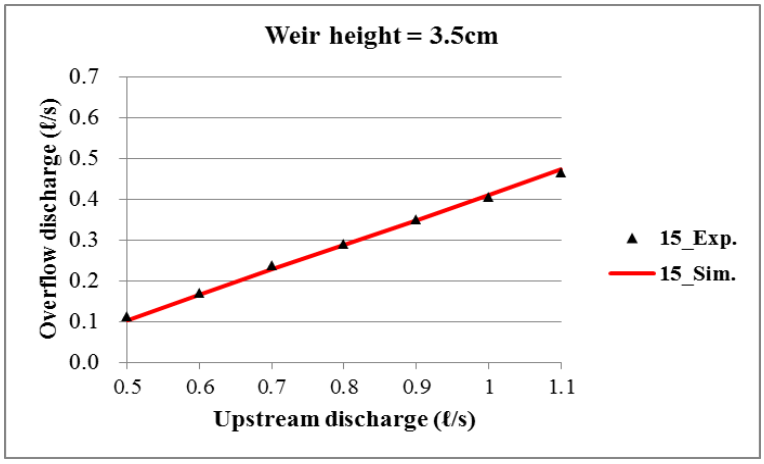

Figure 3.11 Comparisons between the experimental and simulated results (p = 3.5cm, L = 15cm)

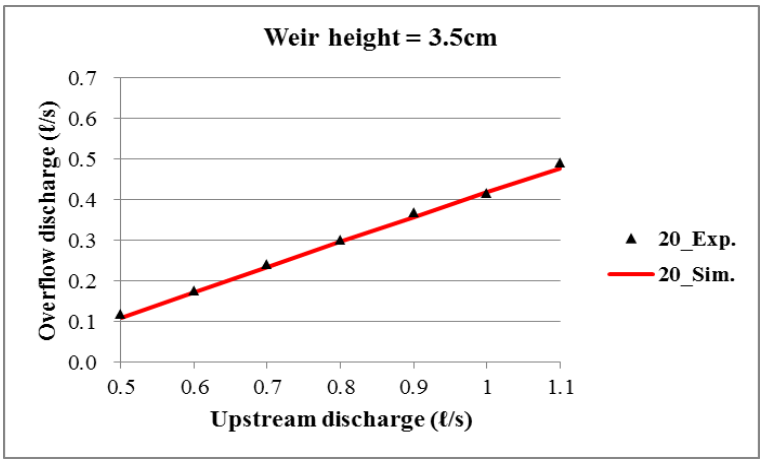

Figure 3.12 Comparisons between the experimental and simulated results (p = 3.5cm, L = 20cm)

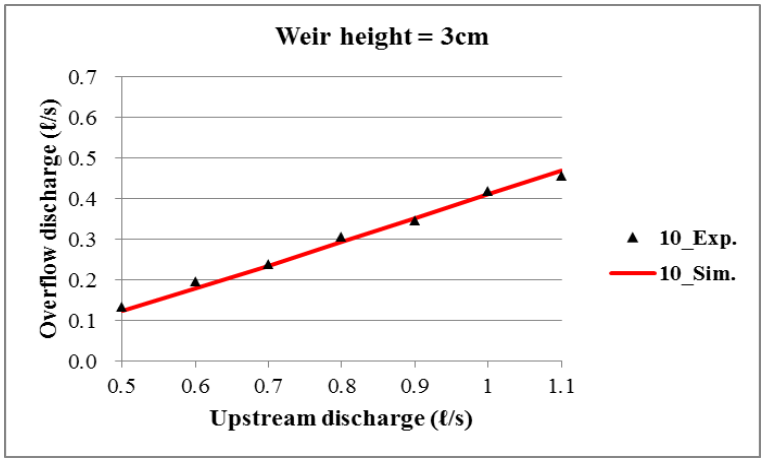

Figure 3.13 Comparisons between the experimental and simulated results (p = 3cm, L = 10cm)

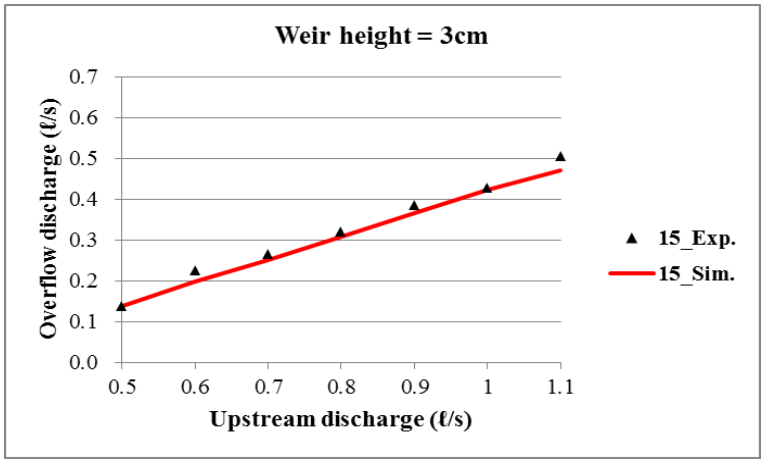

Figure 3.14 Comparisons between the experimental and simulated results (p = 3cm, L = 15cm)

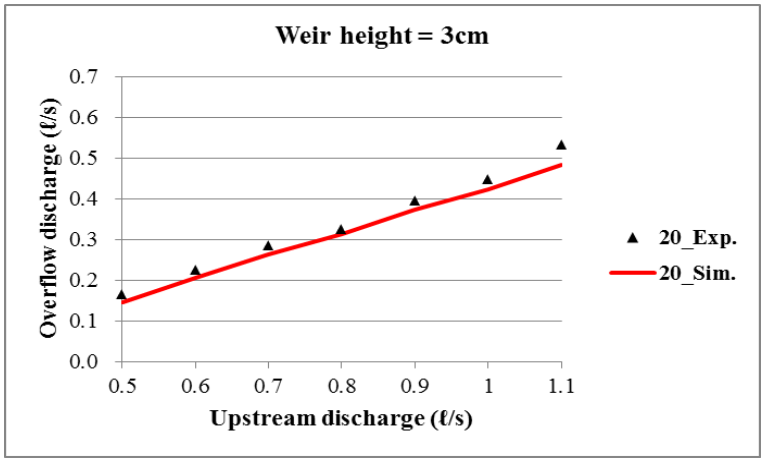

Figure 3.15 Comparisons between the experimental and simulated results (p = 3cm, L = 20cm)

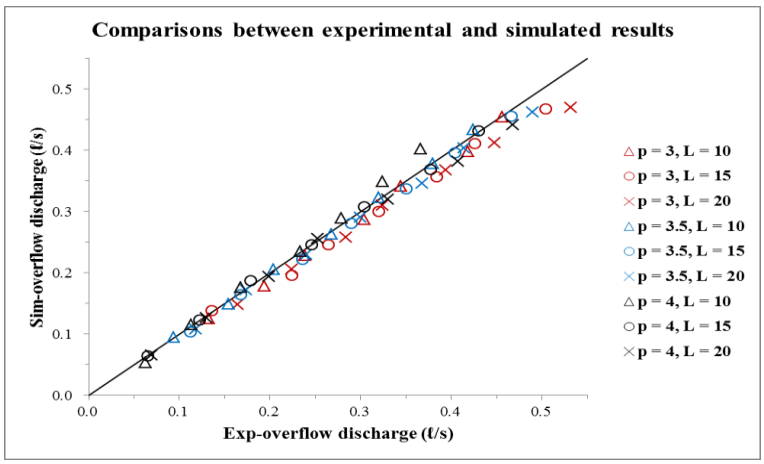

Figure 3.16 Comparisons between the experimental and simulated results

When applying the overflow discharge coefficient to the actual field, the constant coefficient value would be easy to handle. Therefore, a suitable coefficient was determined within the limited experimental results for each different side weir condition. As a result, suitable coefficients from 0.57 to 0.64 were suggested. Additionally, an empirical correlation to predict the discharge coefficient was developed for the ratio of weir height to length using the suitable coefficients. However, previous C_d empirical correlations in terms of the above function are not applicable to my study because each experiment was carried out along different experimental conditions, like open channel or differing weir scale. The applicability of h and F on the equation of C_d is limited due to the limited input discharge range in the experiment, compared with other research. Thus, in this study, I decided to use the function of p/L, since p and L are already fixed, as shown in Figure 3.17. The resulting correlation is given in Equation (3.23):

$$C_d = -0.2604\frac{p}{L} + 0.6736 \tag{3.23}$$

where the deterministic coefficient(R^2) is 0.9619.

Suitable values were selected within the range of the lowest and highest coefficients in the experimental results along the weir condition and were determined through the least square method, where the triangle is the lowest coefficient, the circle is the highest coefficient, and the cross is the most suitable coefficient, as shown in Figures 3.18 ~ 3.26.

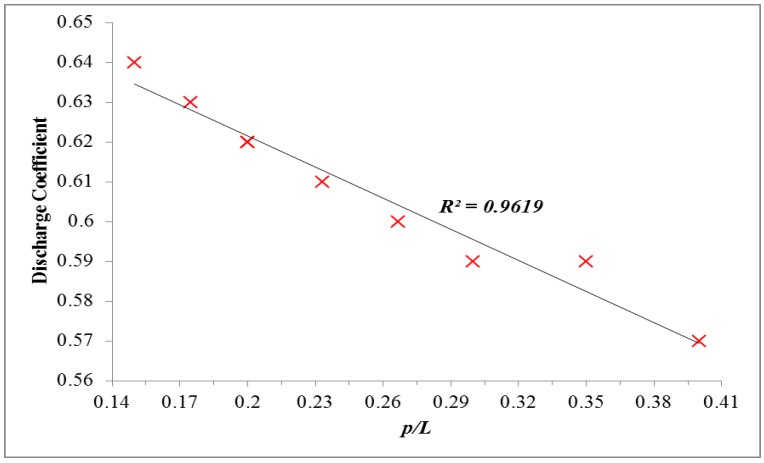

Figure 3.17 C_d empirical correlations using the function of *p/L*

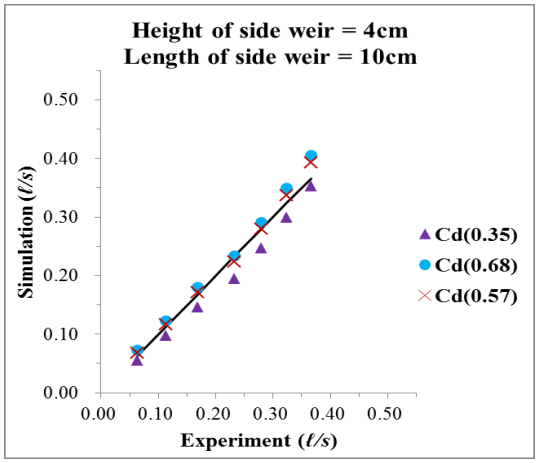

Figure 3.18 Suitable discharge coefficients (*p* = 4cm, *L* = 10cm)

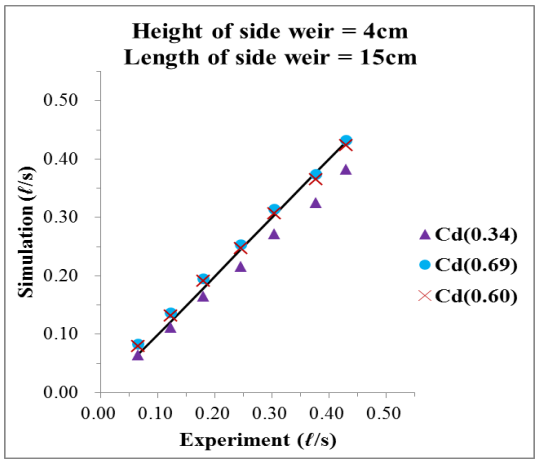

Figure 3.19 Suitable discharge coefficients (p = 4cm, L = 15cm)

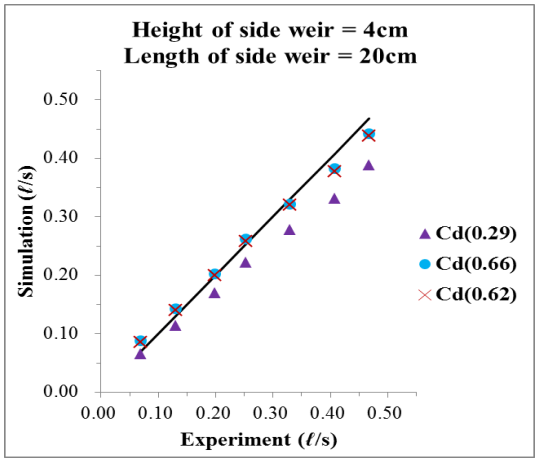

Figure 3.20 Suitable discharge coefficients (p = 4cm, L = 15cm)

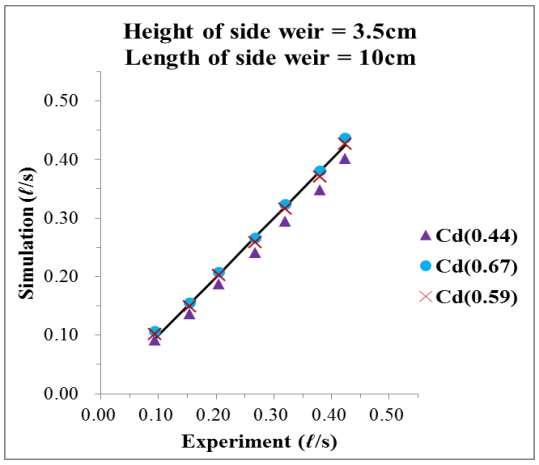

Figure 3.21 Suitable discharge coefficients (p = 3.5cm, L = 10cm)

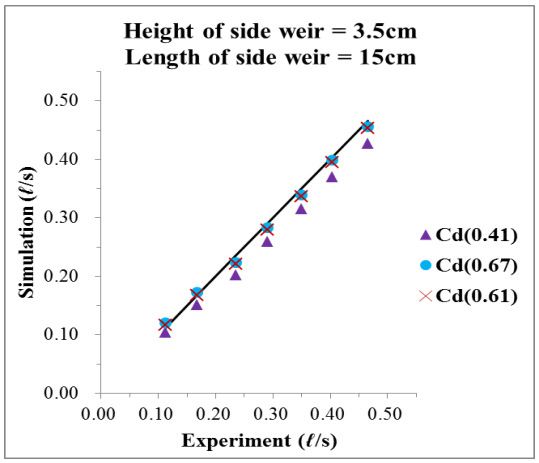

Figure 3.22 Suitable discharge coefficients (p = 3.5cm, L = 15cm)

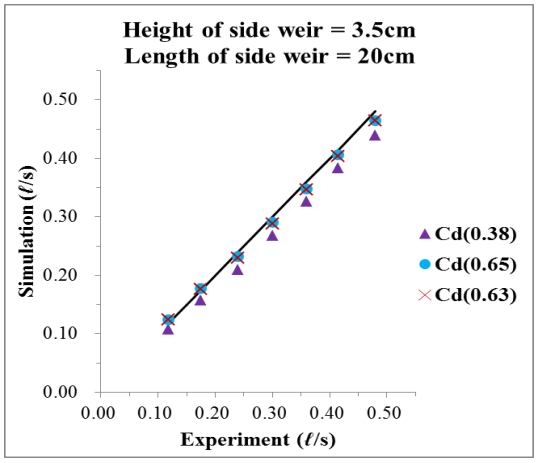

Figure 3.23 Suitable discharge coefficients (p = 3.5cm, L = 20cm)

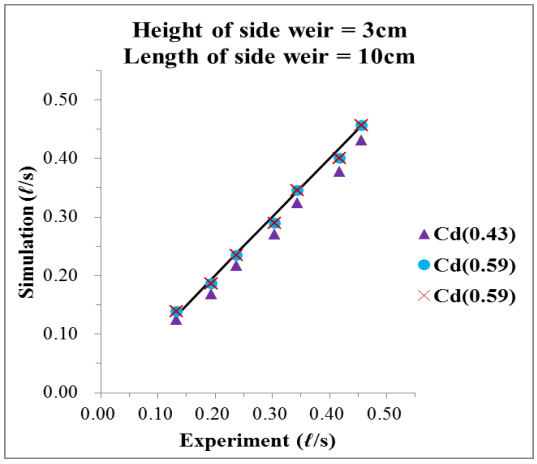

Figure 3.24 Suitable discharge coefficients (p = 3cm, L = 10cm)

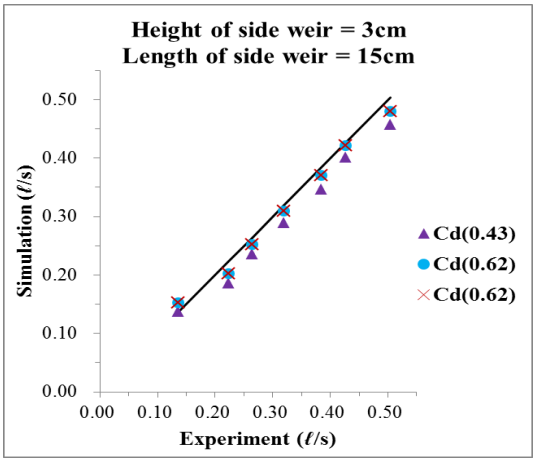

Figure 3.25 Suitable discharge coefficients (p = 3cm, L = 15cm)

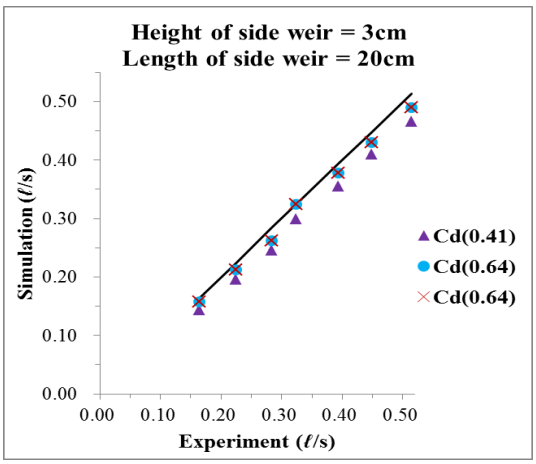

Figure 3.26 Suitable discharge coefficients (p = 3cm, L = 20cm)

3.4 Summary

This chapter, under the assumption that De Marchi's equation is applicable to the pressurized flow conditions, a numerical model is used to validate the experimental results, like the discharge coefficients obtained by the experiment, so that effective conclusions can be drawn regarding the suitability of De Marchi's equation for these cases.

In this study, the discharge coefficients for each different weir condition were applied to numerical simulation. And, each overflow discharge simulated was compared with the overflow discharge data obtained from the experiment. Consequently, the overflow discharge simulated could reproduce the experimental results, although there are still small differences as a whole.

When applying the overflow discharge coefficient to the actual field, the constant coefficient value would be easy to handle. Therefore, a suitable coefficient was determined within the limited experimental results for each different side weir condition. As a result, suitable coefficients from 0.57 to 0.64 were suggested. Additionally, an empirical correlation to predict the discharge coefficient was developed for the ratio of weir height to length using the suitable coefficients as follows:

$$C_d = -0.2604\frac{p}{L} + 0.6736$$

Next step will be to verify a numerical model under unsteady condition, which would enable to estimate the overflow discharge from sewerage to storage box and the mitigation effects of these storage boxes.

Chapter 4

Field application studies on the effect of an underground storage box

4.1 Introduction

One of the major components of storm water management is flow control, particularly in newly developed areas in which buildings, parking lots, roads, and other impervious surfaces have replaced open spaces. As imperviousness increases, there is less area available for infiltration, and the amount of runoff increases. This may cause streams to be more prone to flash floods. Storm water flowing into sewer pipes from residential land and roads, etc., are collected in the main sewer in increased the amounts as it goes downstream. It is drained into rivers and the sea directly or through pump station, as shown in Figure 4.1.

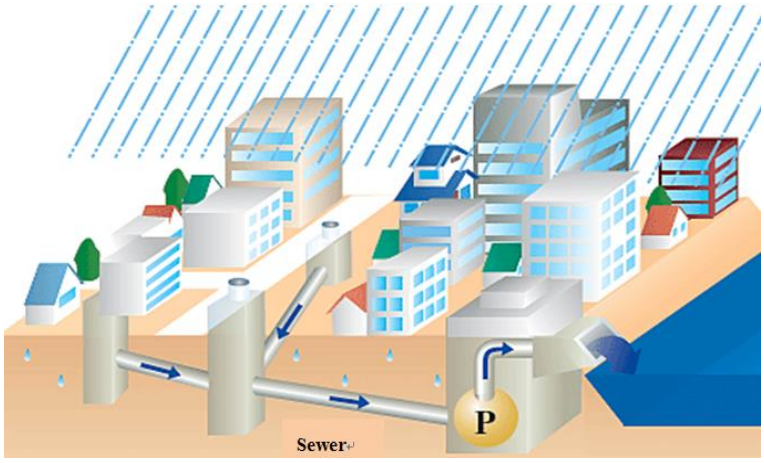

Figure 4.1 Drainage systems (Source: http://www.nikkeibp.co.jp/sj/2/special/10/index1.html)

Metropolises and central city areas such as Tokyo and Osaka in Japan are no exception, and flood damage has also occurred in underground spaces associated with such areas. This is highly dangerous and can be lead to catastrophe. The design criteria for sewerage is often 10-year probability rainfall, which corresponds to about 50mm/hr all over the country in Japan, but

the rainfall intensity has frequently exceeded this level in recent years. In order to promptly remove the storm water, drainage systems and pumping stations must be maintained to increase the efficiency of the sewerage treatment capacity. However, huge costs and amounts of time are required to conduct this maintenance. Therefore, underground storm water storage boxes are installed ideally in order to temporarily capture and store runoff in a large space. The storm water poured down onto the ground is reduced using various storage methods, which such as lower parking lots, the ground, tanks installed onto houses and buildings, and side weirs attached to the sewer system. Figure 4.2 ~ 4.5 show each of the storage systems. These systems provide peak runoff control, and the stored storm water can be drained back into the environment later, making these systems ideal for highly urbanized areas. Accordingly, those systems help to maintain pre-development runoff conditions at newly developed sites. However, storm water storage systems are not prevalent due to budgetary reasons and uncertain effects (Kawaike et al., 2015).

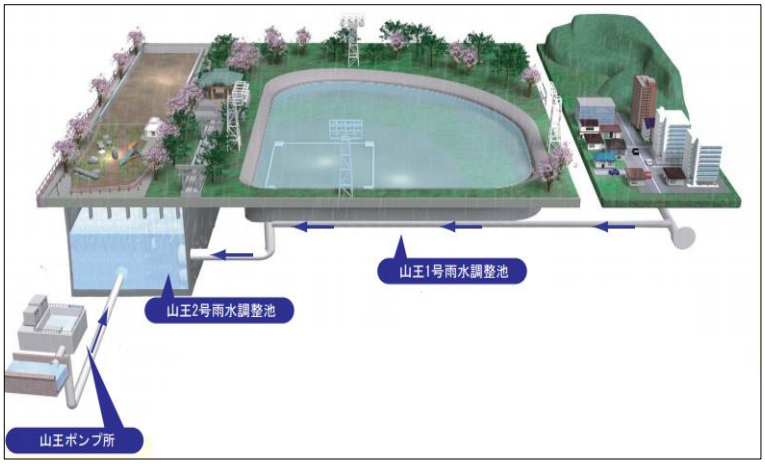

Figure 4.2 Storage system (Source: Neyagawa Water System Renovation Engineering Camp

Figure 4.3 Storage system (Source: http://www.kitchener.ca/en/livinginkitchener/Managing_Stormwater_for_your_business.asp)

Figure 4.4 Storage system (Source: http://www.raincell.co.za/products/products_raincell.asp)

Figure 4.5 Storage system (Source: http://www.city.saitama.jp/001/006/003/001/002/p001648.html)

I considered the side weir attached to the sewer for this research. The storm water drainage and diversion process of the side weir were presented using a numerical model, and the reduction ratio of inland flooding due to installing the storage box was verified.

4.2 Study area

Osaka has been conducting countermeasures against 60mm/hour rainfall, which is estimated as having 10-year rainfall frequency; however, inundation still occurs when heavy rain occurs. Since most of the storm water cannot be discharged naturally. 90% of the city area is prone to flooding by heavy rain, and storm water should be drained with pumping systems to

the river. In addition, most storm water cannot infiltrate the ground due to the high pavement ratio. Because of this, storm water can exceed the capacity of the sewer network systems, which may naturally cause inundation, as shown in Figure 4.6. Therefore, Osaka undertook the construction of major trunk sewers, such as the Yodo Grand Floodway, which is 22.5km long, has 145,000m^3 maximum storage capacity, and 105m^3/s maximum flow discharge, as well as the expansion of pumping facilities as drastic countermeasures against inland flooding. In addition, as much time is required to construct such large-scale underground storage facilities, Osaka has also pursued localized flood control facilities, as shown in Figure 4.7.

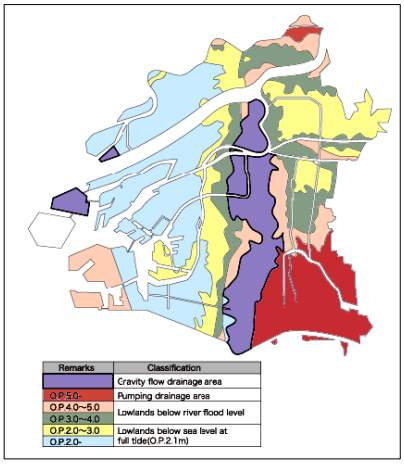

Figure 4.6 Configuration of Osaka City

(Source: http://nett21.gec.jp/GESAP/themes/themes4_5.html)

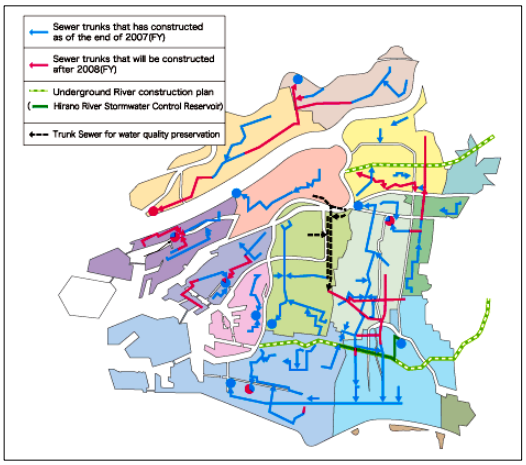

Figure 4.7 Location of major trunk sewers

(Source: http://nett21.gec.jp/GESAP/themes/themes4_5.html)

In this study, Nakahama District in Osaka was the target area, which is located in the eastern part of Osaka City, north of Neyagawa, west of Uehonmachi, surrounded by the Hirano River, as shown in Figure 4.8. This sewerage treatment district is 18.1km^2 long to the south, and the overall topography is inclined from west to east. This area received inundation damage during a heavy rainfall in a short time, in August 27, 2011. The maximum precipitation per 1 hour was 77.5mm for about 3 hours, which was the largest value on record.

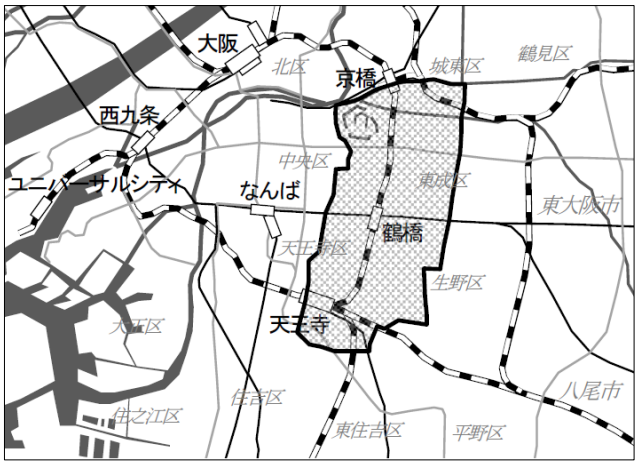

Figure 4.8 Target area (Source: Kawaike. K)

4.3 Integrated model for the ground surface and sewer network

Two-dimensional ground surface and one-dimensional sewer network models (Kawaike et al., 2002) were used to reproduce the inland flood and storm water drainage process, in an integrated flood analysis model developed by Lee et al. (2014).

They obtained sewerage system data of 4,445 sewer pipes, 4,317 manholes, and four pumping stations in total. The data for each sewer pipe included x and y coordinates, upstream and downstream connection data, the manhole shape, diameter, size, elevation, and slope. Similarly, each manhole data entry includes x and y coordinates, bottom elevation, bottom area, and connected pipe data. Therefore, it is possible to arrange all of the pipes and manholes with a pumping station. However, additional work is needed to trace all of the pipes and manholes to clarify the connection information because of data uncertainties. As a result of data sorting, Lee et al. (2014) rearranged 3,026 pipes and 2,903 manholes. The sewer pipe diameter ranged from 8.5m to 0.3m. Figure 4.9 shows the sorted sewer pipe data. A red circle indicates a pumping station, and a blue line is a sewer pipe, respectively.

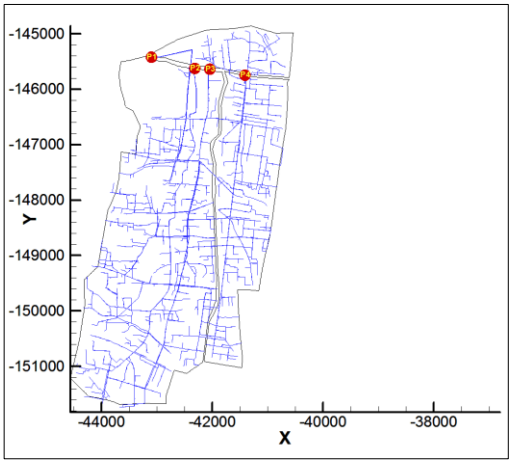

Figure 4.9 Pumping station and sewer network

The ground was divided by a non-structure mesh using the GID software, and it takes into account the influence of the buildings and roads. These data were obtained from the Geospatial Information Authority of Japan. 5m × 5m Digital Elevation Model (DEM) data were used to generate the mesh elevation data, as shown in Figure 4.10. The elevations of both meshes were adjusted to induce flows from building groups to roads artificially.

In reality, manholes and storm drains are bi-directional spots between the ground surface and the sewerage system. Generally, storm drains are widely distributed on roads. However, the connecting works of storm drain distribution data are nearly unavailable because of the shape diversity and welter of storm drains, as well as time limitations. The positions of the manholes are used as exchange spots. To calculate the exchange discharge between the ground and sewer network, the water elevations in a manhole were directly compared with the water elevations on the ground mesh on which the manhole was; then, each bottom area and manhole perimeter was used according to suitable equations (Lee et al., 2015).

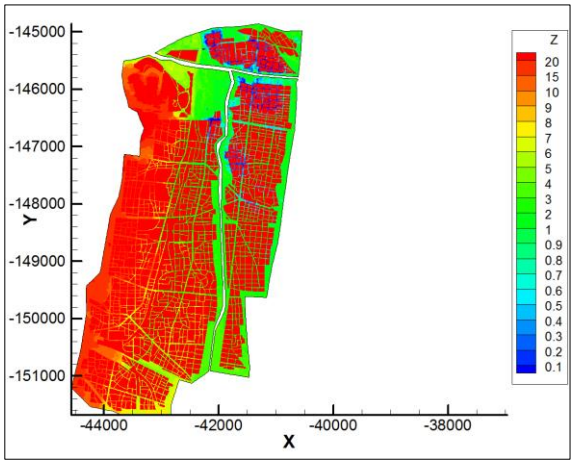

Figure 4.10 Ground elevations in the target area

4.3.1 Two-dimensional ground surface

A two-dimensional ground model was used by the finite different method based on the shallow water-flow equation. Equations (4.1) and (4.2) present the continuity and a momentum equation. The leap-frog method was used to calculate the water depth and flux.

Continuity equation

$$\frac{\partial h}{\partial t}+\frac{\partial M}{\partial x}+\frac{\partial N}{\partial y}=r_e-q_{drain} \tag{4.1}$$

Momentum equation

$$\frac{\partial M}{\partial t}+\frac{\partial (uM)}{\partial x}+\frac{\partial (vM)}{\partial y}=-gh\frac{\partial H}{\partial x}-\frac{gn^2M\sqrt{u^2+v^2}}{h^{4/3}} \tag{4.2}$$

$$\frac{\partial N}{\partial t}+\frac{\partial (uN)}{\partial x}+\frac{\partial (vN)}{\partial y}=-gh\frac{\partial H}{\partial y}-\frac{gn^2N\sqrt{u^2+v^2}}{h^{4/3}} \tag{4.3}$$

where h is the water depth; H is the water level; u, v are the x, y directional velocity; M (=mh), N (=vh) are the x, y directional flow flux, q_{drain} is the inflow discharge from the ground surface to the sewer network unit area, g is the gravity acceleration, and n is the Manning's roughness coefficient.

4.3.1.1 Discretization methods

The x, y direction of the flow flux (M, N), the flow velocity (u, v) at the boundary of the non-structured grid, and the water depth (h) at the centroid of the non-structured grid were defined as shown in Figure 4.11. Figure 4.12 shows the control volume, and equation (4.4) shows the discretization for continuity equation.

$$\frac{h_i^{n+3}-h_i^{n+1}}{2\Delta t}+\frac{1}{A_i}\sum_{l=1}^{m_i}\left\{M_l^{n+2}(\Delta y)_l-N_l^{n+2}(\Delta x)_l\right\}=r_e-q_{drain}^{n+2} \tag{4.4}$$

where h_i is the depth of grid i; m_i is the number of sides surrounding grid i; A_i is the area of the control volume; and M_l, N_l are the x, y directions of flow flux at the boundaries of adjacent grids,

respectively. Δx, Δy are the difference of each coordinate at both ends' boundaries of adjacent grids. Each Δx, Δy is calculated as follows (4.5), (4.6), (4.7):

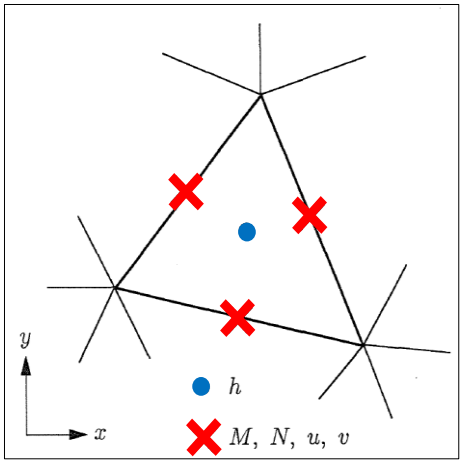

Figure 4.11 Location of parameters

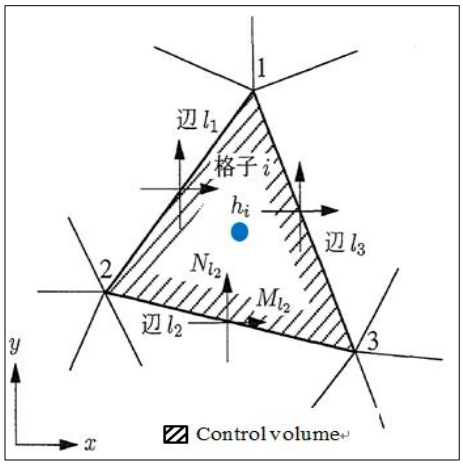

Figure 4.12 control volume of continuity equation

$$(\Delta x)_{l_1} = x_2 - x_1,\ (\Delta y)_{l_1} = y_2 - y_1 \tag{4.5}$$

$$(\Delta x)_{l_2} = x_3 - x_2,\ (\Delta y)_{l_2} = y_3 - y_2 \tag{4.6}$$

$$(\Delta x)_{l_3} = x_1 - x_3,\ (\Delta y)_{l_3} = y_1 - y_3 \tag{4.7}$$

The momentum equation can be calculated at the boundary of adjacent grids, as shown in Figure 4.13. Figure 4.14 shows calculation process for the convection term. Equations (4.8) and (4.9) show the discretization for momentum equation along each direction.

***x*-direction**

$$\frac{M_L^{n+2}-M_L^n}{2\Delta t}+M1+M2=-g\tilde{h}_L^{n+1}(\nabla H)_x-\frac{g\tilde{n}_L^2\dfrac{M_L^{n+2}+M_L^n}{2}\sqrt{\left(u_L^n\right)^2+\left(v_L^n\right)^2}}{\left(\tilde{h}_L^{n+1}\right)^{3/4}} \tag{4.8}$$

***y*-direction**

$$\frac{N_L^{n+2}-N_L^n}{2\Delta t}+N1+N2=-g\tilde{h}_L^{n+1}(\nabla H)_x-\frac{g\tilde{n}_L^2\dfrac{N_L^{n+2}+N_L^n}{2}\sqrt{\left(u_L^n\right)^2+\left(v_L^n\right)^2}}{\left(\tilde{h}_L^{n+1}\right)^{3/4}} \tag{4.9}$$

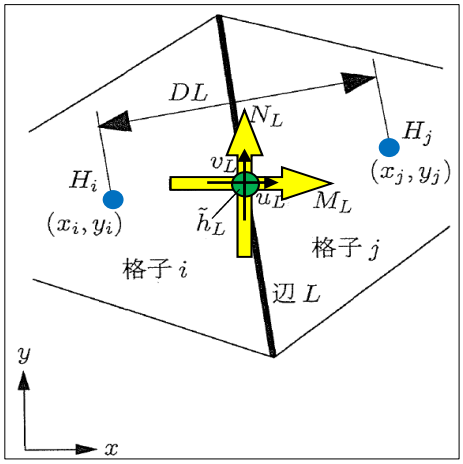

Figure 4.13 Calculation process for the momentum equation

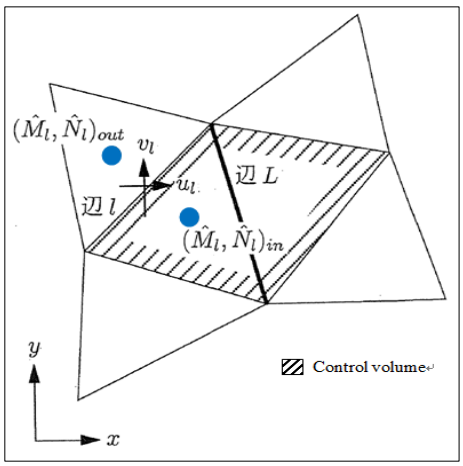

Figure 4.14 Calculation process for the convection term

where, M_l, N_l is the x, y directions of the flow flux at the boundary of adjacent grids, which is an interlocked grid line. u_l, v_l is the x, y directions of the flow velocity at the boundary of adjacent grids. The convection terms of the x, y directions are calculated as follows (4.10), (4.11):

$$M1+M2=\frac{1}{A_{cv}}\sum_{l=1}^{m'}\left\{\left(u_l\hat{M}_l\right)(\Delta y)_l-\left(v_l\hat{M}_l\right)(\Delta x)_l\right\} \tag{4.10}$$

$$N1+N2=\frac{1}{A_{cv}}\sum_{l=1}^{m'}\left\{\left(u_l\hat{N}_l\right)(\Delta y)_l-\left(v_l\hat{N}_l\right)(\Delta x)_l\right\} \tag{4.11}$$

where A_{cv} is the area of the control volume and m' is the number of sides surrounding the control volume. M, N is the flow flux on the centroid, which is obtained by interpolating the flow flux on the grid boundary, as shown in Figure 4.15, and each equation is as follows (4.12), (4.13):

$$\hat{M}=\frac{\frac{1}{d_1}M_1+\cdots+\frac{1}{d_m}M_m}{\frac{1}{d_1}+\cdots+\frac{1}{d_m}} \tag{4.12}$$

$$\hat{N}=\frac{\frac{1}{d_1}N_1+\cdots+\frac{1}{d_m}N_m}{\frac{1}{d_1}+\cdots+\frac{1}{d_m}} \tag{4.13}$$

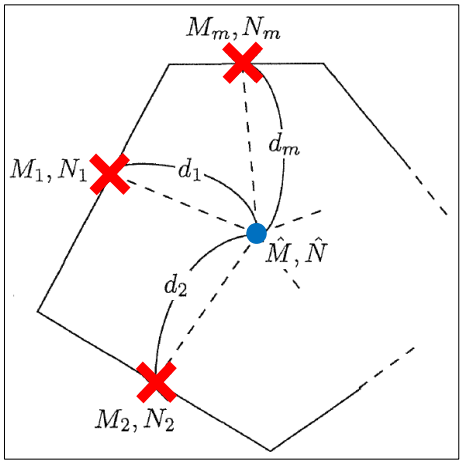

Figure 4.15 Interpolation of flow flux

According to the u_l, v_l of directions, the interpolated flow flux of different direction is used to calculate the $\widehat{M_l}$, $\widehat{N_l}$ as follows (4.14), (4.15),(4.16), (4.17):

Case of $(\boldsymbol{u_l} \times (\Delta \boldsymbol{y})_{\boldsymbol{l}} \geq \boldsymbol{0})$ **for** $\boldsymbol{u_l \widehat{M_\iota}}$, $\boldsymbol{u_l \widehat{N_\iota}}$

$$\widehat{M_\iota} = (\widehat{M_l})_{in},\ \widehat{N_\iota} = (\widehat{N_l})_{in} \tag{4.14}$$

Case of $(\boldsymbol{u_l} \times (\Delta \boldsymbol{y})_{\boldsymbol{l}} < \boldsymbol{0})$ **for** $\boldsymbol{u_l \widehat{M_\iota}}$, $\boldsymbol{u_l \widehat{N_\iota}}$

$$\widehat{M_\iota} = (\widehat{M_l})_{out},\ \widehat{N_\iota} = (\widehat{N_l})_{out} \tag{4.15}$$

Case of $(\boldsymbol{v_l} \times (\Delta \boldsymbol{x})_{\boldsymbol{l}} \geq \boldsymbol{0})$ **for** $\boldsymbol{v_l \widehat{M_\iota}}$, $\boldsymbol{v_l \widehat{N_\iota}}$

$$\widehat{M_\iota} = (\widehat{M_l})_{out},\ \widehat{N_\iota} = (\widehat{N_l})_{out} \tag{4.16}$$

Case of $(\boldsymbol{v_l} \times (\Delta \boldsymbol{x})_{\boldsymbol{l}} < \boldsymbol{0})$ **for** $\boldsymbol{v_l \widehat{M_\iota}}$, $\boldsymbol{v_l \widehat{N_\iota}}$

$$\widehat{M_\iota} = (\widehat{M_l})_{in},\ \widehat{N_\iota} = (\widehat{N_l})_{in} \tag{4.17}$$

where the definitions of *in* and *out* are described in Figure 4.14. $(\nabla H)_x$, $(\nabla H)_y$ are the water surface gradient of the *x*, *y* directions, as follows (4.18), (4.19):

$$(\nabla H)_x = \frac{(h_j + z_j) - (h_i + z_i)}{DL}\cos\theta \tag{4.18}$$

$$(\nabla H)_y = \frac{(h_j + z_j) - (h_i + z_i)}{DL}\sin\theta \tag{4.19}$$

where *DL* is the distance between the centroids of the adjacent grids, which are described in Figure 4.13 and calculated as follows (4.20),

$$DL = \sqrt{(x_j - x_i)^2 - (y_j - y_i)^2} \tag{4.20}$$

and, $\cos\theta = \frac{x_j - x_i}{DL}$, $\sin\theta = \frac{y_j - y_i}{DL}$

$\tilde{h}_L$, $\tilde{n}_L$ are also calculated by interpolating the centroid values following (4.21) and (4.22), and Figure 4.16 shows the calculation process of water depth and roughness coefficient by interpolation:

$$\tilde{h}_L = \frac{\frac{1}{d_i}h_i + \frac{1}{d_j}h_j}{\frac{1}{d_i} + \frac{1}{d_j}} = \frac{d_j h_i + d_i h_j}{d_i + d_j} \tag{4.21}$$

$$\tilde{n}_L = \frac{\frac{1}{d_i} n_i + \frac{1}{d_j} n_j}{\frac{1}{d_i} + \frac{1}{d_j}} = \frac{d_j n_i + d_i n_j}{d_i + d_j} \tag{4.22}$$

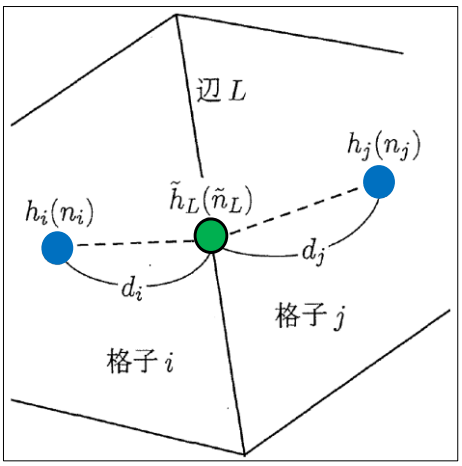

Figure 4.16 Calculation process of water depth and roughness coefficient by interpolation

4.3.2 One-dimensional sewer network

As mentioned in the previous chapter, the storm water in the sewer pipe was calculated based on the following 1D continuity (4.23), (4.24) and momentum (4.25) equations. Overflow discharge over the side weir was calculated by De Marchi's equation (4.26), in which the C_d value was calculated using a correlation equation (4.27) by weir height (p) and length (L) (Ko et al., 2014). Figure 4.17 shows a schematic diagram of the diverted portion by side weir within the sewer pipe.

Continuity equation

(a) Case of originally sewer network:

$$\frac{\partial A}{\partial t} + \frac{\partial Q}{\partial x} = q_{ex} \tag{4.23}$$

(b) Case of installed the storage system within sewer network:

$$\frac{\partial A}{\partial t} + \frac{\partial Q}{\partial x} = q_{ex} - q_{out} \tag{4.24}$$

Momentum equation

$$\frac{\partial Q}{\partial t} + \frac{\partial (uQ)}{\partial x} = -gA\frac{\partial H}{\partial x} - \frac{gn^2|Q|Q}{R^{\frac{4}{3}}A} \quad (4.25)$$

De Marchi's equation

$$q_{out} = \frac{dQ_{out}}{dL} = \frac{2}{3}C_d\sqrt{2g}(h-p)^{1.5} \quad (4.26)$$

and $C_d = -0.2604\frac{p}{L} + 0.673$ (4.27)

where A is the cross-sectional area of flow, Q is the discharge, q_{ex} is the lateral inflow discharge per unit pipe length, q_{out} is the overflow discharge per unit length over the side weir, u is the flow velocity, n is the Manning's roughness coefficient (0.012 was used in this study), R is the hydraulic radius, H is the piezometric head ($H = z + h$), z is the bottom elevation of the pipe, and h is the water depth in the pipe measured from the bottom, which is calculated as follows:

$$h = \begin{cases} f(A) & : (A \le A_p) \\ B` + \frac{A - A_p}{B_s} & : (A > A_p) \end{cases} \quad (4.28)$$

$$B_s = \frac{gA}{a^2} \quad (4.29)$$

$$A_p = \frac{D^2}{8}(\theta - sin\,\theta) \quad (4.30)$$

$$W = D\ sin\frac{\theta}{2} \quad (4.31)$$

$$h = \frac{D}{2}\left(1 - \cos\frac{\theta}{2}\right) \quad (4.32)$$

and $\theta = 2\ cos^{-1}(1 - \frac{2h}{D})$ (4.33)

where f is a function expressing a relationship between the flow cross-section area and water depth in a circular pipe, the case of $A \le A_p$ is an open-channel flow condition and that of $A > A_p$ is a pressurized flow condition, $B`$ is the height of the pipe ceiling, A_p is the cross-sectional area of the pipe, B_s is the slot width, and a is pressure propagation velocity for the pipe (10m/s was used).

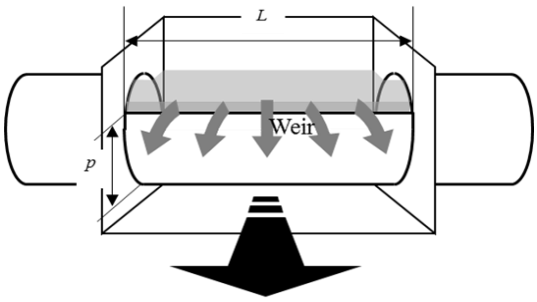

Figure 4.17 Schematic diagram of the diverted portion by side weir within the sewer pipe

4.3.3 Connecting model

4.3.3.1 Drain box

The governing equation of a drain box is as follows (4.34):

$$F_d \frac{dZ}{dt} = q_{drain} - q_{sew-d} \tag{4.34}$$

where F_d is the horizontal area of the drain box, Z is the water level at the drain box, and $q_{sew\text{-}d}$ is the drainage discharge from the drain box to the sewer pipe.

4.3.3.2 Interaction model between the ground and drain box

The discharge for interaction between the ground and drain box was calculated by the weir and orifice formulas, as follows (4.35), (4.36), (4.37), (4.38):

Case of drainage ($h_m > h_d$), as shown in Figure 4.18:

Weir equation

$$Q = \frac{2}{3} C_{dw} L_1 \sqrt{2g} (h_m - h_d)^{\frac{2}{3}} \ : \ (h_m - h_d) \leq B_{01}/2 \tag{4.35}$$

Orifice equation

$$Q = C_{d0} A_d \sqrt{2g(h_m - h_d)} \ : (h_m - h_d) > B_{01}/2 \tag{4.36}$$

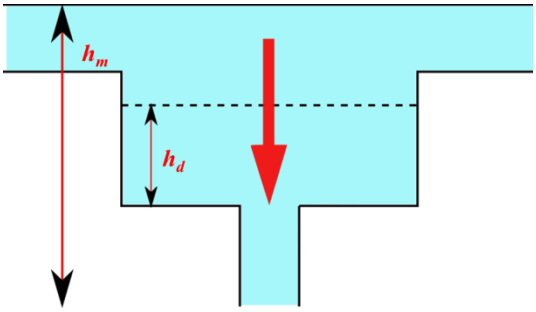

Figure 4.18 Case of drainage

Case of spurt ($h_m < h_d$), as shown in Figure 4.19:

Weir equation

$$Q = -\frac{2}{3} C_{dw} L_1 \sqrt{2g} (h_m - h_d)^{\frac{2}{3}} : \ (h_m - \ h_d) \leq B_{01}/2 \tag{4.37}$$

Orifice equation

$$Q = -C_{d0} A_d \sqrt{2g(h_m - h_d)} : \ \ (h_m - \ h_d) > B_{01}/2 \tag{4.38}$$

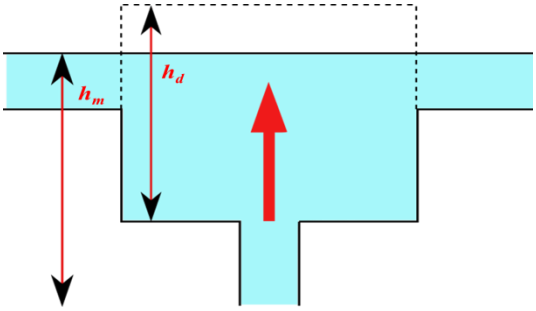

Figure 4.19 Case of spurt

where Q is the drainage discharge from the ground surface into the drain channel, h_m is the water level on the ground, h_d is the piezometric head of the drain box, and A_d is the vertical area storm drain.

C_{dw} and C_{do} are the coefficients, which were 0.48 and 0.57, respectively. B_{01} is the smallest width of the storm drain, while L_1 is the perimeter length of the storm drain.

4.3.3.3 Interaction model between a drain box and sewer pipe

The discharge for the interaction between a drain box and sewer pipe is calculated by the weir and orifice formulas as follows (4.39), (4.40), (4.41), (4.42):

Case of drainage ($h_d > h_p$), as shown in Figure 4.20:

Weir equation

$$Q = \frac{2}{3} C_{dw} L_2 \sqrt{2g} (h_d - h_p)^{\frac{2}{3}} \ : \ (h_d - \ h_p) \leq B_{01}/2 \tag{4.39}$$

Orifice equation

$$Q = C_{d0} A_u \sqrt{2g(h_d - h_p)} \ : (h_d - \ h_{dp}) > B_{01}/2 \tag{4.40}$$

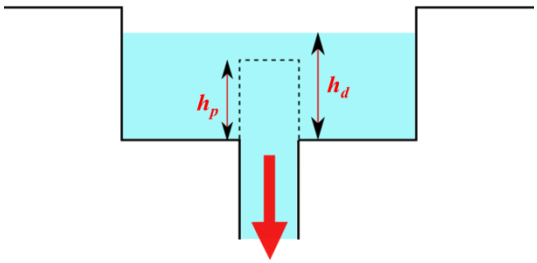

Figure 4.20 Case of drainage

Case of spurt ($h_d < h_p$), as shown in Figure 4.21:

Weir equation

$$Q = -\frac{2}{3} C_{dw} L_2 \sqrt{2g} \left(h_d - h_p\right)^{\frac{2}{3}} \ : \ (h_d - \ h_p) \leq B_{01}/2 \tag{4.41}$$

Orifice equation

$$Q = -C_{d0} A_u \sqrt{2g(h_d - h_p)} \ : \ (h_d - \ h_{dp}) > B_{01}/2 \tag{4.42}$$

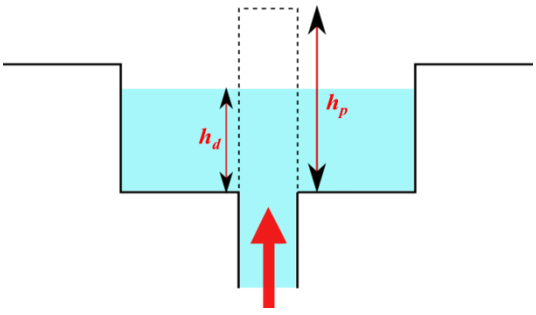

Figure 4.21 Case of spurt

where h_d is the piezometric head of the drain box, h_p is the piezometric head of the pipe, and A_d is the vertical area storm drain. B_{02} is the smallest width of the drainage tube, and L_1 is the perimeter length of the drainage tube.

4.3.3.4 Interaction model between a manhole and sewer pipe

The discharge for the interaction between a manhole and sewer pipe is calculated by the weir and orifice formulas, as follows:

Tank is located in the upstream part:

Case of flowing toward the pipe ($h_t > h_p$), as shown in Figure 4.22:

$$Q = C_1 A_t \sqrt{2gh_t} \quad : h_p/h_t \leq 2/3 \tag{4.43}$$

$$Q = C_2 A_p \sqrt{2g(h_t - h_p)} \; : h_p/h_t > 2/3 \tag{4.44}$$

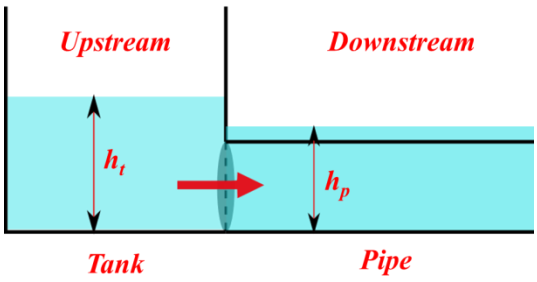

Figure 4.22 Case of flowing toward to pipe

Case of flowing toward the tank ($h_t < h_p$), as shown in Figure 4.23:

$$Q = -C_1 A_p \sqrt{2gh_p} \quad : h_t/h_p \leq 2/3 \tag{4.45}$$

$$Q = -C_2 A_t \sqrt{2g(h_p - h_t)} \; : h_t/h_p > 2/3 \tag{4.46}$$

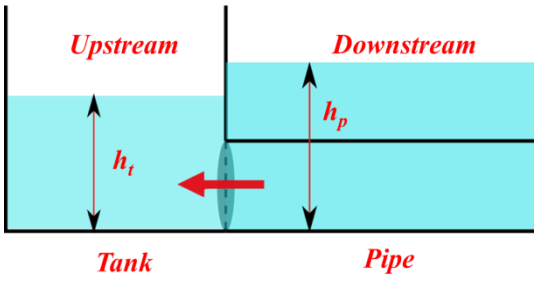

Figure 4.23 Case of flowing toward to tank

Tank is located in the downstream part:

Case of flowing toward to manhole ($h_t < h_p$):

$$Q = C_1 A_p \sqrt{2gh_p} \quad : h_t/h_p \leq 2/3 \tag{4.47}$$

$$Q = C_2 A_t \sqrt{2g(h_p - h_t)} \; : h_t/h_p > 2/3 \tag{4.48}$$

Case of flowing toward the pipe ($h_t > h_p$):

$$Q = -C_1 A_t \sqrt{2gh_t} \quad : h_p/h_t \leq 2/3 \tag{4.49}$$

$$Q = -C_2 A_p \sqrt{2g(h_t - h_p)} \; : h_p/h_t > 2/3 \tag{4.50}$$

where Q is the positive direction of the outlet discharge, A_t is the wet area of the pipe cross section in the upstream tank, h_t is the water depth from the bottom of the tank, A_p is the wet area of the pipe cross-section, h_p is the water head in the bottom of pipe, and c_1 and c_2 are coefficients (0.35 and 0.91 were used, respectively).

4.4 Evaluation of an underground storage box's effects

If a virtual underground storage box is installed in the Nakahama area, then the amount of inundation damage that is reduced must be considered, using the integrated model mentioned previously. Three installation sites were determined after considering different area features, where A is the lowland, B is the middle, and C is the upstream portion in the Nakahama area, as shown in Figure 4.24. Figures 4.25 ~ 4.27 show the installation positions along each of the A, B, and C areas in detail. In addition, the capacity of the storage box is 50,000 m^3, which is the largest capacity of an installed storage box in the Neyagawa basin. Also, it is assumed that the storage box will no longer operate if this capacity becomes full. The calculation time is 10 hours from the start of rainfall. An inundated area was used to evaluate the mitigation effect. However, since the effects of storage box influence the installed area topically, a comparison between an inundated area and the whole target area is not suitable. Therefore, it is assumed that an inundated area within a radius of 500m is compared.

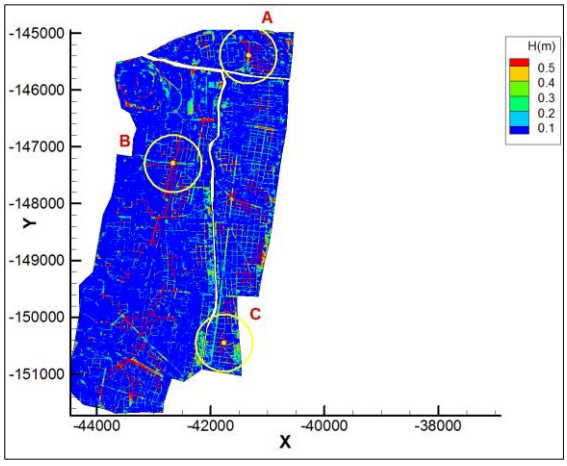

Figure 4.24 Installation areas (whole)

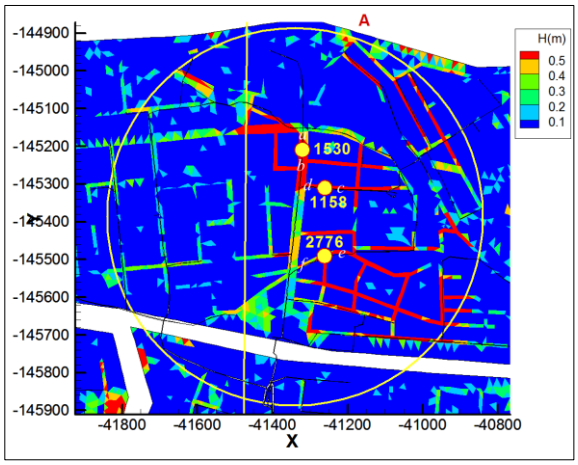

Figure 4.25 Installation areas (A)

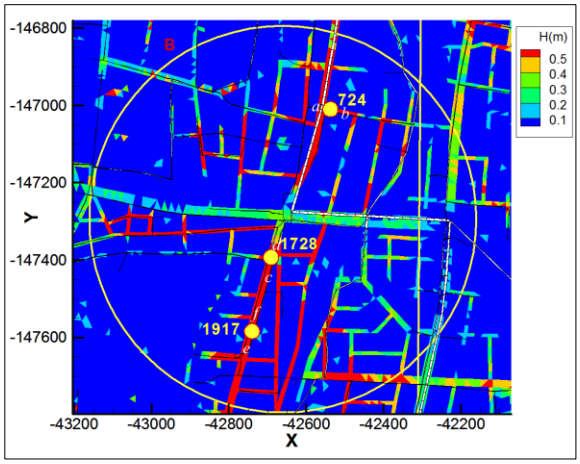

Figure 4.26 Installation areas (B)

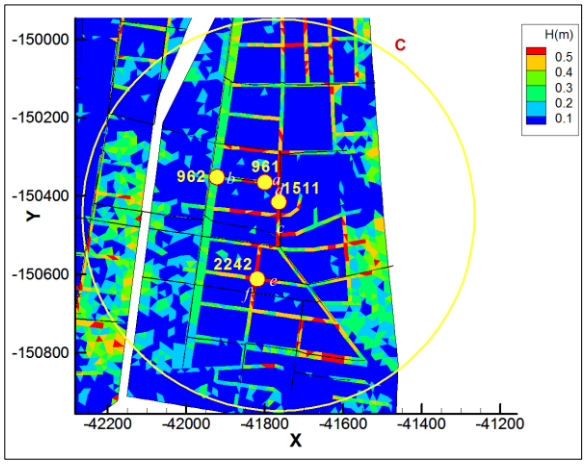

Figure 4.27 Installation areas (C)

4.4.1 Comparison by rainfall type and weir shape

4.4.1.1 Setting of the rainfall type

The effects of the storage box are different from those of the rainfall type, even if the rainfall intensity is same. Therefore, I provide three hyetographs as a virtual rainfall model, in which 50-year probability rainfall was used as the intensity of greater than 10-year probability rainfall as the design rainfall. Duration time is 3 hours equal to actual rainfall recorded in Nakahama area, 2011. Rainfall was calculated using the AMeDAS rainfall probability calculation program of the Public Works Research Institute, in which 3 hours of total rainfall at 50-year probability was calculated to be 168mm, which was distinguished as fore, center, and rear intensity rainfall, as shown in Figure 4.28. Here, the GEV distribution (generalized extreme value distribution) was adopted, and the probability of rainfall intensity was calculated a by fair formula, which was used to calculate that the original GEV distribution had a high correlation. The maximum rainfall intensity was 22.5mm/min when the Nakahama area was inundated. This is 25.57% of all rainfall events. Therefore, 25.57% of 168mm was given as the maximum intensive distribution for each rainfall type.

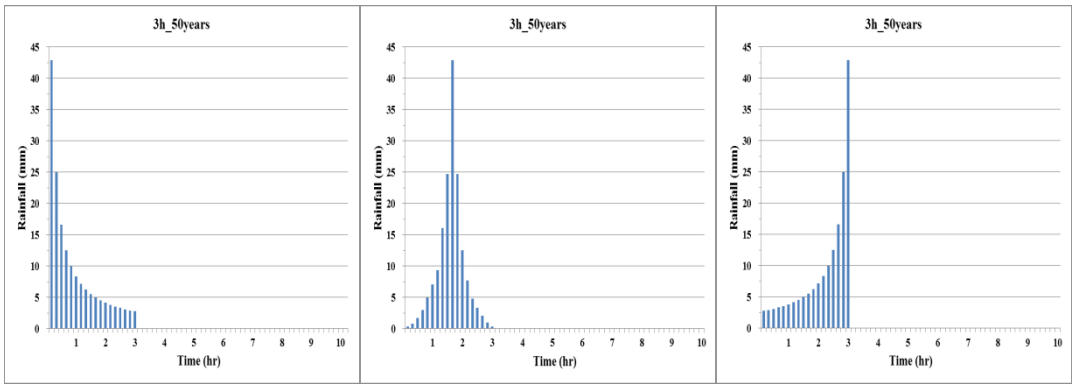

Figure 4.28 Fore, center, and rear intensity rainfall

4.4.1.2 Setting of the weir shape

Overflow discharge at the side weir differs based on the weir shape. If the weir height is lower or the weir length is longer, the overflow starts earlier by that much. Thus, it is expected that the reduction effect of flooding and peak sewer capacity differ by weir shape.

In this study, the weir heights (p) were 0.86m (86% of diameter, basic), 0.65m (65%), 0.45m (0.45%), and 0.25m (25%); the weir lengths (L) were 4.09m (basic) and 2.05m (50%) in the A area; the weir heights (p) were 0.78m (86% of diameter, basic), 0.59m (65%), 0.41m (0.45%),

and 0.23m (25%); the weir lengths (*L*) were 3.68m (basic) and 1.84m (50%) in the B area; the weir heights (*p*) were 1.17m (86% of diameter, basic), 0.88m (65%), 0.61m (0.45%), and 0.34m (25%); and the weir lengths (*L*) were 5.52m (basic) and 2.76m (50%) in the C area. In other words, four kinds of weir heights and two kinds of weir lengths, led to 8 cases being investigated, as shown in Table 4.1.

Table 4.1 Cases by rainfall type and weir condition

Target area	Rainfall type	Class number of pipe	Installation position	Pipe diameter (m)	Classification of cases	Weir length (m)	Weir height (m)	Capacity (m^3)
A	Fore Center Rear	1530	b	1	Case(a)	4.09	0.86	50,000
					Case(b)	4.09	0.65	
					Case(c)	4.09	0.45	
					Case(d)	4.09	0.25	
					Case(e)	2.05	0.86	
					Case(f)	2.05	0.65	
					Case(g)	2.05	0.45	
					Case(h)	2.05	0.25	
B	Fore Center Rear	1728	d	0.9	Case(a)	3.68	0.78	
					Case(b)	3.68	0.59	
					Case(c)	3.68	0.41	
					Case(d)	3.68	0.23	
					Case(e)	1.84	0.78	
					Case(f)	1.84	0.59	
					Case(g)	1.84	0.41	
					Case(h)	1.84	0.23	
C	Fore Center Rear	962	b	1.35	Case(a)	5.52	1.17	
					Case(b)	5.52	0.88	
					Case(c)	5.52	0.61	
					Case(d)	5.52	0.34	
					Case(e)	2.76	1.17	
					Case(f)	2.76	0.88	
					Case(g)	2.76	0.61	
					Case(h)	2.76	0.34	

4.4.1.3 Results and discussion

Figures 4.29 ~ 4.46 show the inundation areas corresponding to more than 10cm and 50cm inundation areas by changes in weir length and height for the different rainfall types. According to these results, the inundation areas were still decreased, compared with the case of without a storage box, even if the rainfall intensive distribution is changed.

In the case of area A, the inundated area was the largest with rear intensity rainfall more than 10cm. However, the center intensity rainfall caused the large inundation area of more than 50cm. In case of the fore intensity rainfall, relatively smooth drainage was conducted. Since the time of peak rainfall into sewerage systems was quick at the beginning, the drainage effect was better than other rainfall intensity type. In the case of area B, rear intensity rainfall caused a large inundation area of more than 10cm and even more than 50cm. Damage by fore intensity rainfall was still smaller than at other areas. In the case of area C, the rear intensity rainfall also caused a large inundation area of more than 10cm and center intensity rainfall caused large damage of more than 50cm. Furthermore, the largest inundated area was represented under fore intensity rainfall, compared to the other study areas.

As a whole, the rear and center intensity rainfall conditions influenced urban inundation. The impact of the fore intensity rainfall condition was less than the other rainfall distributions. The inundation mitigation effects by different weir height and length were that the peak inundation area decreased as the weir height decreased or length increased because the overtopping time had begun by decreasing the weir height and the quantity of discharge increased. The peak inundation area was decreased by adjusting the weir size, but the variation in the inundation mitigation effect was not so great. On the other hand, in the case of area C, the effect was the opposite. As the weir height decreased, the peak inundation area increased, and changes in weir shape were not effective at more than 50cm, even if the inundation area corresponding to more than 50cm was less than A, B area.

The mitigation effect of the inundation area due to the installation of a storage box was the best in area C. This means that the quantity of overflow discharge was large due to the active capacity of the sewer network. Therefore, as seen in the results above, when the capacity of a sewer pipe is great, the changes in weir height and length are not as effective. Inundation mitigation due to changes in weir height is more pronounced than by changes in weir length. Figures 4.47 ~ 4.58 show the correlation in reduction effect along the change in weir height and lengths corresponding to more than 10cm and 50cm inundation areas. Therefore, regarding the shape of the side weir, weir height is a greater influence on flood mitigation than weir length.

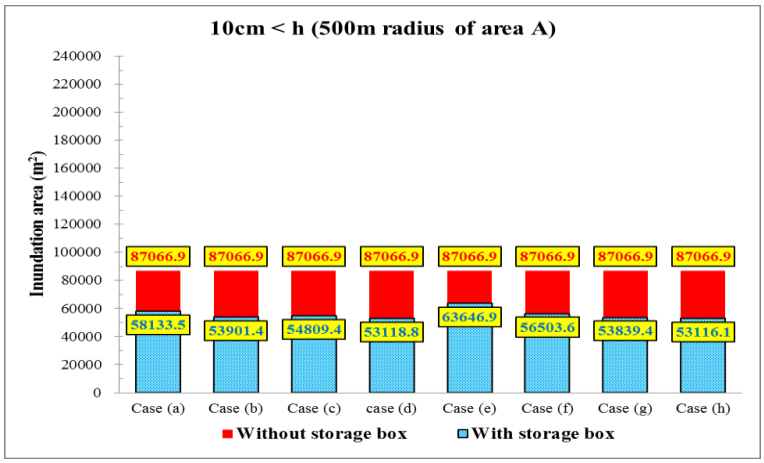

Figure 4.29 Mitigation effect by changes in weir shape (fore intensity rainfall, area A)

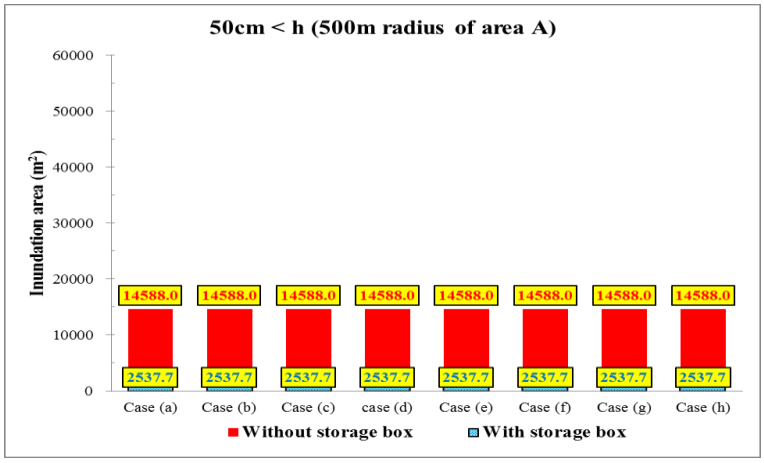

Figure 4.30 Mitigation effect by change of weir shape (fore intensity rainfall, A area)

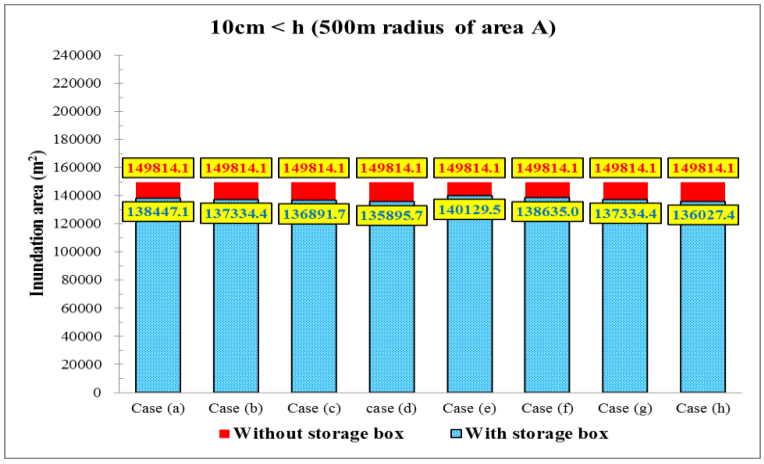

Figure 4.31 Mitigation effect by changes in weir shape (center intensity rainfall, area A)

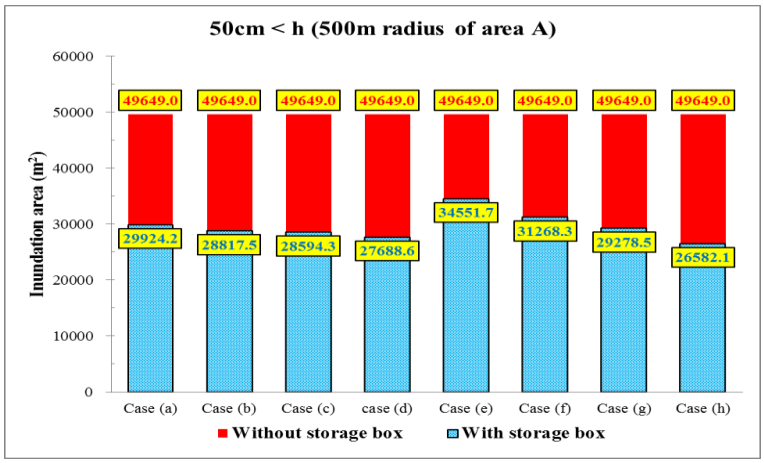

Figure 4.32 Mitigation effect by changes in weir shape (center intensity rainfall, area A)

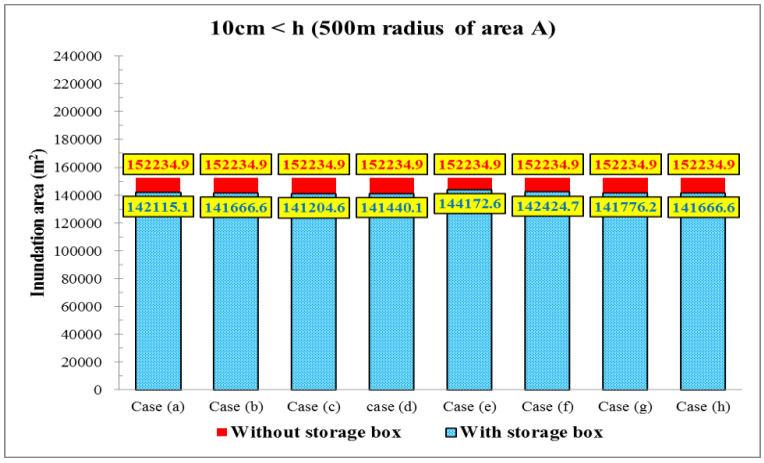

Figure 4.33 Mitigation effect by changes in weir shape (rear intensity rainfall, area A)

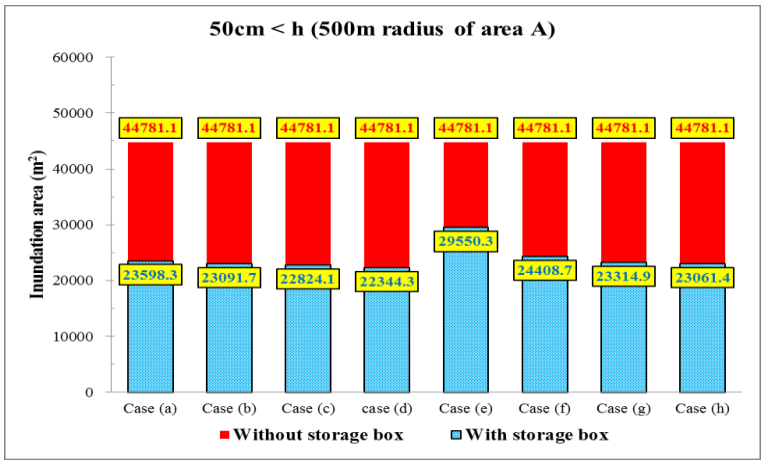

Figure 4.34 Mitigation effect by changes in weir shape (rear intensity rainfall, area A)

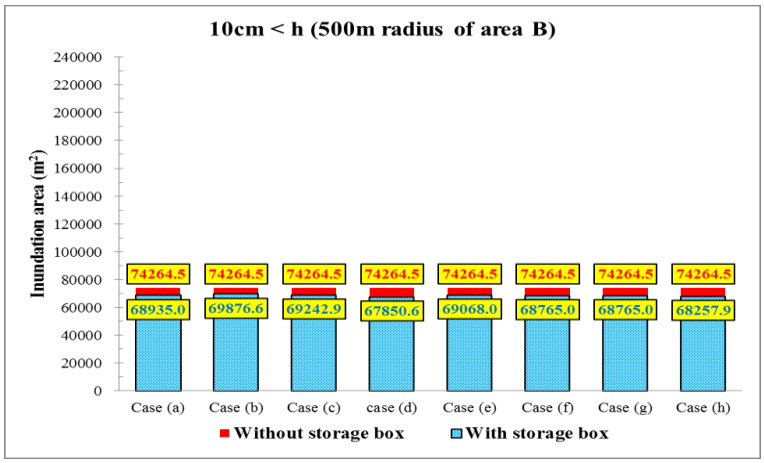

Figure 4.35 Mitigation effect by changes in weir shape (fore intensity rainfall, area B)

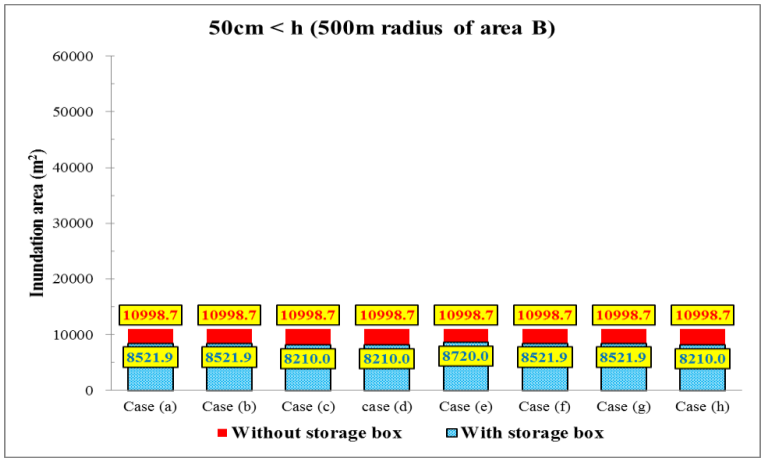

Figure 4.36 Mitigation effect by changes in weir shape (fore intensity rainfall, area B)

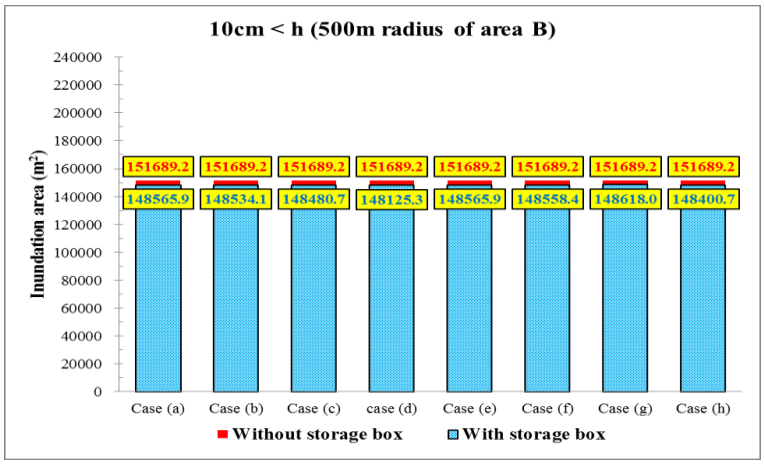

Figure 4.37 Mitigation effect by changes in weir shape (center intensity rainfall, area B)

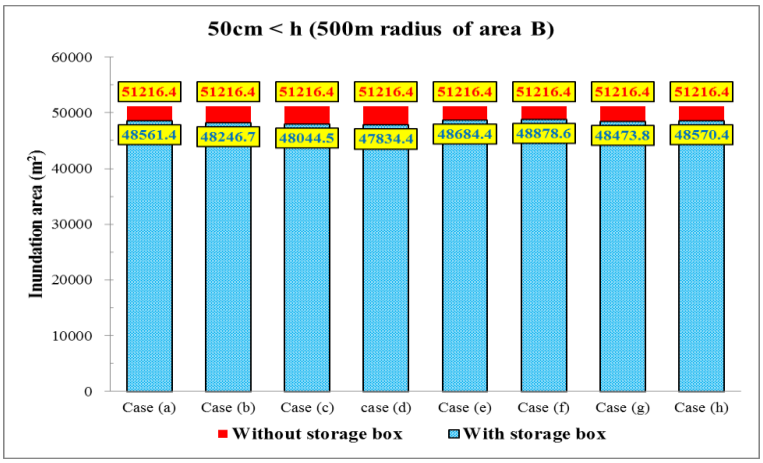

Figure 4.38 Mitigation effect by changes in weir shape (center intensity rainfall, area B)

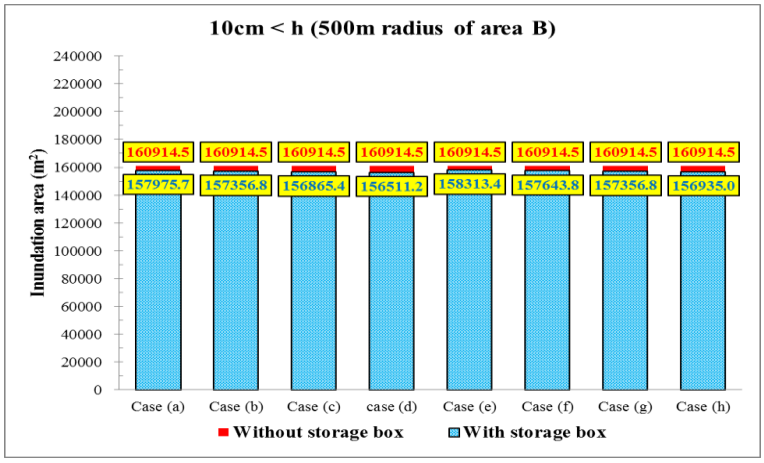

Figure 4.39 Mitigation effect by changes in weir shape (rear intensity rainfall, area B)

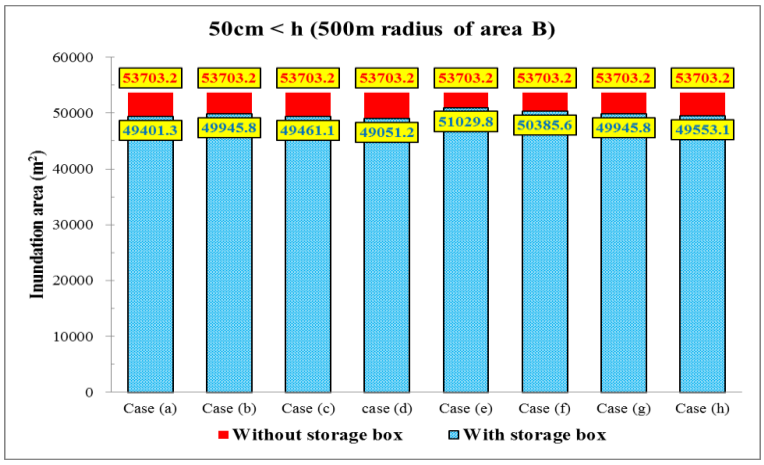

Figure 4.40 Mitigation effect by changes in weir shape (rear intensity rainfall, area B)

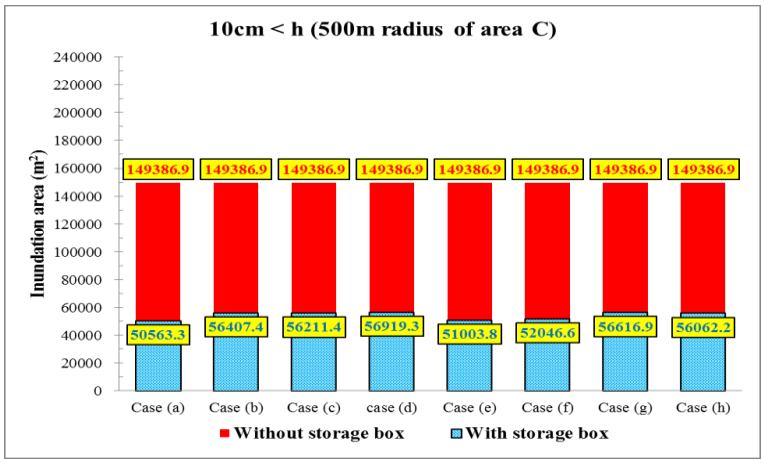

Figure 4.41 Mitigation effect by changes in weir shape (fore intensity rainfall, area C)

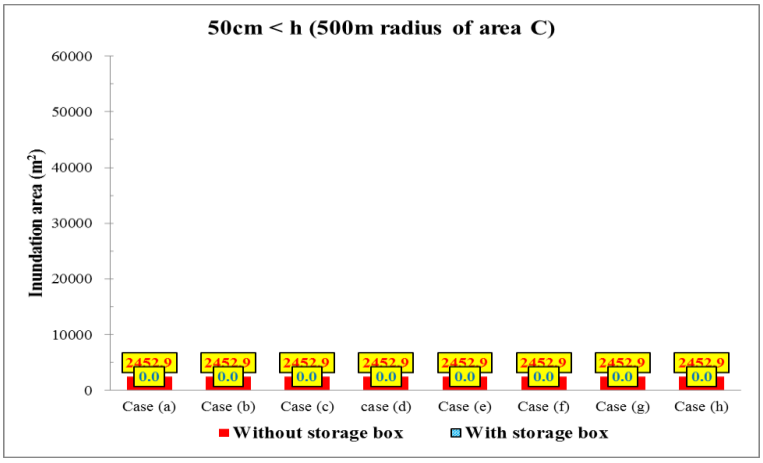

Figure 4.42 Mitigation effect by changes in weir shape (fore intensity rainfall, area C)

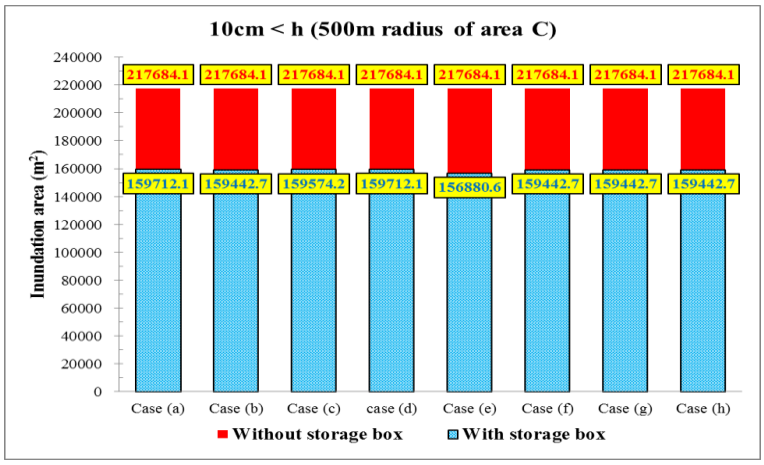

Figure 4.43 Mitigation effect by changes in weir shape (center intensity rainfall, area C)

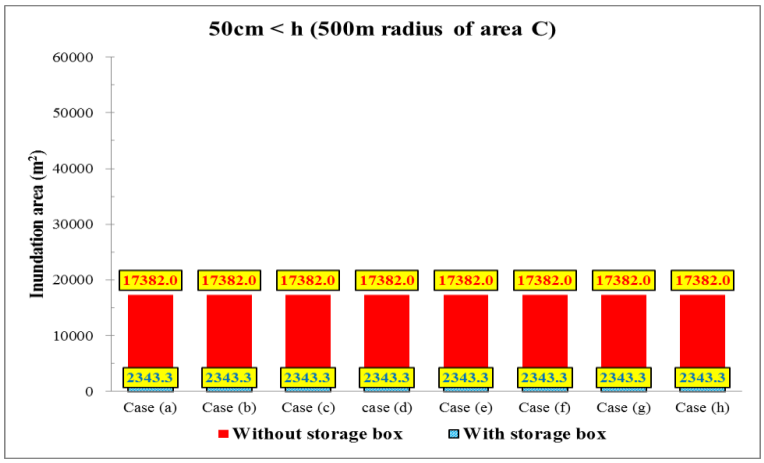

Figure 4.44 Mitigation effect by changes in weir shape (center intensity rainfall, area C)

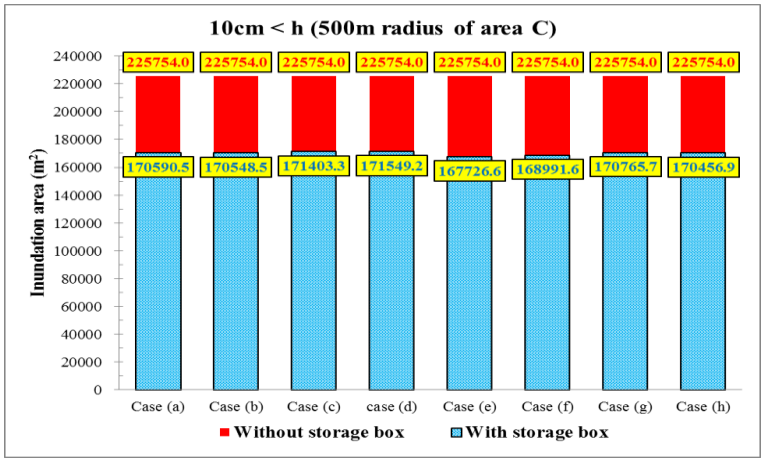

Figure 4.45 Mitigation effect by changes in weir shape (rear intensity rainfall, area C)

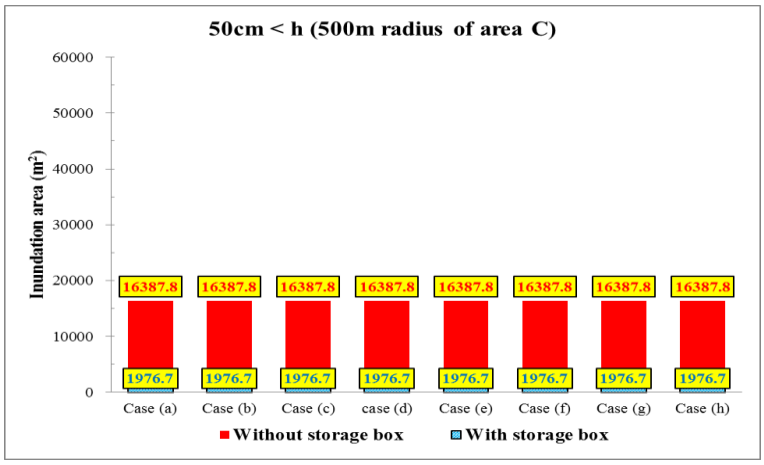

Figure 4.46 Mitigation effect by changes in weir shape (rear intensity rainfall, area C)

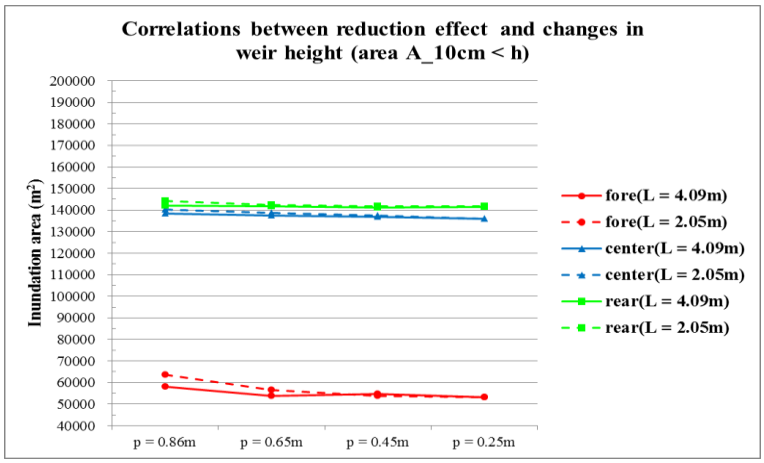

Figure 4.47 Correlations between reduction affect and changes in weir height (10cm < h, area A)

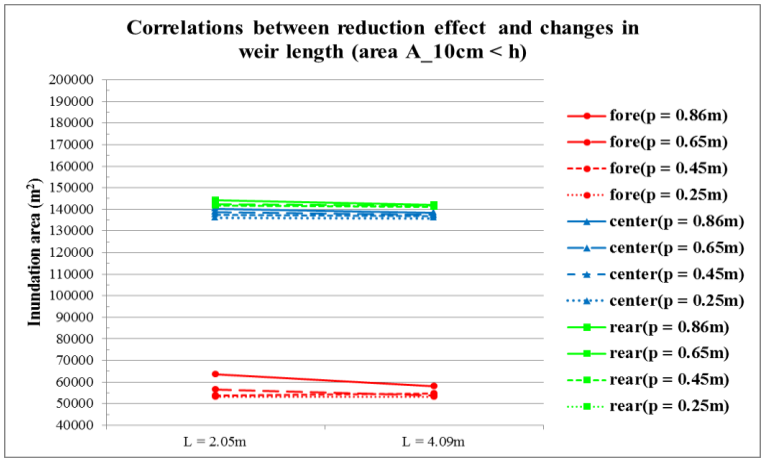

Figure 4.48 Correlations between reduction affect and changes in weir length (10cm < h, area A)

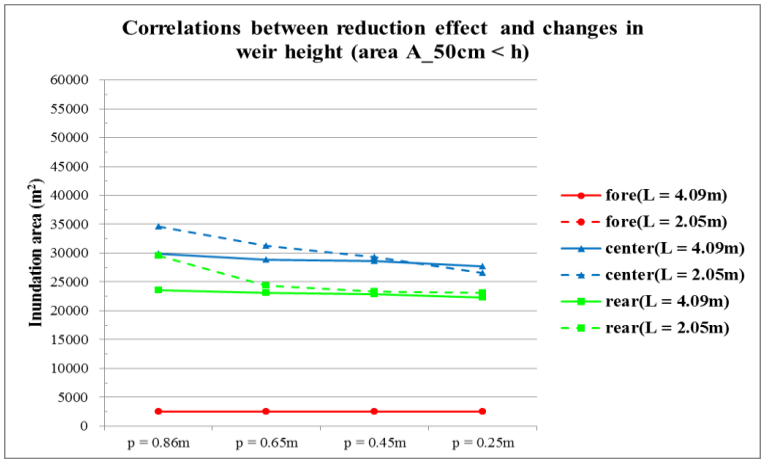

Figure 4.49 Correlations between reduction affect and changes in weir height (50cm < h, area A)

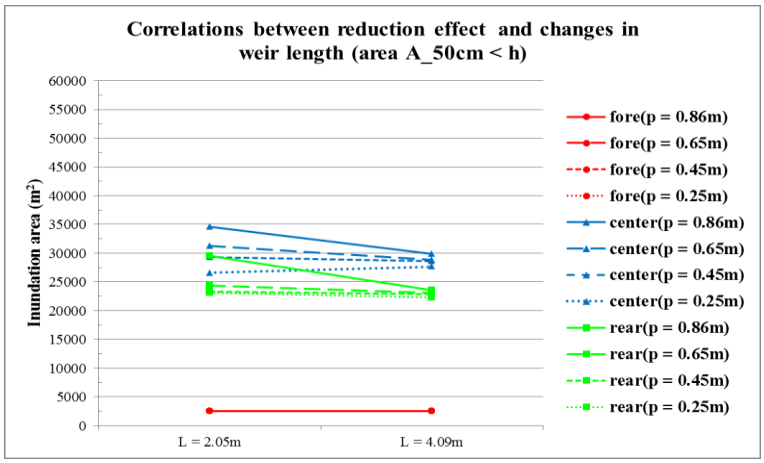

Figure 4.50 Correlations between reduction affect and changes in weir length (50cm < h, area A)

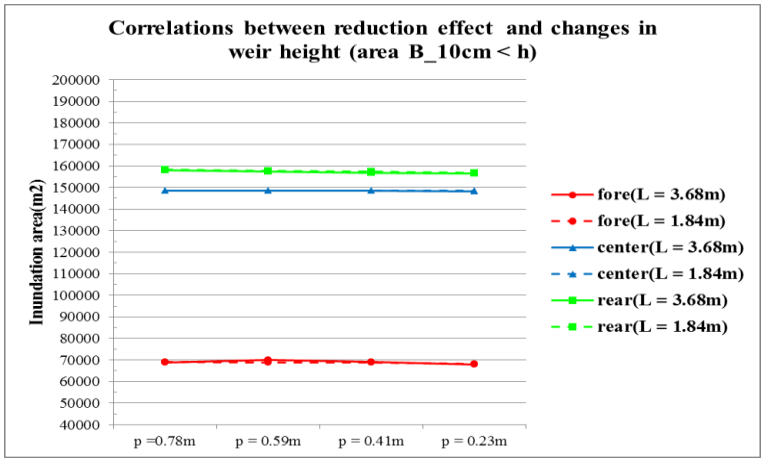

Figure 4.51 Correlations between reduction affect and changes in weir height (10cm < h, area B)

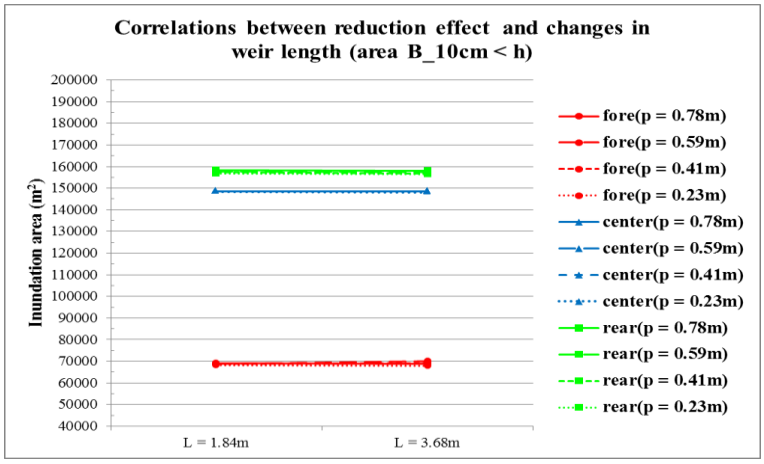

Figure 4.52 Correlations between reduction affect and changes in weir length (10cm < h, area B)

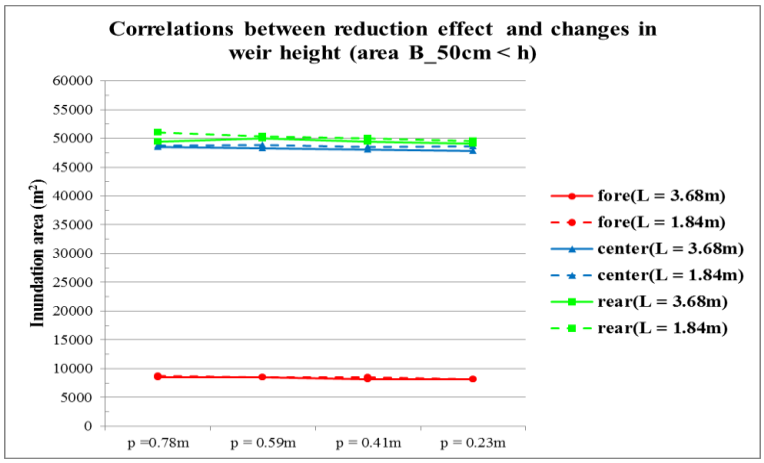

Figure 4.53 Correlations between reduction affect and changes in weir height (50cm < h, area B)

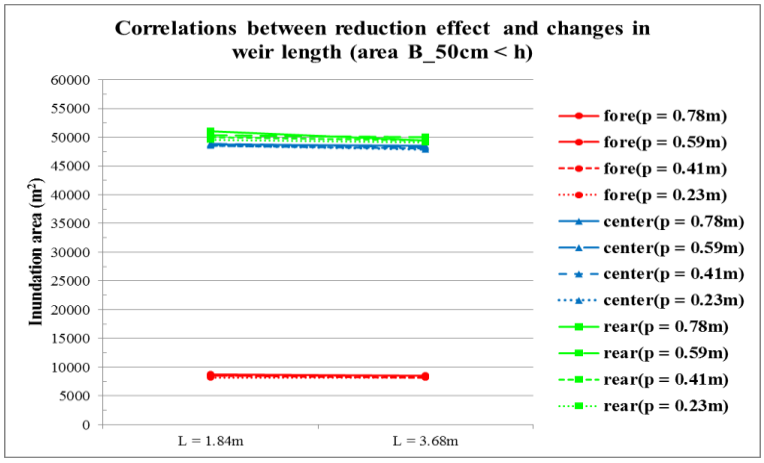

Figure 4.54 Correlations between reduction affect and changes in weir length (50cm < h, area B)

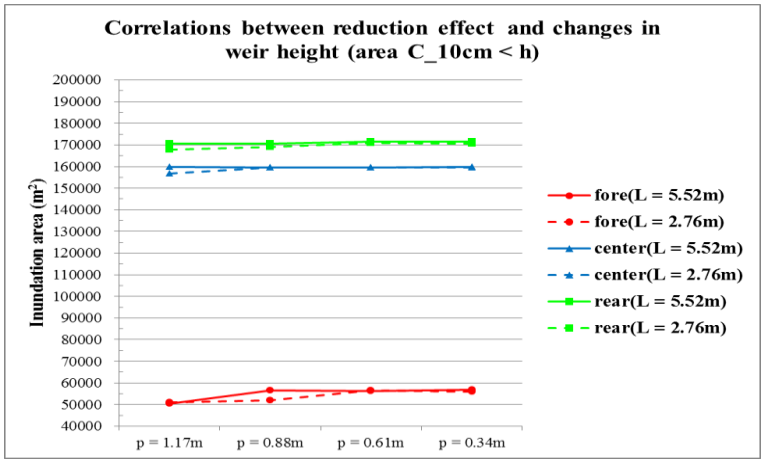

Figure 4.55 Correlations between reduction affect and changes in weir height (10cm < h, area C)

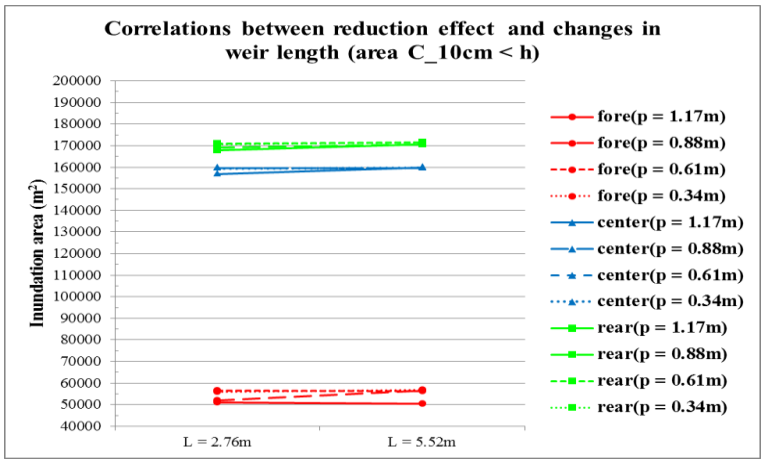

Figure 4.56 Correlations between reduction affect and changes in weir length (10cm < h, area C)

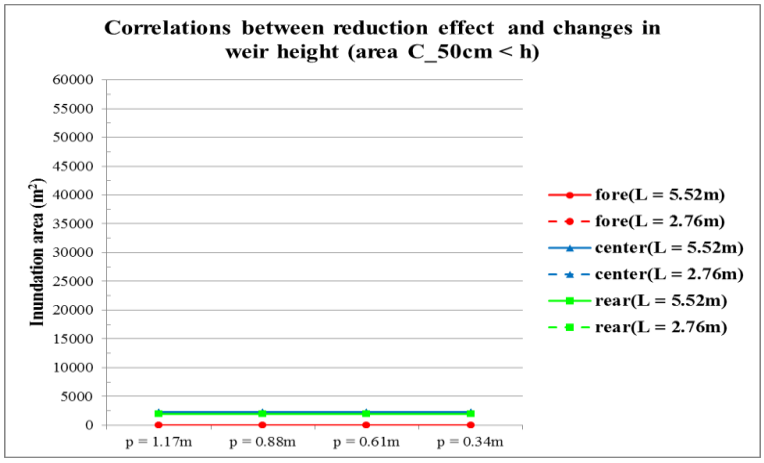

Figure 4.57 Correlations between reduction affect and changes in weir height (50cm < h, area C)

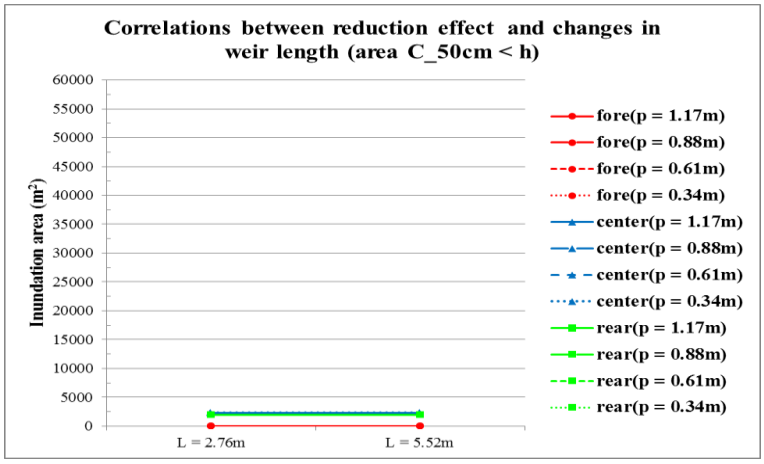

Figure 4.58 Correlations between reduction affect and changes in weir length (50cm < h, area C)

4.4.2 Comparison by the installation position of the storage box

When installing the storage box, different effects are expected according to the installation position, such as at the upstream and downstream portions of the sewer pipe. Each storage box was installed on the upstream and downstream portion within one sewer pipe, and six storage boxes were installed in each of areas A, B, and C, as shown in Figures 4.25 ~ 4.27. Pipe diameters of 0.7m ~ 1.35m were chosen after considering the drain capacity of the sewer pipe, depending on the pipe diameter and shape of actual storage box in Moriguchi City in, the Neyagawa basin. The weir height and length were determined following the ratio to the actual model. Also, rear intensity was adopted because the largest inundation area was caused under that rainfall condition, as shown in Table 4.2.

Table 4.2 Cases along the storage box positions

Rainfall type	Target area	Class number of pipe	Classification of cases	Pipe diameter (m)	Weir length (m)	Weir height (m)	Capacity (m^3)
Rear intensity	A	1530_up	a	1	4.09	0.86	50,000
		1530_down	b				
		1158_up	c	1.2	4.91	1.04	
		1158_down	d				
		2776_up	e	0.7	2.86	0.60	
		2776_down	f				
	B	724_up	a	1.52	6.22	1.31	
		724_down	b				
		1728_up	c	0.9	3.68	0.78	
		1728_down	d				
		1917_up	e	0.83	3.40	0.72	
		1917_down	f				
	C	961_up	a	1.35	5.52	1.17	
		962_down	b				
		1511_up	c	1	4.09	0.86	
		1511_down	d				
		2242_up	e	0.8	3.27	0.63	
		2242_down	f				

4.4.2.1 Results and discussion

Strictly speaking, although a comparison of mitigation effects based on different weir lengths and heights is difficult, the mitigation effect differed depending on the installation position of the storage box.

In the case of area A, the best mitigation effect was represented when the storage box was located at position (b), which is the downstream section of pipe (1530). Even though the diameter of pipe (1530) is smaller than the others, it showed the best mitigation effect. In other words, as the overflow discharge into the storage box increases, the mitigation effect of inundation also increases. Since overflow discharge is influenced by the drainage capacity of the pipe, the diameter of the pipe is not related to the mitigation effect. The best reduction rates of 6.6% and 47.3% showed under the more than 10cm and 50cm inundation area. In the case of area B, the best mitigation effect was represented when the storage box was located at position (d), which is the downstream section of pipe (1728). As discussed with area A, even though the diameter of pipe (1728) is smaller than the others, it showed the best mitigation effect. However, the overall mitigation effect was less than areas A and C. The best reduction rate was extremely low: 1.8% and 8.0% under the more than 10cm and 50cm inundation areas. In the case of area C, the mitigation effect on position (b), located at the downstream section of pipe (962), was larger than the others. The mitigation effect under any of the positions was great. The best reduction rates of 24.4% and 87.9% showed under the more than 10cm and 50cm inundation area. It seemed that the drainage capacity of pipe network in area C (upstream portion in Nakahama) was greater than in the other areas.

An important point was that when the storage box was located at the downstream portion of the sewer pipe, the mitigation effect was better than at the upstream position, as shown in Figures 4.59 ~ 4.70.

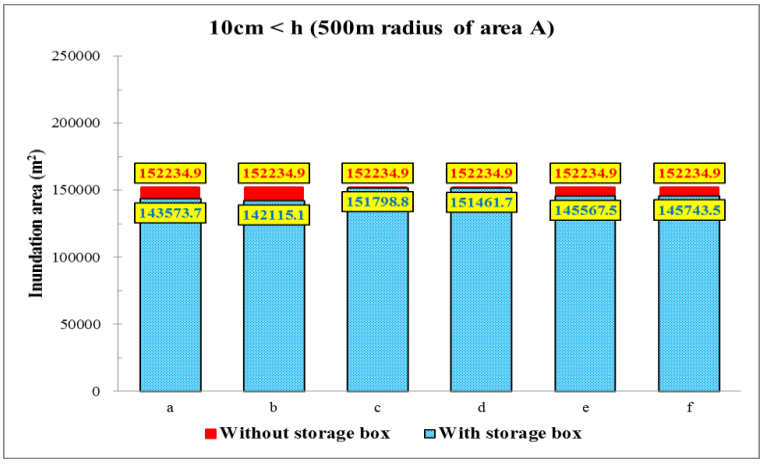

Figure 4.59 Mitigation effect along installation position (10cm < h, area A)

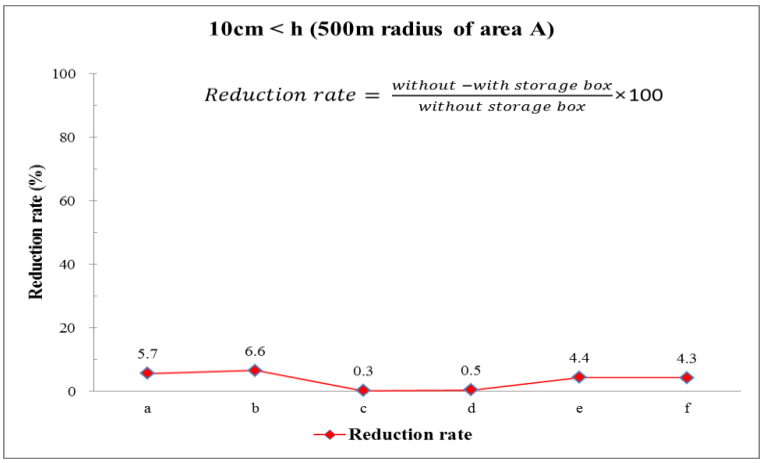

Figure 4.60 Reduction rate along the installation position (10cm < h, area A)

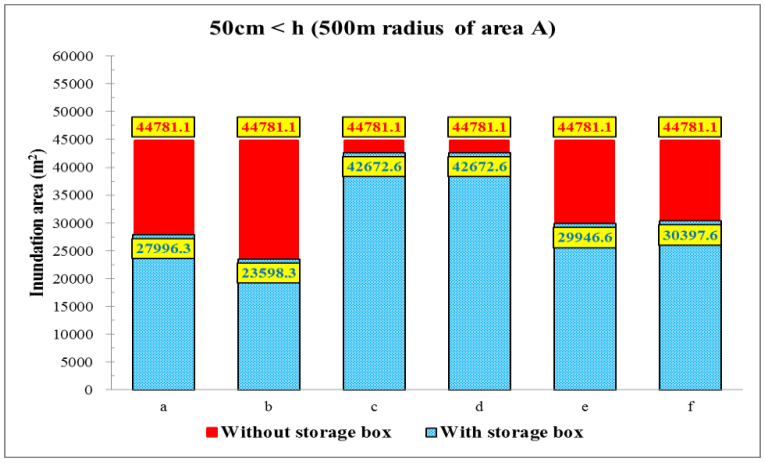

Figure 4.61 Mitigation effect along installation position (50cm < h, area A)

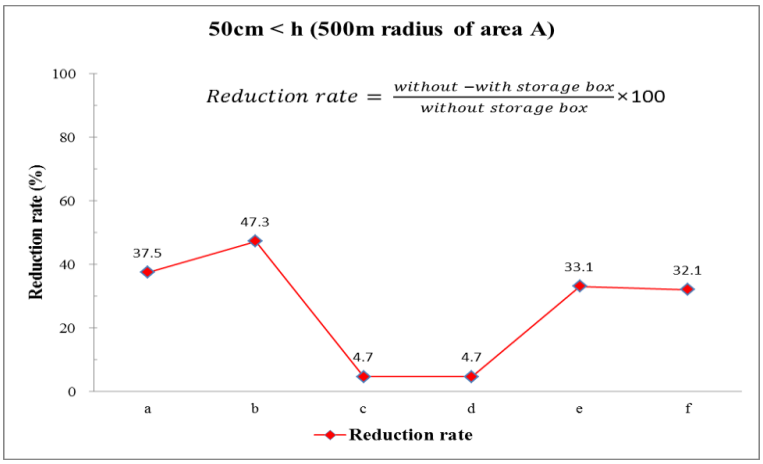

Figure 4.62 Reduction rate along the installation position (50cm < h, area A)

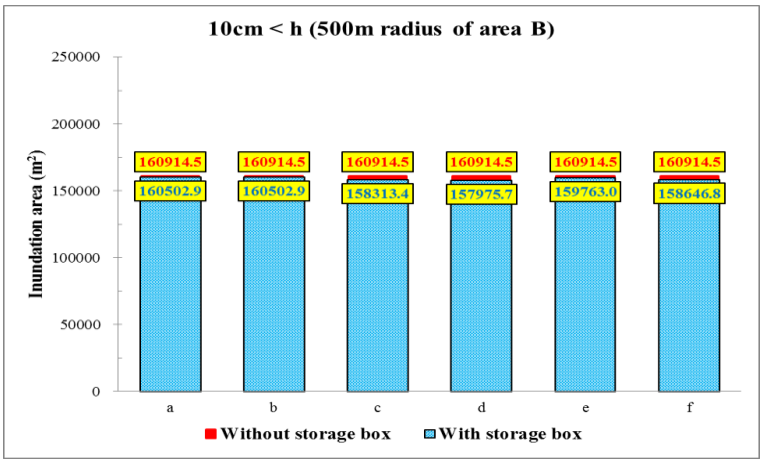

Figure 4.63 Mitigation effect along installation position (10cm < h, area B)

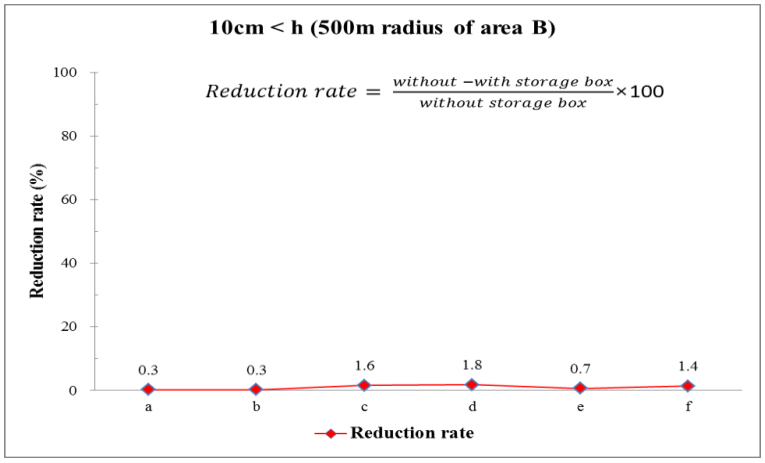

Figure 4.64 Reduction rate along installation position (10cm < h, area B)

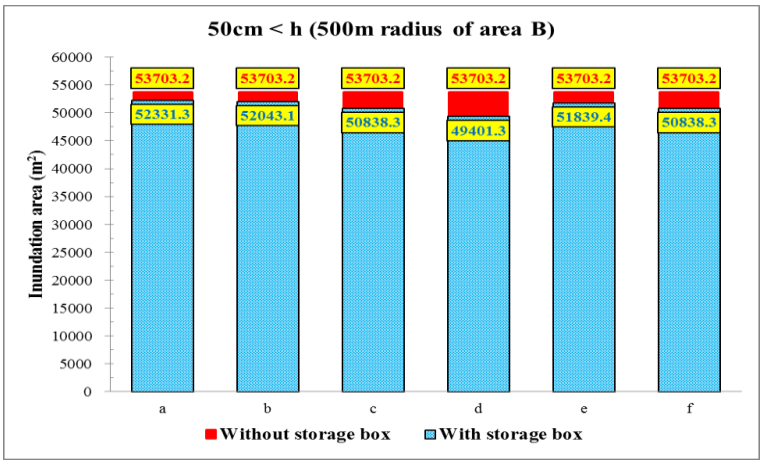

Figure 4.65 Mitigation effect along installation position (50cm < h, area B)

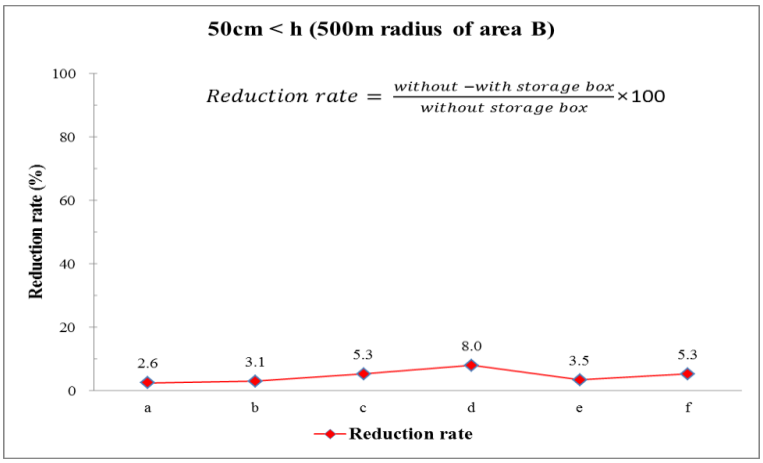

Figure 4.66 Reduction rate along installation position (50cm < h, area B)

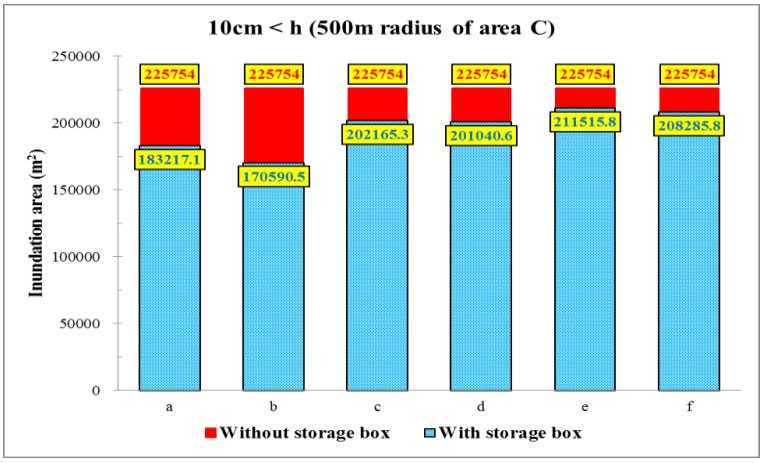

Figure 4.67 Mitigation effect along installation position (10cm < h, area C)

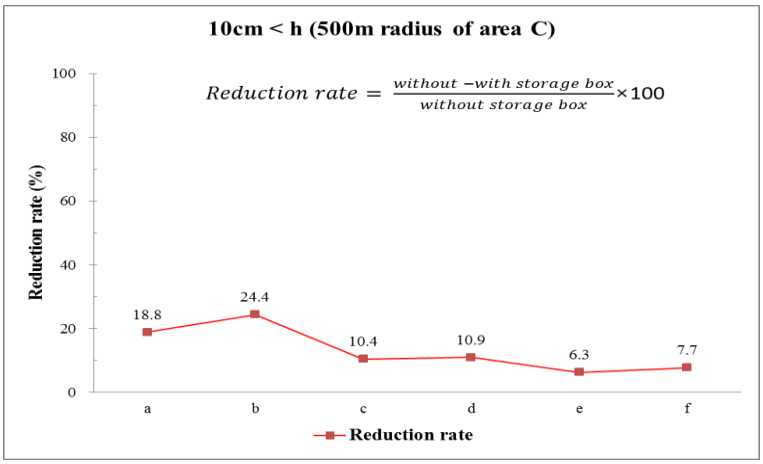

Figure 4.68 Reduction rate along installation position (10cm < h, area C)

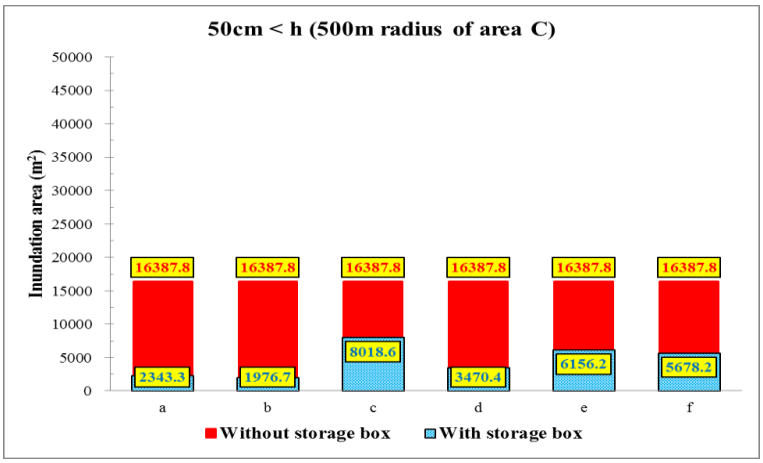

Figure 4.69 Mitigation effect along installation position (50cm < h, area C)

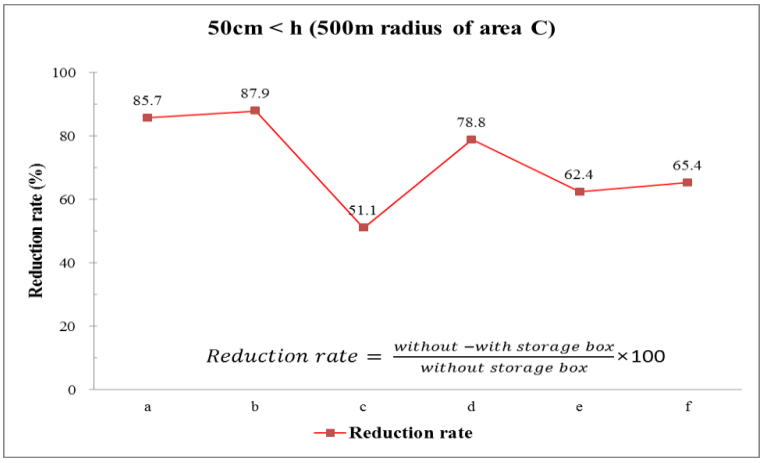

Figure 4.70 Reduction rate along installation position (50cm < h, area C)

4.4.3 Comparison by storage capacity.

Naturally, larger capacities can demonstrate the mitigation effect of inundation, although there is a limit to storage capacity. The small capacity possible is desirable, when considering construction cost and time. Moreover, the mitigation effect may not increase over a certain size while using a large storage capacity. Therefore, a study to obtain the mitigation effects of the degree to which the storage capacity changes would need to indicate the suitable results. Four cases of storage capacities were investigated along each of areas A, B, and C, as shown in Table 4.3. Each storage capacity was determined depending on the previously analyzed results, and rear intensity rainfall was adopted.

Table 4.3 Cases along the storage capacity

Rainfall type	Target area	Class number of pipe	Installation position	Classification of cases	Pipe diameter (m)	Weir length (m)	Weir height (m)
Rear intensity	A	1530	b	Case(5000)	1	4.09	0.86
				Case(10000)			
				Case(15000)			
				Case(20000)			
	B	1728	d	Case(5000)	0.9	3.68	0.78
				Case(10000)			
				Case(13000)			
				Case(15000)			
	C	962	b	Case(30000)	1.35	5.52	1.17
				Case(40000)			
				Case(50000)			
				Case(60000)			

4.4.3.1 Results and discussion

Figures 4.71 ~ 4.76 show the variations in the inundation area along the calculated time corresponding to inundation areas more than 10cm and 50cm depths.

In the case of area A, the storage capacity of case (5000) could have an influence by reducing the inundation area at inundation peak time, but it had filled soon. Cases (10000) and (15000) also had filled within around 4 ~ 5 hours after the inundation peak time. Case (20000) was not filled, and it showed sufficient mitigation effects to the end of the calculation time. However, if the storage capacity was exceeded until case (10000), its effect was insufficient at the inundation peak time. The difference was the drainage process from the past inundation peak time. Therefore, when intended to reduce the peak inundation area, case (10000) was financially suitable, and all of the capacities were effective in reducing the inundation areas corresponding to inundation area more than 50cm depth. In the case of area B, the maximum inundation area was not much different from the case of no installation.

Even though the mitigation effect increased as the capacity increased, the variation from case (5000) to case (15000) was too small, and it cannot be expected to be highly effective at case (15000). In the case of area C, if the storage capacity was exceeded until case (30000), its effect was insufficient at the inundation peak time. However, as the storage capacity increased, a large

difference in the drainage process from the past inundation peak time was shown, compared to areas A and B, and case (30000) was suitable for reducing the inundation areas corresponding to inundation area more than 50cm depth.

However, since the mitigation is thought to differ depending on the installation position for storage capacity and its effects, it is necessary to be compared in a variety of combined cases.

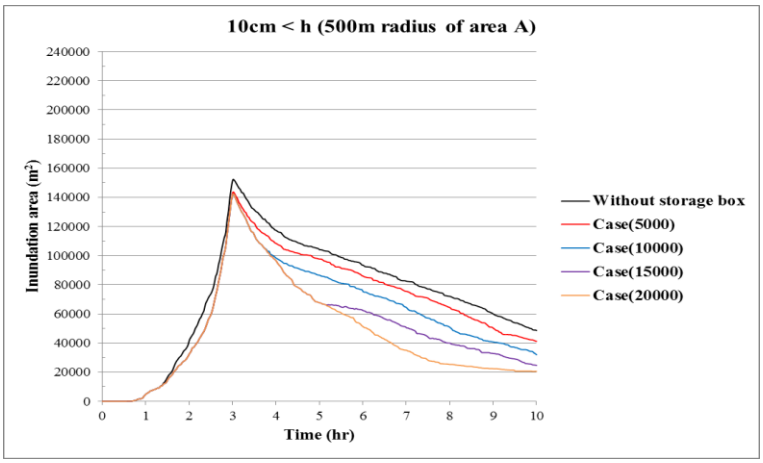

Figure 4.71 Variation in inundation area along the calculated time (10cm, area A)

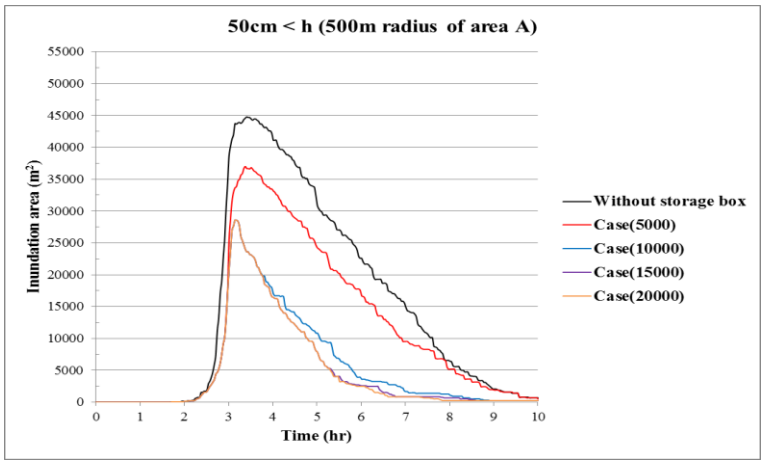

Figure 4.72 Variation in inundation area along the calculated time (50cm, area A)

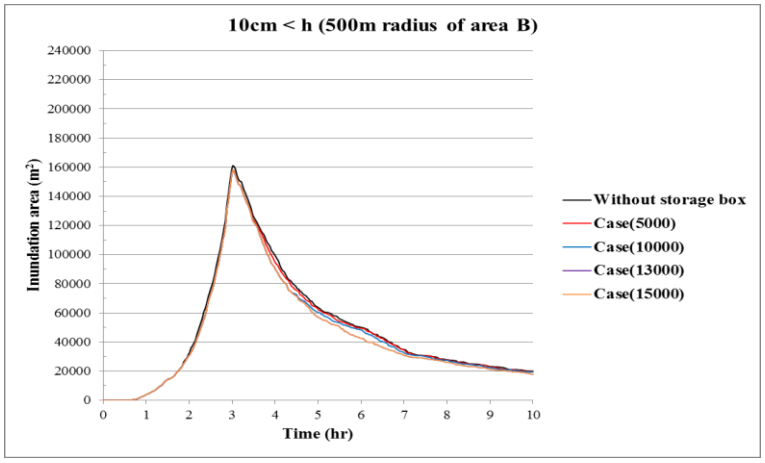

Figure 4.73 Variation in inundation area along the calculated time (10cm, area B)

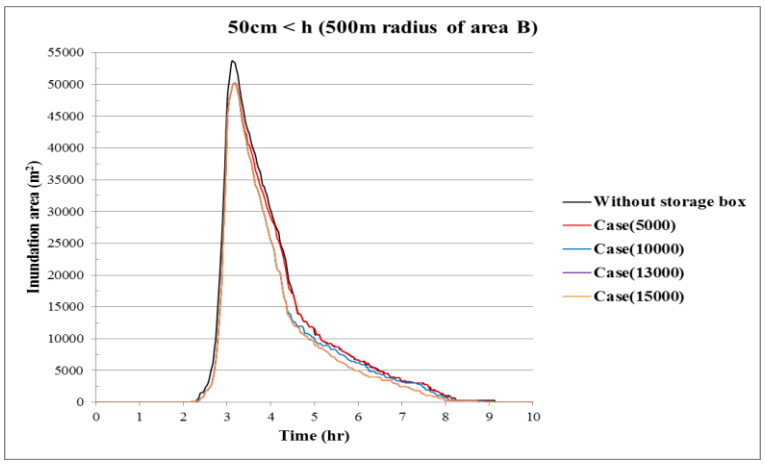

Figure 4.74 Variation in inundation area along the calculated time (50cm, area B)

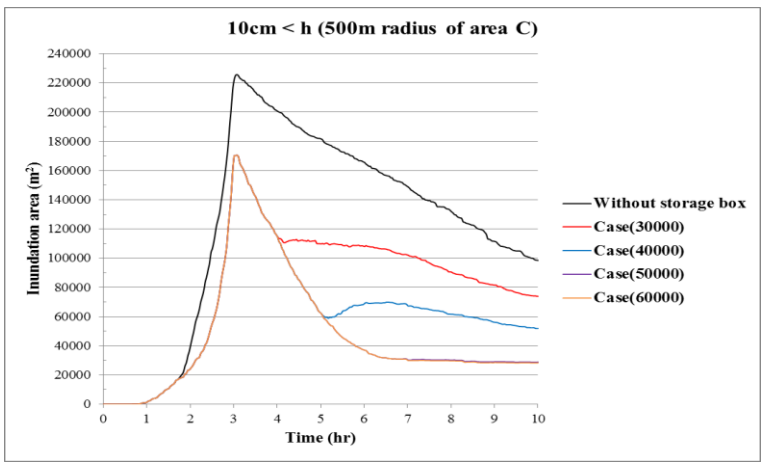

Figure 4.75 Variation in inundation area along the calculated time (10cm, area C)

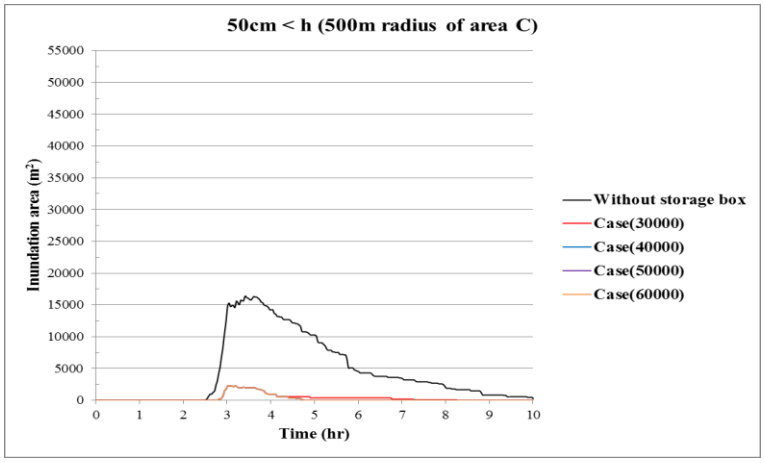

Figure 4.76 Variation in inundation area along the calculated time (50cm, area C)

4.4.4 Assessment of inundation damage costs

Assessments of inundation damage have obtained greater importance, as flood risk management is becoming the dominant approach of flood control policies. Also, flood control systems like an underground storage box should be installed, preferably in areas that receive significant damage, depending on quantitative analyses, such as assessments of inundation damage costs. The storage box in area C seems to have the most salient effect, in view of the results achieved so far. However, its relatively small inundation area compared with the other areas corresponding to inundation areas more than 50cm depth had an effect on its results. Therefore, a suitable installation sites at areas A, B, and C in Nakahama would need to be found through assessments of inundation damage costs. Inundation damage costs are estimated by considering the calculated inundation depth using a numerical model, the amount of damage per unit area in the corresponding area, and the damage rate of house assets depending on inundation depth. Table 4.4 shows the amount of damage per unit area in corresponding administrative districts (the Ministry of Land, Infrastructure, and Transport's water management and Land conservation stations run by the River Planning Division), and Table 4.5 shows the damage rates of house assets when considering the ground gradient (Ministry of Land, Infrastructure and Transport River Bureau: Flood Control Economic Research Manual).

Table 4.4 Amount of damage per unit area in corresponding administrative district

Index	Basic unit	District	Value
House assets	Amount per $1m^2$ ($1,000yen/m^2$)	Tokyo	220.6 ($1,000yen/m^2$)
		Osaka	158.3 ($1,000yen/m^2$)
		Aichi	165.8 ($1,000yen/m^2$)

Table 4.5 Damage rate of house assets considering the ground gradient

Index	Ground gradient	Under the floor	Over the floor				
			Less than 50cm	50~99 cm	100~199 cm	200~299 cm	More than 300cm
House assets	Less than 1/1,000	0.032	0.092	0.119	0.266	0.580	0.834
	1/1,000 ~1/500	0.044	0.126	0.176	0.343	0.647	0.870
	More than 1/500	0.050	0.144	0.205	0.382	0.681	0.888

4.4.4.1 Results and discussion

Figure 4.77 shows the inundation area distributions for areas A, B, and C. Area A had about 90% of inundation areas corresponding more than 1cm but less than 50cm depths, area B had 88%, and area C had 97%; while corresponding to more 50cm but less than 2m depth, area A had 10%, area B had 12%, area C had 3%. Deep inundation depth occurring serious damage was happened a lot in area B, and area C had small inundation distribution relatively.

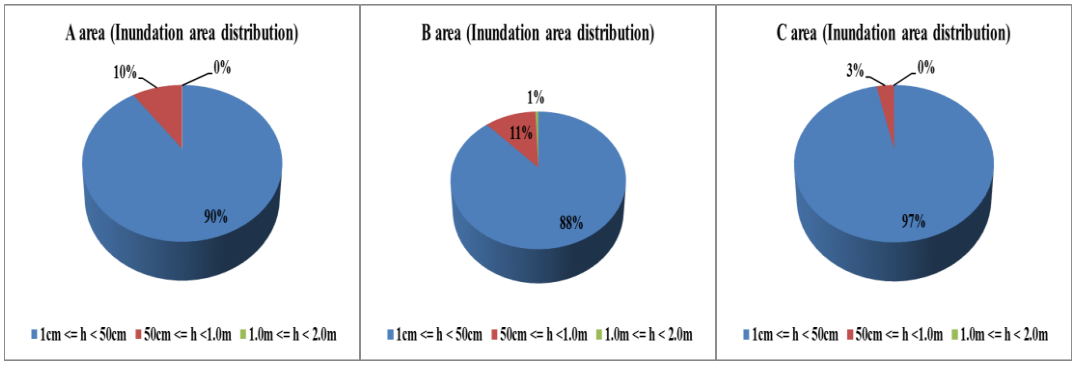

Figure 4.77 Inundation area distributions

The inundation damage costs were calculated by equation (4.51):

$$\text{Damage cost} = \text{Amount of damage per unit area} \times \text{Damage rate of house assets} \times \text{Inundation area} \quad (4.51)$$

where 158.3 (1,000yen/m^2) was used as the amount of damage per unit area. The damage rates of house assets were divided into three inundation depth sections. 0.032 was adopted for inundation areas with more than 1cm but less than 50cm depths, 0.119 was adopted for

inundation areas with more than 50cm but less than 1m depths, and 0.266 was adopted for inundation areas with more than 1m but less than 2m depths.

Figures 4.78 ~ 4.83 show the reduction effects of damage costs after installing at each position in areas A, B, and C, as well as the rate of damage cost (R), compared to the cases without the storage box.

In the case of area A, the costs of the inundation damage were assessed at 2,257,485,000yen without the storage box. When the storage box was installed at position b, the damage costs were reduced by about 255,258,000yen. In the case of area B, the costs of the inundation damage were assessed at 2,466,030,000 yen without the storage box. The most significant damage occurred in this case. When the storage box was installed at position d, the damage cost was reduced by about 91,206,000yen. The storage box did not greatly influence inundation damage. In the case of area C, the costs of the inundation damage were assessed at 2,046,573,000yen without the storage box. Relatively little inundation damage occurred compared with areas A and B. When the storage box was installed at position b, the damage costs were reduced by about 255,473,000yen.

Consequently, the storage box reduced the inundation damage but did not have a significant effect. Since area B was estimated to receive the highest inundation damage, compared with the other areas, if a storage box will be installed in one of areas A, B, and C, the area B is most suitable as an installation location. However, since the effect of the storage box is smaller than in the other areas, the installation position and storage box's effects should be considered carefully to obtain greater effects, financially.

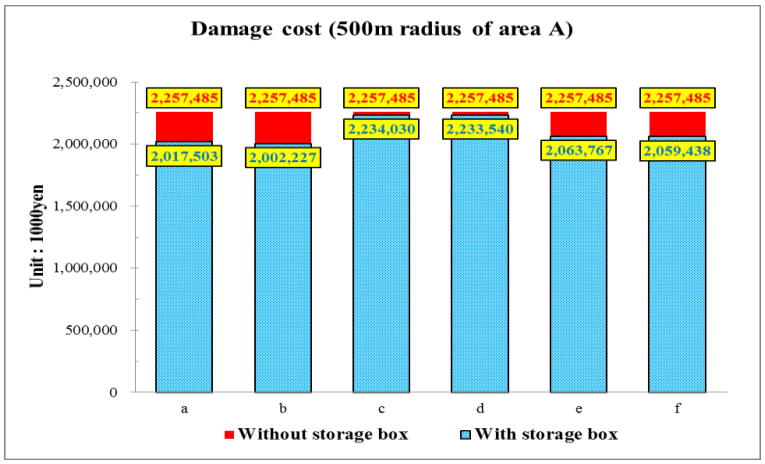

Figure 4.78 Reduction effects of damage costs when installing at each position (area A)

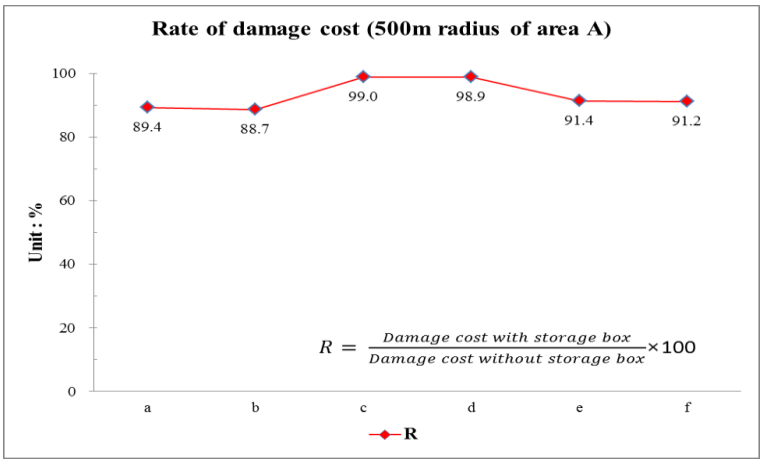

Figure 4.79 Rates of damage costs when installing at each position (area A)

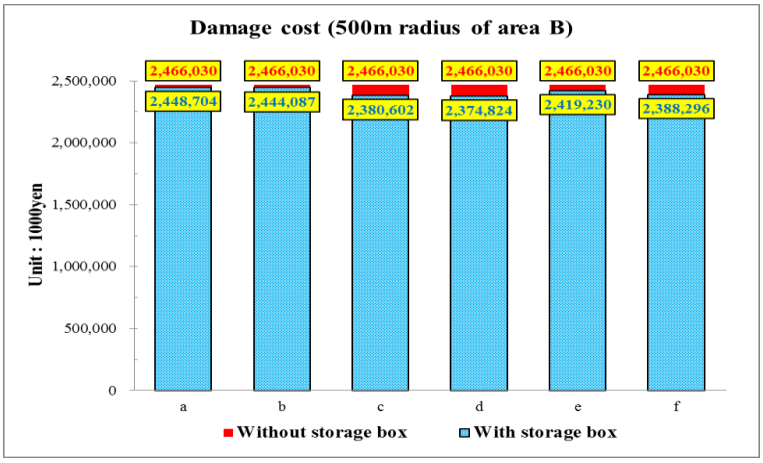

Figure 4.80 Reduction effects of damage costs when installing at each position (area B)

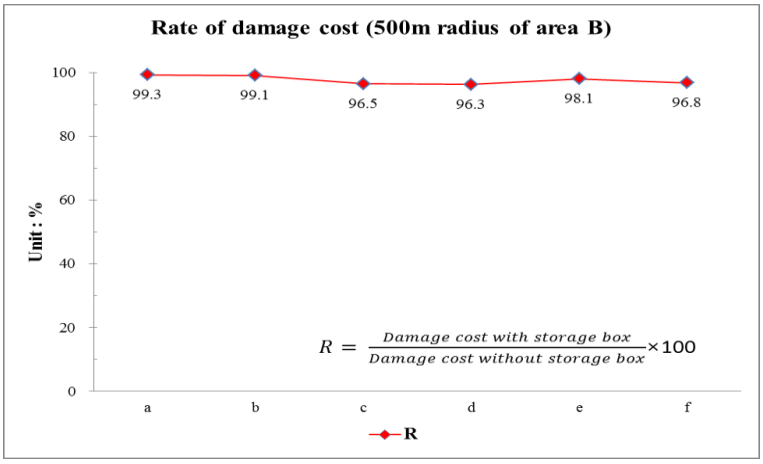

Figure 4.81 Rates of damage costs when installing at each position (area B)

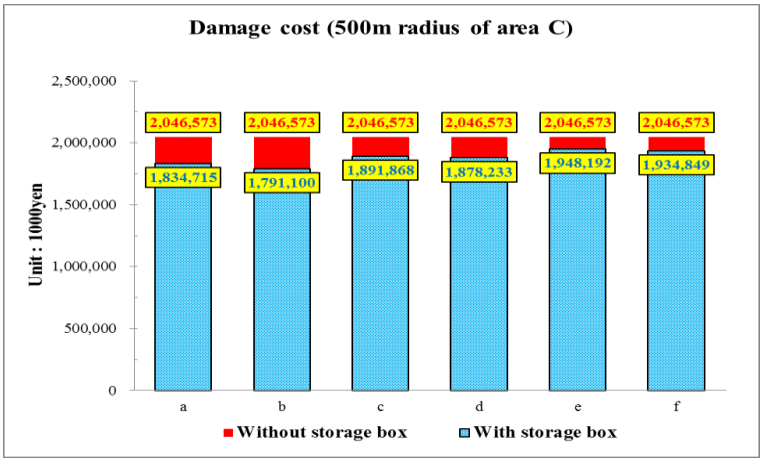

Figure 4.82 Reduction effects of damage costs when installing at each position (area C)

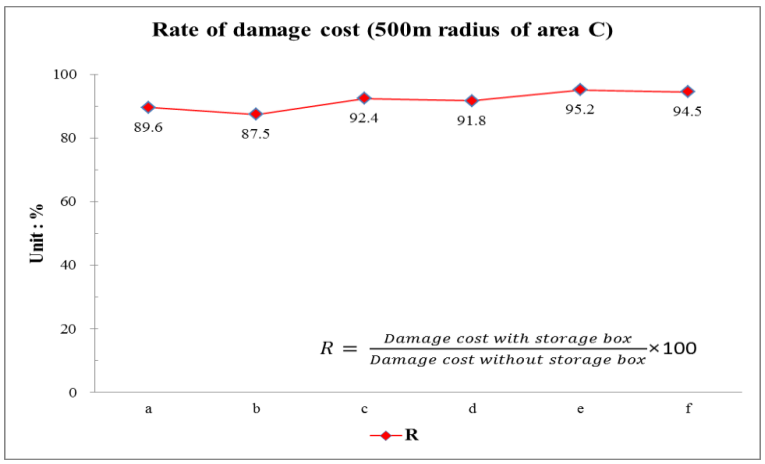

Figure 4.83 Rates of damage costs when installing at each position (area C)

4.5 Summary

In order to promptly remove the storm water, drainage systems and pumping stations must be maintained to increase the efficiency of the sewerage treatment capacity. However, huge costs and amounts of time are required to conduct this maintenance. Therefore, underground storm water storage boxes are installed ideally in order to temporarily capture and store runoff in a large space. I considered the side weir attached to the sewer as one of methods for storage system. The storm water drainage and diversion process of the side weir were presented using a numerical model, and the reduction ratio of inland flooding due to installing the storage box was verified.

In this study, Nakahama District in Osaka was the target area, which is located in the eastern part of Osaka City. Two-dimensional ground surface and one-dimensional sewer network models (Kawaike et al., 2002) were used to reproduce the inland flood and storm water drainage process, in an integrated flood analysis model developed by Lee et al. (2014). Three installation sites were determined after considering different area features, where A is the lowland, B is the middle, and C is the upstream portion in the Nakahama area. Firstly, the differences in the storage box's effects were verified due to rainfall type and weir shape changes. Secondly, the lowland, middle, and upstream portions of the Nakahama area were investigated to verify the storage box's effect along locations that have different area features. Thirdly, the differences in the storage box's effect were verified by the changes in storage capacity volume. Lastly, a suitable installation site was verified though assessments of inundation damage costs.

The rear and center intensity rainfall conditions influenced urban inundation. The impact of the fore intensity rainfall condition was less than the other rainfall distributions. The mitigation effect of the inundation area due to the installation of a storage box was the best in area C. The inundation mitigation effects by different weir height and length were that the peak inundation area decreased as the weir height decreased or length increased because the overtopping time had begun by decreasing the weir height and the quantity of discharge increased. The peak inundation area was decreased by adjusting the weir size, but the variation in the inundation mitigation effect was not so great. In conclusion, inundation mitigation due to changes in weir height is more pronounced than by changes in weir length.

The mitigation effect differed depending on the installation position of the storage box. In the case of area A, the best mitigation effect was represented when the storage box was located at position (b), which is the downstream section of pipe (1530). In the case of area B, the best mitigation effect was represented when the storage box was located at position (d), which is the downstream section of pipe (1728). However, the overall mitigation effect was less than areas A and C. In the case of area C, the mitigation effect on position (b), located at the downstream section of pipe (962), was larger than the others. The mitigation effect under any of the positions was great. It seemed that the drainage capacity of pipe network in area C (upstream portion in Nakahama) was greater than in the other areas. An important point was that when the storage box was located at the downstream portion of the sewer pipe, the mitigation effect was better than at the upstream position.

The small capacity possible is desirable, when considering construction cost and time. Moreover, the mitigation effect may not increase over a certain size while using a large storage

capacity. Therefore, a study to obtain the mitigation effects of the degree to which the storage capacity changes would need to indicate the suitable results. In the case of area A, Case (20000) was not filled, and it showed sufficient mitigation effects to the end of the calculation time. However, if the storage capacity was exceeded until case (10000), its effect was insufficient at the inundation peak time. In the case of area B, the maximum inundation area was not much different from the case of no installation. In the case of area C, if the storage capacity was exceeded until case (30000), its effect was insufficient at the inundation peak time. Consequently, since the mitigation is thought to differ depending on the installation position for storage capacity and its effects, it is necessary to be compared in a variety of combined cases.

A suitable installation sites at areas A, B, and C in Nakahama would need to be found through assessments of inundation damage costs. In the case of area A, the costs of the inundation damage were assessed at 2,257,485,000yen without the storage box. When the storage box was installed at position b, the damage costs were reduced by about 255,258,000yen. In the case of area B, the costs of the inundation damage were assessed at 2,466,030,000 yen without the storage box. When the storage box was installed at position d, the damage cost was reduced by about 91,206,000yen. In the case of area C, the costs of the inundation damage were assessed at 2,046,573,000yen without the storage box. When the storage box was installed at position b, the damage costs were reduced by about 255,473,000yen. Consequently, the storage box reduced the inundation damage but did not have a significant effect. Since area B was estimated to receive the highest inundation damage, compared with the other areas, if a storage box will be installed in one of areas A, B, and C, the area B is most suitable as an installation location. However, since the effect of the storage box is smaller than in the other areas, the installation position and storage box’s effects should be considered carefully to obtain greater effects, financially.

Chapter 5

Conclusions and recommendations

The present study was undertaken to determine the appropriate equation to estimate the diversion discharge to a storage box. The experiment was to obtain the overtopping discharge under different conditions, like upstream discharge and weir condition, and to determine the discharge coefficient. Also, the numerical model was used to validate the experimental results using the discharge coefficient obtained by experiment. Therefore, the applicability of De Marchi's equation must also be verified in my experimental cases, and the correlation equation of discharge coefficient in the changing hydraulic structure conditions, like side weir length and height, was suggested under pressurized flow conditions.

Finally, actual field application studies on the effects of underground storage box were carried out using a numerical model, adopting the suggested correlation equation of the discharge coefficient. An integrated model consisting of a two-dimensional ground surface model was developed, and a one-dimensional sewer model was used.

5.1 Conclusions

The conclusions of this study are summarized as follows:

5.1.1 Water surface profile

In the experimental results, as the upstream discharge increased, the hydraulic gradient became steeper, compared with the results of the smaller discharge cases. The rate of the rise in pressurized flow conditions was larger than that in the open channel condition, and a high water head at the downstream end of the side weir has an effect on the water heads of the downstream pipe. This phenomenon was due to the water spurting quickly from the upstream to downstream portion, so that it takes the pressure at the downstream portion. This result shows the difference between open channel flow and pressurized flow conditions.

5.1.2 Discharge coefficient

This discharge coefficient depends on the hydraulic conditions including the weir length, weir height, and water head on the side weir and the overflow discharge. As the upstream discharge increases, the overflow rate also increases, in comparison with the results under the low-discharge conditions. The water head was the most important parameter from which to derive the discharge coefficient in this study. Some previous studies used the water head at the upstream end of the side weir to calculate the discharge coefficient. However, there is excessively larger variation in the water heads on the side weir, compared with those of previous studies on the characteristics of pressurized flow. From this perspective, the mean of the integral water heads along the entire side weir length was adopted, which was derived from the side weir's length and the water head integrated along the side weir.

5.1.3 De Marchi's equation's applicability and suitable discharge coefficient

Under the assumption that De Marchi's equation is applicable to the pressurized flow conditions, a numerical model was used to validate the experimental results, like the discharge coefficients obtained by the experiment, so that effective conclusions can be drawn regarding the suitability of De Marchi's equation for these cases.

First, the discharge coefficients for each different weir condition were applied to numerical simulation. Secondly, each overflow discharge simulated was compared with the overflow discharge data obtained from the experiment. Consequently, the overflow discharge simulated could reproduce the experimental results, although there are still small differences as a whole. However, when applying the overflow discharge coefficient to the actual field, the constant coefficient value is easy to handle. Therefore, a suitable coefficient was determined within the limited experimental results for each different side weir condition. As a result, an empirical correlation to predict the discharge coefficient was developed for the ratio of weir height to length using the suitable coefficients as follows:

$$C_d = -0.2604\frac{p}{L} + 0.6736$$

5.1.4 Analysis of storage box's effects when applied to an actual field in Osaka.

In this study, Nakahama District in Osaka was the target area, which is located in the eastern part of Osaka City. This area received inundation damage during a heavy rainfall in a short time, in August 27, 2011. The maximum precipitation per 1 hour was 77.5mm for about 3 hours, which was the largest value on record.

Three installation sites were determined after considering different area features, where A is the lowland, B is the middle, and C is the upstream portion in the Nakahama area. In addition, the capacity of the storage box is 50,000 m^3, which is the largest capacity of an installed storage box in the Neyagawa basin. Firstly, the differences in the storage box's effects were verified due to rainfall type and weir shape changes. Secondly, the lowland, middle, and upstream portions of the Nakahama area were investigated to verify the storage box's effect along locations that have different area features. Thirdly, the differences in the storage box's effect were verified by the changes in storage capacity volume. Lastly, a suitable installation site was verified though assessments of inundation damage costs.

The rear and center intensity rainfall conditions influenced urban inundation. The impact of the fore intensity rainfall condition was less than the other rainfall distributions. The mitigation effect of the inundation area due to the installation of a storage box was the best in area C. The inundation mitigation effects by different weir height and length were that the peak inundation area decreased as the weir height decreased or length increased because the overtopping time had begun by decreasing the weir height and the quantity of discharge increased. The peak inundation area was decreased by adjusting the weir size, but the variation in the inundation mitigation effect was not so great. In conclusion, inundation mitigation due to changes in weir height is more pronounced than by changes in weir length.

The mitigation effect differed depending on the installation position of the storage box. In the case of area A, the best mitigation effect was represented when the storage box was located at position (b), which is the downstream section of pipe (1530). Even though the diameter of pipe (1530) is smaller than the others, it showed the best mitigation effect. In other words, as the overflow discharge into the storage box increases, the mitigation effect of inundation also increases. Since overflow discharge is influenced by the drainage capacity of the pipe, the diameter of the pipe is not related to the mitigation effect. In the case of area B, the best mitigation effect was represented when the storage box was located at position (d), which is the downstream section of pipe (1728). As discussed with area A, even though the diameter of pipe (1728) is smaller than the others, it showed the best mitigation effect. However, the overall mitigation effect was less than areas A and C. In the case of area C, the mitigation effect on position (b), located at the downstream section of pipe (962), was larger than the others. The mitigation effect under any of the positions was great. It seemed that the drainage capacity of pipe network in area C (upstream portion in Nakahama) was greater than in the other areas. An

important point was that when the storage box was located at the downstream portion of the sewer pipe, the mitigation effect was better than at the upstream position.

The small capacity possible is desirable, when considering construction cost and time. Moreover, the mitigation effect may not increase over a certain size while using a large storage capacity. Therefore, a study to obtain the mitigation effects of the degree to which the storage capacity changes would need to indicate the suitable results. In the case of area A, Case (20000) was not filled, and it showed sufficient mitigation effects to the end of the calculation time. However, if the storage capacity was exceeded until case (10000), its effect was insufficient at the inundation peak time. The difference was the drainage process from the past inundation peak time. In the case of area B, the maximum inundation area was not much different from the case of no installation. Even though the mitigation effect increased as the capacity increased, the variation from case (5000) to case (15000) was too small, and it cannot be expected to be highly effective at case (15000). In the case of area C, if the storage capacity was exceeded until case (30000), its effect was insufficient at the inundation peak time. In conclusion, since the mitigation is thought to differ depending on the installation position for storage capacity and its effects, it is necessary to be compared in a variety of combined cases.

As a whole, the storage box in area C seems to have the most salient effect, in view of the results achieved so far. However, its relatively small inundation area compared with the other areas corresponding to inundation areas more than 50cm depth had an effect on its results. Therefore, a suitable installation sites at areas A, B, and C in Nakahama would need to be found through assessments of inundation damage costs. Inundation damage costs are estimated by considering the calculated inundation depth using a numerical model, the amount of damage per unit area in the corresponding area, and the damage rate of house assets depending on inundation depth. In the case of area A, the costs of the inundation damage were assessed at 2,257,485,000yen without the storage box. When the storage box was installed at position b, the damage costs were reduced by about 255,258,000yen. In the case of area B, the costs of the inundation damage were assessed at 2,466,030,000 yen without the storage box. The most significant damage occurred in this case. When the storage box was installed at position d, the damage cost was reduced by about 91,206,000yen. In the case of area C, the costs of the inundation damage were assessed at 2,046,573,000yen without the storage box. Relatively little inundation damage occurred compared with areas A and B. When the storage box was installed at position b, the damage costs were reduced by about 255,473,000yen. Consequently, the storage box reduced the inundation damage but did not have a significant effect. Since area B was estimated to receive the highest inundation damage, compared with the other areas, if a storage box will be installed in one of areas A, B, and C, the area B is most suitable as an installation location. However, since the effect of the storage box is smaller than in the other

areas, the installation position and storage box's effects should be considered carefully to obtain greater effects, financially.

5.2 Recommendations for future studies

Future studies are essential to enhance the knowledge about performance of the model. Several recommendations for further study can include:

1. In the case of experimental study, limited range of discharge was taken due to laboratory limitations. So, it is recommended to increase the variation of discharge to understand its effect.

2. In this study, the steady flow cases were considered during all experiments but in reality, it might not be true. So it is recommended to perform unsteady analysis for more in depth knowledge. Also, the storm drain considered in the experiment is flat with parallel to the road but it is advised to check the slope type storm drain to analyze its effect.

3. Damage costs due to inundation were obtained and compared with and without storage box but those cost considered only inundation in the roads because the two-dimensional model cannot calculate the inundation under the house. So, it will be realistic to modify the code, so that the damage cost will be calculated assuming the house inundation. Also, it is recommended to perform Benefit-Cost analysis (B/C ratio) of the proposed storage box for the optimum capacity and location.

Reference

Allen, J.W.: The discharge of water over side weir in circular pipes, ICE Proc, Vol. 6, No. 2, pp. 270-287, 1957.

Borghei, M., Jalili, M.R., Ghodsian, M.: Discharge coefficient for sharp-crested side weir in subcritical flow, ASCE Journal of Hydraulic Engineering, Vol. 125, No.10, pp. 1051-1056, 1999.

Chaudhry, M. H.: Applied Hydraulic Transients, Van Nostrand Reinold, 1979.

Chen, A., Djordjević, S., Leandro, J., Evans, B. and Savic, D.: Simulation of the building blockage effect in urban flood modelling, Proc. 11th International Conference on Urban Drainage, pp. 1-10, 2008.

Chen, A., Djordjević, S., Leandro, J., Savic., D.: The urban inundation model with bidirectional flow interaction between 2D overland surface and 1D sewer networks, Workshop, 2007.

Chen, A. S., Hsu, M. H., Chen, T. S. and Chang, T. J.: An integrated inundation model for highly developed urban areas Wat. Sci. and Tech., Vol.51, No.2, 221-229, 2005.

Cheong, H. F.: Discharge coefficient of lateral diversion from trapezoidal channel, ASCE Journal of Irrigation and Drainage Engineering, Vol. 117, No. 4, pp. 321-333, 1991.

Choi, H., Han, K., Yi, J., Cho, W.: Study on installation of underground storage facilities for reducing the flood damage, Journal of Korean Society of Hazard Mitigation, Vol. 12, No. 4, pp. 115-123, 2012.

Cunge, J. A. and Wagner, M.: Numerical integration of Barre de Saint-Venant's flow equations by means of an implicit scheme of finite difference, Applications in the case of alternately free and pressurized flow in a tunnel, La Houille Blanch, No. 1, pp. 33-39, 1964.

De Marchi, G.: Saggio di teoria del funzionamento degli stramazzi laterali, L'Energia Elettrica, Vol. 11, No. 11, pp. 849–860 (in Italian), 1934.

Farid, M., Mano, A. and Udo, K.: Modelling flood runoff response to land cover change with rainfall spatial distribution in urbanized catchment, Annual J. Hydraulic Engineering, Vol. 55, pp. 19-24, 2011.

Ghodsian, M.: Supercritical flow over rectangular side weir, Canadian Journal of Civil Engineering, Vol. 30, No. 3, pp. 596–600, 2003.

Granata, F., Marinis, G.D., Gargano, R., Tricarico, C.: Novel approach for side weir in supercritical Flow, J. Irrigation and Drainage Engineering, Vol. 139, No. 8, pp. 672-679, 2013.

Hager, W.H.: Lateral outflow over side weirs, J. Hydraulic Engineering, Vol. 113, No. 4, 1987.

Inoue, K.: Study on its application to water engineering and numerical analysis of open channel unsteady flow, Kyoto University, pp. 189-197, 1986.

Inoue, K., Nakagawa. H. and Toda, K.: Numerical analysis of overland flood flows by mean of one and two-dimensional model, The 5th JSPS-VCC Seminar on Integrated Engineering, "Engineering Achievment and Challenges", pp. 388-397, 1994.

Iwasa, Y. and Inoue, K.: Mathematical simulation of channel and overland flood flows in view of flood disaster engineering, Journal of Natural Disaster Science, Vol. 4, No. 1, pp. 1-30, 1982.

Kawaike, K., Inoue, K. and Toda, K.: Inundation flow modeling in urban area based on the unstructured meshes, Hydrosoft 2000, Hydraulic Engineering Software, VIII, WIT Press, pp. 457-466, 2000.

Kawaike, K. and Nakagawa, H.: Recent inundation disaster in Japan and numerical modeling of urban flooding, International Symposium, 2006.

Kawaike, K., Nakagawa, H., Oomoto, T., Lee. S.: Study on mitigation effects of inundation damage in terms of storm water regulating pond, Journal of Jorean Society of Civil Engineers, 2015.

Khorchani, M., Blanpain, O.: Free surface measurement of flow over side weirs the video monitoring concept, Flow Measurement and Instrumentation, Vol. 15, No. 2, pp. 111-117, 2004.

Kim, Y., Han, K. and Cho, W.: Analysis on the effects of flood damage mitigation according to installation of underground storage facility, Journal of Korean Society of Civil Engineers, Vol. 30, No. 1B, pp. 41-51, 2010.

Lee, S., Nakagawa, H., Kawaike, K.: Urban inundation simulation considering road network and building configurations, Journal of flood risk management, 2015.

Muslu, Y.: Lateral weir flow model using a curve fitting analysis, ASCE Journal of Hydraulic Engineering, Vol. 128, No. 7, pp. 712-715, 2002.

Preissmann, M. A. and Cunge, J. A.: calculation of Wave Propagation on Electronic ~achines, Proceedings, 9th Congress, IAHR, Dubrovnik, pp. 656-664, 1961.

Ryu, S. and Lee, J.: Determination of optimal locations and size of storage in the urban sub-surface using genetic algorithm, Journal of Korean Society of Hazard Mitigation, Vol. 12, No. 3, pp. 285-290, 2012.

Schubert, J. E., Sanders, B. F., Smith, M. J. and Wright, N. G.: Unstructured mesh generation and land cover-based resistance for hydrodynamic modelling of urban flooding, Adv. Water Resource, Vol. 31, pp. 1603-1621, 2008.

Son, J. and Im, J.: An experimental study on runoff reduction effect of infiltration-storage system due to rainfall intensity, Journal of Korean Society of Hazard Mitigation, Vol. 7, No. 4, pp. 85-95, 2007.

Song, C., Seo, I. and Jung, Y.: Reduction of rainfall runoff by constructing underground Storage Tank, Journal of the Korean Society of Civil Engineers, Vol. 33, No. 3, pp. 927-935, May 2013.

Subramanya, K., Awasthy, S. C.: Spatially varied flow over side weirs, ASCE Journal of the Hydraulics Division, Vol. 98, No.1, pp. 1-10, 1972.

Tayefi, V., Lane, S. N., Hardy, R. J. and Yu, D.: A comparison of one and two-dimensional approaches to modeling flood inundation over complex upland floodplains, Hydrol. Processes, Vol. 21, pp. 3190-3202, 2007.

Uyumaz, A. and Muslu, Y.: Flow over side weirs in circular channels, J. Hydraulic Engineering, Vol. 111, No.1, pp. 144-160, 1985.

Vatankhah, A.R.: New solution method for water surface profile along a side weir in a circle channel, J. Irrigation and Drainage Engineering, Vol. 138, No.10, pp. 948-954, 2012.

Yen, B. C. and Pansic, N.: Surcharge of Sewer Systems, WRC Report No. 149, University of Illinois, USA, 1980.

Yuksel, E.: Effect of specific variation on lateral overflows, Flow measurement and instrumentation, Vol. 15, No. 5-6, pp. 259-269, 2004.

Yu-Tech, L.: Discussion of spatially varied flow over side weir, ASCE Journal of the Hydraulics Division, Vol. 98, No.11, pp. 2046-2048, 1972.

List of Figures

List of Tables

Curriculum Vitae

Name KO Dongwoo

Citizenship Republic of Korea

Birth October 13, 1984 Daegu, Republic of Korea

Ph.D. Student (2012 ~ 2015)
Department of Civil and Earth Resources Engineering,
Kyoto University, Kyoto, Japan

M. Sc. (2010~2012)
Department of Civil Engineering
Inje University, Republic of Korea

B.E. (2003~2009)
Department of Civil Engineering
Inje University, Republic of Korea

Paper based on the Thesis

Ko, D., Nakagawa, H., Kawaike, K. and Zhang, H.: Experimental study on the discharge coefficient for side weir with pressurized flow in circular channel, *Annual of the Disaster Prevention Research Institute*, Kyoto University, No. 57B, pp. 425- 431, June, 2014.

Ko, D., Nakagawa, H., Kawaike, K. and Zhang, H.: Study on estimation of inflow discharge to underground storage system for mitigation of urban inundation damage, *Annual Journal of the Japan Society for Natural Disaster Science*, Vol. 33, pp. 177-184, September, 2014.

Ko, D., Nakagawa, H., Kawaike, K. and Zhang, H.: Study on suitable coefficient of overflow discharge equation under pressurized flow condition, *Annual Journal of Hydraulic Engineering, JSCE*, Vol. 59, pp. 169-174, February, 2015.

Ko, D., Nakagawa, H., Kawaike, K.: Study on Applicability of Overflow Discharge Equation Under Pressurized Flow Condition, *Annual of the Disaster Prevention Research Institute*, Kyoto University, No. 58B, June, 2015 (In printing).